# Dynamics of Structures

*description of projects in the research programme*

Hansen, Lars Pilegaard

*Publication date:*
1998

*Document Version*
Publisher's PDF, also known as Version of record

## Description of the projects in the research programme

# DYNAMICS OF STRUCTURES

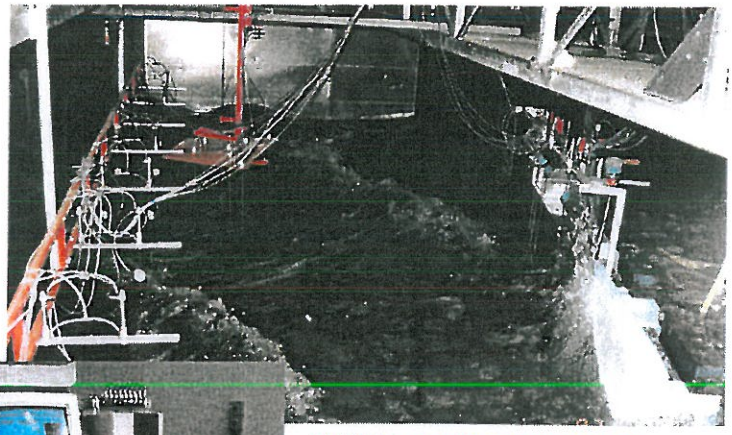

WAVE LOADS ON BREAKWATER

MODAL ANALYSIS OF MODEL BRIDGE

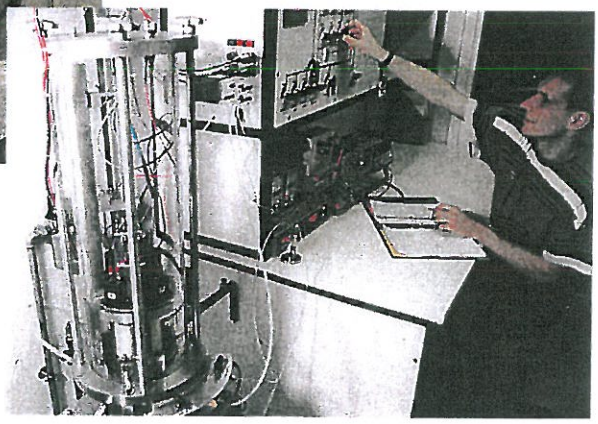

RESONANT COLUMN TEST ON SOIL

DEPARTMENT OF CIVIL ENGINEERING , AALBORG UNIVERSITY
DEPARTMENT OF BUILDING TECHNOLOGI AND STRUCTURAL ENGINEERING , AALBORG UNIVERSITY

SOHNGAARDSHOLMSVEJ 57, DK 9000 AALBORG , DENMARK

R 9808

MARCH 1998

# CONTENTS



ISSN 1395 - 7953 - R9808
Printed at Aalborg University

# Introduction

"Dynamics of Structures" was a research programme sponsored by the Danish Technical Research Council. The programme started in 1993 and continued until the end of 1997. It was a cooperative effort of the Department of Building Technology and Structural Engineering and the Department of Civil Engineering at Aalborg University and the Department of Structural Engineering at the Technical University of Denmark.

The purpose of the programme was to conduct research and provide research education and results relating to dynamic loads and response of civil engineering structures and foundations. Characterization and modelling of materials under time varying loads were also parts of the research programme. The research has developed and used both analytical, numerical and experimental methods.

The problem areas dealt with in the research programme were:

- Analysis of structures
- Wind and wave loads
- Soil mechanics
- System identification
- Damage detection
- Fatigue and crack propagation
- Man induced vibrations
- Experimental methods

A description of the research programme is given in "Final report for the research programme DYNAMICS OF STRUCTURES", Department of Civil Engineering and Department of Building Technology and Structural Engineering, Aalborg University, R 9807, March 1998.

In this report the following projects are described and the numbering refers to the above-mentioned report:

A.1: Mode shape and reduced base techniques
Paper: ***A generalized Lanczos - QR techniques for structural analysis***

A.2: Wind and wave loads on structures
Paper: ***Vortex-induced vibrations of structural elements***
Paper: ***Active vibration control of monopile offshore platforms***

A.3: Dynamic response of structures with stochastic properties and excitation
Paper: ***Response and damage assessment of reinforced concrete frames subject to earthquakes***
Paper: ***Influence of surface irregularities and vehicle uncertainties on the dynamic response of shortspan highway bridges***

B.1: Damage detection in structures under random loading
Paper: ***Identification of civil engineering structures using vector ARMA models***

B.2: Modal analysis based on the random decrement techniques
Paper: ***Modal analysis based on the random decrement technique - Application to civil engineering structures***

B.3: Fatigue and crack propagation
Paper: ***Fatigue and crack propagation***

C.1: Behaviour of soil subjected to dynamic loads
Paper: ***Behaviour of soil subjected to dynamic loads***

C.2: Dynamic response of coarse granular materials to wave loads
Paper: ***Dynamic response of coarse granular material to wave load (Steen Krenk)***
Paper: ***Advanced numerical analysis of caisson breakwater on Frictional materials***
Paper: ***Dynamic response of coarse granular material to wave load (Lars Bo Ibsen)***
Paper: ***Hydraulic response of caisson breakwaters in multidirectional breaking and non-breaking waves***

C.3: Dynamics of sports stadiums
Paper: ***Development of a model for determination of the dynamic load from spectator movement***

C.4: Dynamic measurements on the Frejlev mast
Paper: ***Dynamic measurements on the Frejlev Mast***

A complete publication list for all the publications written in the research programme is included in "Final report for the research programme DYNAMICS OF STRUCTURES", Department of Civil Engineering and Department of Building Technology and Structural Engineering, Aalborg University, R 9807, March 1998.

This report or the publication list can be ordered free of charge from:

Lars Pilegaard Hansen
Department of Building Technology and Structural Engineering
Aalborg University
Sohngaardsholmsvej 57
DK 9000 Aalborg
Denmark

Direct phone: +45 9635 8585
Direct fax: +45 9814 2366
Email: i6lph@civil.auc.dk

# A.1 MODE SHAPE AND REDUCED BASE TECHNIQUES

This project is described by the summary given in the Ph.D. thesis : "Steffen Vissing: A generalized Lanczos- QR techniques for structural analysis. ISSN 1395 - 7953. R9606, February 1996"

For more information, see also appendices H and I in the report "Final report for the research programme DYNAMICS OF STRUCTURES", Department of Building Technology and Structural Engineering, Aalborg University, R9807, March 1998.

The aim of this thesis *A Generalized Lanczos-QR Technique for Structural Analysis* has been the development of efficient algorithms for large matrix systems with positive and sparse matrices. The background is that matrix problems within the field of solid mechanics are often in a generalized form with two symmetric matrices which is banded or profiled due to a finite element or finite difference discretization. The engineering interest is therefore to develop a set of algorithms in which the special properties of the matrices are maintained.

The thesis consists of three main parts. The first part (chapter 1) presents the physical problem and a strategy for its solution. The second part (chapters 2-5) contains a description and development of four different algorithms and the third part (chapter 6) concerns the implementation of algorithms into a MATLAB toolbox for dynamic finite elements.

The types of problems are illustrated by an offshore structure modelled by finite elements. A dynamic analysis corresponding to an undamped vibration leads to a matrix system with two matrices describing the stiffness and mass of the structure. The matrices are symmetric with the same structure and sparsity. For this example the number of non-zero elements is approximately 1%. In the corresponding damped vibration a mass matrix with the same structure as the stiffness and mass matrices are introduced.

An eigenvalue analysis determines the eigenfrequencies and the corresponding vibration modes of the structure. Typically, a small fraction of the modes is important in the overall response of the structure. It is therefore advantageous to divide into a reduction and solution process. The reduction consists of a transformation into a smaller system including the lower modes. The solution step is an iterative process in which eigenvalues and eigenmodes are approximated via a sequence of elementary transformations.

The basic strategy for eigenvalue problems of this type of engineering problems

consists of

- similarity transformations
- inverse vector iteration

In the symmetric problem similarity transformations are made by a sequence of elementary transformations such as plane rotations, distortions or reflections either as part of an iterative solution step or as part of a finite reduction process in order to obtain an optimized format of the matrices.

The basis of inverse vector iterations is the solution of the eigenvalue problem in an iterative sequence. In a vector format the process converges towards the dominating eigenmode represented by the smallest eigenvalue. In practical problems a small fraction of the lower modes is required. There are in principle the following two ways of generalizing inverse vector iteration

- Subspace iteration
- Lanczos reduction

In subspace iterations a subspace of iteration vectors is used and by an orthogonalization procedure the subspace is forced to converge towards a subspace including only the lower modes. The alternative is the Lanczos type in which the iteration is formed with a single vector at the time, but without rejecting the information from the previous steps. The sequence is combined with an orthogonalization scheme ensuring orthogonality to the previous iteration vectors. In this way a subspace of orthogonal vectors is gradually formed. A special property of the Lanczos method is that the reduced problem is already in an optimized format with a tridiagonal matrix.

In the analysis of an undamped vibration the Lanczos reduction leads to a symmetric tridiagonal system on standard form, i.e. with a single matrix. The eigenvalues of the reduced problem, therefore, have a light coupling. In the solution step the matrices are transformed into diagonal form. This process is iterative. However, with a good implementation of a standard QR algorithm, the eigenvalues may be approximated by a limited number of operations. The QR iteration uses elementary transformation in a way that the symmetry is preserved during iteration.

In traditional methods this cannot be transferred into indefinite or quadratic problems such as stability problems and damped vibrations. The original symmetry is destroyed either by the reduction process into optimized format or by the iteration to evaluate the required eigenvalues. These problems are traditionally an order of magnitude more expensive to solve.

In this thesis a symmetry-preserving technique has been developed for symmetric generalized indefinite and quadratic eigenvalue problems. This may open up possibilities since it may require less computer power to handle e.g. the damped vibration.

The basis is the generalized indefinite eigenvalue problem which is reduced by a generalized Lanczos algorithm into a generalized form with a symmetric tridiagonal matrix and a diagonal matrix with $\pm 1$ elements instead of the identity matrix. The symmetric QR iteration is generalized to this type of problem in a way that the symmetry is maintained. This is obtained by a generalized form of orthogonality with respect to the diagonal $\pm 1$ matrix. The algorithms for Lanczos reduction and the generalized QR iteration is presented in the chapters 4 and 5.

The algorithms are implemented into MATLAB for which a toolbox FEMDYN for the dynamic finite element method is developed. FEMDYN contains approximately 50 functions in the form of element functions for global system matrices, algorithms for reduction methods, eigenvalue solutions and time step integrations for the forced vibrations. Chapter 6 contains a description in the form of three examples: a response analysis of a 10 storey building applied to the impact of a car, an eigenvalue analysis of an offshore structure and a stability analysis of a shallow truss dome. A FEMDYN manual is also presented in Appendix A and the functions are available as script files on a disc.

# A.2 WIND AND WAVE LOADS ON STRUCTURES

## VORTEX-INDUCED VIBRATIONS OF STRUCTURAL ELEMENTS

A double oscillator model for vortex-induced vibrations of structural elements based on exact power exchange between fluid and structure has been proposed. The model predicts two different modes of oscillation in the lock-in regime leading to hysteresis effects when the wind speed passes up and down through the lock-in interval. The effect of turbulence is to destabilize the mode with the highest amplification, thereby reducing the response amplitude, and for higher turbulence intensity to change the self-excited harmonic response to stochastic narrow-banded response with changing amplitude, closely resembling observed behaviour in experiments and full-scale structures. The basic mechanics of the model was presented in a paper,[1], submitted for journal publication whereas the influence of the turbulence on the stochastic response of the oscillator was presented at the ICOSSAR '97 conference, [2].

Expenses related to the project was covered partly by the frame program and partly by the EU programme on Human Capital and Mobility within stochastic mechanics.

Wind tunnel experiments have been carried out at the end of 1997 at Svend Ole Hansen Aps in an attempt to quantify the magnitude of the reduction and its dependence on the degree of turbulence.

A circular cylinder mounted on springs was tested in a wind tunnel. The vortex-induced vibrations and the pressure distribution around the central cylinder section were measured in low turbulent flow as well as in turbulent flows with different intensities and length scales. Two sets of springs giving two different fundamental frequencies and critical wind velocities were used in order to investigate the influence of turbulence in two different Reynolds number regimes. The response was measured for many structural damping ratios covering the range giving large as well as small amplitude movements of the circular cylinder.

The results will be used to support the basis for the new guidelines for vortex shedding included in the new Danish wind code expected to be published in June 1998. The report with measuring results obtained in the wind tunnel tests is under preparation and will be finalised late March 1998. The results obtained will be used as basis for a paper published internationally.

### References

[1] S. Krenk and S.R.K. Nielsen (1996).
An Energy Balanced Double Oscillator Model for Vortex-Induced Vibrations. Submitted to Journal of Engineering Mechanics, ASCE.

[2] S.R.K. Nielsen and S. Krenk (1997).
Stochastic Response of Energy Balanced Model for Vortex-Induced Vibrations. Proceedings of the 7th International Conference on Structural Safety and Reliability, ICOSSAR'97, Kyoto, November 24 - 28, 1997.

[3] S. Krenk (1997)
Wind load statistics and models. Symposium on Engineering Structures and Extreme Events, Risk Analysis and Simulation. Royal Institute of Technology, Stockholm, May 29 - 30, 1997.

# A.2 WIND AND WAWE LOADS ON STRUCTURES

## ACTIVE VIBRATION CONTROL OF MONOPILE OFFSHORE PLATFORMS

At the exploitation of marginal fields in the Jutlandian sector of the North Sea monopile platforms have proved beneficial. In the original concept the platform was designed to waterdepths of 35-50 m, and was assumed to be operated unmanned. Vibrations of the structure under these conditions are unimportant in all cases. However, in later applications the concept is under consideration for waterdepth up to 75 m, and the platforms are assumed to be manned. In this case significant dynamic amplification can arise in comparison to the quasi-statical response. The project, which is proposed together with Rambøll, Esbjerg, is aimed at developing an active vibration system for reduction of waveinduced oscillations.

The system is based on control of the boundary layer flow, and hence of the loading on the cylindre. The waveloading consists of a drag component and an inertial component. Only the drag component is under consideration. Normally, the drag coefficient is 0.6-0.9 for a circular cylinder. For a sharp edge body the drag coefficient can amount to 1.5-2.0. The cylinder will effectively acts as sharp edged body, if the boundary layer is forced to separate before the naturally separation points. The separation of the boundary layers will be insured by blowing air from inside the cylinder whenever appropriate.

The idea is to insure a large drag coefficient, when the velocity of structure is opposite to that of the fluid. In this case the boundary layers are blown away. When the velocity of the structure and the fluid are unidirectional no forced separation is impinged on the boundary layers. The velocity of the structure is measured by accellerometers on the platform, and the velocity of the boundary flow relative to the structure is measured by an ultrosonic velocity meter, attached to the structure. The advantage of the principle compared to other active vibration arrangements is that the power for vibration reduction is supplied primary from the fluid itself. Only the power for blowing the boundary layers off need to be supplied externally.

The versability of the principle has been demonstrated by a series of initial tests in January and February 1996, in stationary flow and regular waveloadings, which was reported in, [1]. During March 1998 the final tests with an optimized test setup were performed, showing a reduction of the vibration level of approximately 50%. The results will be reported in a journal paper in the near future, [2].

The project was staffed by S.K.N. Nielsen and P.H. Kirkegaard. The contribution of S.R.K. Nielsen was financed by Aalborg University, whereas P.H. Kirkegaard was financed by the research programme.

## References

[1] S.R.K. Nielsen, P.H. Kirkegaard and L. Thesbjerg (1996). Active Vibration Control of a Monopile Offshore Structure. Proceedings of the 2nd Workshop on Dynamic Loads Response of Structures and Soil Dynamics, November 13-14, 1996, Aalborg University, Denmark, pp. 90-101.

[2] S.R.K. Nielsen and P.H. Kirkegaard (1998). Active Vibration Control of a Monopile Offshore Structure. To be submitted to the Journal of Structural Control.

# A.3 DYNAMIC RESPONSE OF STRUCTURES WITH STOCHASTIC PROPERTIES AND EXCITATION

## RESPONSE AND DAMAGE ASSESSMENT OF REINFORCED CONCRETE FRAMES SUBJECT TO EARTHQUAKES

An algoritm for localization of damage in instrumented structures has been developed and verified by model testing on a scale 1:5 reinforced concrete frame. In Turkey and other middle east countries it is a custom only to build the lower part of a building at first and then leave the upper storeys until later, when the need and the available money turns up. This creates a weakening in the mid of the structure, which turns out to accumulate damage. The same effect of accumulation of damage in the midst of structures was observed in the 1996 Kobe earthquake, where the effect was caused by a discontinous change of the strength and stiffness of the outer columns of the building. The applicability of the devised algoritms in predicting such damage accumulations in the midst of a structure was also demonstrated by laboratory tests.

The project was staffed by Poul S. Skjærbæk, P.H. Kirkegaard, S.R.K. Nielsen from Aalborg University, B. Taşkin from the Technical University of Istanbul, Turkey and A.Ş.Çakmak from the Princeton University, USA. Poul S. Skjærbæk's participation in the project was financed by Aalborg University through a Ph.D. grant. The participation of P.H. Kirkegaard (January 1-June 30, 1997) and B.Taşkin (February 1-February 28, 1997) were financed by the frame programme. S.R.K. Nielsen and A.Ş.Çakmak were financed by their respective universities.

Totally 14 publications were written during the project. Of these have 3 papers been published in international journals, [1-3], one in a Nordic journal, [4], and one has been submitted for publication in an international journal, [5]. 5 papers have been presented at international conferences, [6-10], 1 paper was presented at a national conference, [11], and 3 laboratory reports with measurement data were published as internal department reports, [12-14].

### References

[1] P.S. Skjærbæk, S.R.K. Nielsen and A.Ş.Çakmak (1996). Identification of Damage in Reinforced Concrete Structures from Earthquake Records Optimal Location of Sensors. Soil Dynamics and Earthquake Engineering, 15, No. 6, pp. 347-358.

[2] P.S. Skjærbæk, B.Taşkin, S.R.K. Nielsen and P.H. Kirkegaard (1997). An Experimental Study of a Midbroken 2-Bay, 6-Storey Reinforced Concrete Frame subject to Earthquake. Accepted for publication in Soil Dynamics and Earthquake Engineering.

[3] P.S. Skjærbæk, S.R.K. Nielsen, P.H. Kirkegaard and A.Ş.Çakmak (1997). Damage Localization and Quantification of Earthquake Excited RC-Frame. An Experimental

Study of a Midbroken 2-Bay, 6-Storey Reinforced. Accepted for publication in Earthquake Engineering Structural Dynamics.

[4] P.S. Skjærbæk, S.R.K. Nielsen and P.H. Kirkegaard (1997). Earthquake Tests of Reinforced Concrete Frames. Accepted for publication in Nordic Concrete Research, Publication No. 20, 1-2, 1997,pp 94 -107.

[5] P.S. Skjærbæk, S.R.K. Nielsen, P.H. Kirkegaard and A.Ş.Çakmak (1997). Experimental Study of Damage Indicators for a 2-Bay, 6-Storey RC-Frame. Submitted for publication in Journal of Structural Engineering, ASCE.

[6] P.S. Skjærbæk, S.R.K. Nielsen and A.Ş.Çakmak (1996). Assessment of Damage in Seismically Excited RC-Structures from a Single Measured Response. Proceedings of the 14th International Modal Analysis Conference , Dearborn, Michigan, USA, February 12-15, 1996, pp. 133-139.

[7] P.S. Skjærbæk, S.R.K. Nielsen and A.Ş.Çakmak (1996).Damage Localization of Severely Damaged RC-Structures based on Measured Eigenperiods from a Single Response. Proceedings of the 4th International Conference on Computer-Aided Damage Assessment and Control. Localized Damage'96, Fukuoka, Japan, June 1996, pp. 815-822.

[8] P.S. Skjærbæk, S.R.K. Nielsen and P.H. Kirkegaard (1997). Case Study of Damage Indicators for a 2-Bay, 6-Storey RC-Frame subject to Earthquake. Proceedings of IMAC XV, Orlando, USA, February 3-6, 1997, pp. 1181-1187.

[9] P.S. Skjærbæk, P.H. Kirkegaard and S.R.K. Nielsen (1997). Modal Identification of a Time-Invariant 6-Storey Model Test RC-Frame from Free Decay Tests using Multivariate Models. Proceedings of IMAC XV, Orlando, USA, February 3-6, 1997, pp. 510-516.

[10] P.S. Skjærbæk, P.H. Kirkegaard and S.R.K. Nielsen (1997). Shaking Table Tests of Reinforced Concrete Frames. Proceedings of DAMAS'97, International Workshop on Structural Damage Assessment using Advanced Signal Processing Procedures, University of Sheffield, UK, June 30 - July 2, 1997, pp. 441 - 450.

[11] P.S. Skjærbæk, P.H. Kirkegaard and S.R.K. Nielsen (1996). Earthquake Tests of Reinforced Concrete Frames. Proceedings of the 2nd Workshop on Dynamic Loads Response of Structures and Soil Dynamics, November 13-14, 1996, Aalborg University, Denmark, pp. 112-124.

[12] P.H. Kirkegaard, P.S. Skjærbæk and S.R.K. Nielsen (1997). Identification Report: Earthquake Tests on 2-Bay, 6-Storey RC-Frames. Laboratory Report, Aalborg University. Fracture and Dynamics, Paper No. 85, ISSN 1395-7953 R9703.

[13] P.S. Skjærbæk, S.R.K. Nielsen and P.H. Kirkegaard (1997).Laboratory Report: Earthquake Tests on Scale 1:5 RC-Frames. Aalborg University. Fracture and Dynamics,

Paper No. 86, ISSN 1395-7953 R9713.

[14] P.S. Skjærbæk, S.R.K. Nielsen, P.H. Kirkegaard and B.Taşkin (1997). Earthquake Tests on Midbroken Scale 1:5 Reinforced Concrete Frame. Laboratory Report, Aalborg University. Fracture and Dynamics, Paper No. 99, ISSN 1395-7953 R9712.

# A.3 DYNAMIC RESPONSE OF STRUCTURES WITH STOCHASTIC PROPERTIES AND EXCITATION

## INFLUENCE OF SURFACE IRREGULARITIES AND VEHICLE UNCERTAINTIES ON THE DYNAMIC RESPONSE OF SHORTSPAN HIGHWAY BRIDGES

A common problem in bridge engineering practice in these years is the upgrading of minor highway bridges (span=5-20 m) to carry heavier loads partly due to a tendency of heavier trucks moving at larger speeds, and partly because the authorities want to permit transportation of heavier goods at a larger part of the road net. These needs will in many cases cause that strengthening of the bridge becomes necessary. In order to keep the cost of such strengthening projects at a minimum it is necessary to obtain accurate estimates of the dynamic amplification factor (defined as the dynamic load effect divided by the static load effect from the vehicle). For the minor highway bridges the critical design scenario occurs at the simultaneous passage of two heavy trucks, which according to the present Danish regulations are taken as a 50t and a heavier 100-150 t vehicle. For both these vehicles the dynamic amplification factor is taken as 1.25, which is generally considered too conservative among bridge engineers. The dynamic amplification factor depends on many factors, such as the dynamic properties of the bridge and the vehicle suspension system, the speed of the vehicles, surface irregularities and bumps due to attritioned surface dressings and expansion joints. Many of these parameters are uncertain and should be modelled as random variables.

In the project some investigations on the probability distribution of the dynamic amplification factor is presented, based on Monte Carlo simulation studies. Numerical 3D-models have been formulated for the vehicles with parameters calibrated to a 50t Scania and a 100t Goldhofer truck. A characteristic highway bridge has been selected, and a numerical FEM-model has been formulated with due consideration to the dominating quasi-static response of minor highway bridges.

First the velocities and the parameters describing the vehicles are assumed to be deterministic at characteristic values and the influence of the surface irregularities are investigated. Based on measured data, a 2D stochastic model has been formulated for the surface roughnesses. A stochastic is also formulated for the bumps at the expansion joints. Based on the Monte Carlo studues the mean values and variational coefficients of several dynamic amplification factors have been calculated.

Overtaking scenarios, where the trucks cross the crests and troughs of the whell tracking, have been considered as well. The overall conclusion from this part of the investigation is that the most important impact on magnitude of the dynamic amplification factor stems from short waved bumps, whereas the attrition of the surface dressing is less important.

Next, the influence of the uncertainty of the parameters of the suspension system and the vehicle velocities has been investigated. The conclusion drawn from these studies is that the especially the spring stiffness of the suspension systems may influence the mean value and variational coefficients of the dynamic amplification factors significantly. However, with modern softer springs the amplification factors are significantly smaller than the design value of 1.25 prescribed in the Danish regulations. This conclusion even holds, when the uncertainty of the vehicle dynamics is combined with surface irregularities and other sources of uncertainty.

The results of the project have been met with interest among bridge engineers, and have initiated discussion on the reduction of the safety factors for reinforcement projects.

The project was staffed by P.H. Kirkegaard, S.R.K. Nielsen from Aalborg University and I. Enevoldsen, Rambøll A/S, Virum. The participation of I. Enevoldsen was financed by a special grant of 108.000,00 DKK from The Danish Research Council (grant No. 9502738). The participations of P.H. Kirkegaard (January 1-June 30, 1997) and S.R.K. Nielsen were financed by the research programme and by the Aalborg University, respectively.

Totally 7 publications were written during the project. Initially 4 internal department reports were carried out presenting an extensive literature survey on the subject ,and details of the applied mathematical modelling, [1-4]. At present (March 1998) 1 contribution to international conferences for bridge engineers, [5], and and two contributions to an international conference on stochastic dynamics, [6-7], are under preparation.

## References

[1] P.H. Kirkegaard, S.R.K. Nielsen and I. Enevoldsen (1997). Heavy Vehicles on Minor Highway Bridges - A Literature Review. Structural Reliability Theory, Paper No. 169. ISSN 1395-7953 R9719, Aalborg University.

[2] S.R.K. Nielsen, P.H. Kirkegaard and I. Enevoldsen (1997). Heavy Vehicles on Minor Highway Bridges - Stochastic Modelling of Surface Irregularities. Structural Reliability Theory, Paper No. 170. ISSN 1395-7953 R9720, Aalborg University.

[3] P.H. Kirkegaard, S.R.K. Nielsen and I. Enevoldsen (1997). Heavy Vehicles on Minor Highway Bridges - Dynamic Modelling of Vehicles and Bridges. Structural Reliability Theory, Paper No. 171. ISSN 1395-7953 R9721, Aalborg University.

[4] P.H. Kirkegaard, S.R.K. Nielsen and I. Enevoldsen (1997). Heavy Vehicles on Minor Highway Bridges - Calculation of Dynamic Impact Factors from Selected Crossing Scenarios. Structural Reliability Theory, Paper No. 172. ISSN 1395-7953 R9722, Aalborg University.

[5] P.H. Kirkegaard, S.R.K. Nielsen and I. Enevoldsen (1998). Dynamic Vehicle Impact for Safety Assessment of Bridges. Structural Reliability Theory, Paper No. 173, Aalborg University. To be presented at the 2nd Conference on VIM of Road Vehicles, Lisbon,

September 1998.

[6] R.K. Nielsen and P.H. Kirkegaard (1998). Influence of Surface Irregularities on the Dynamic Response of Minor Highway Bridges. To be presented at the 4th International Conference on Stochastic Structural Dynamics, University of Notre Dame, USA, August 6-8, 1998.

[7] P.H. Kirkegaard and S.R.K. Nielsen (1998). Influence of Uncertainty of Vehicle Dynamics on the Dynamic Response of Minor Highway Bridges. To be presented at the 4th International Conference on Stochastic Structural Dynamics, University of Notre Dame, USA, August 6-8, 1998.

# B.1

# Identification of Civil Engineering Structures using Vector ARMA Models

Palle Andersen, Rune Brincker & Poul Henning Kirkegaard

*Aalborg University*
*Department of Building Technology and Structural Engineering*
*Sohngaardsholmsvej 57,*
*DK-9000 Aalborg, Denmark*

SYNOPSIS: This paper describes the work which have been carried out in the project B.1: *Damage Detection in Structures under Random Loading*. The project is a part of the research programme *Dynamics of Structures* founded by the *Danish Technical Research Council*. The planned contents of and the requirements to the project prior to its start is described together with the results obtained during the project. The project was mainly carried out as a Ph.D. project by the first author from September 1993 to May 1997 under supervision of Professor Rune Brincker and Associate Professor Poul Henning Kirkegaard both from department of Building Technology and Structural Engineering, Aalborg University.

## 1. INTRODUCTION

In the mid eighties, researchers at the Department of Building Technology and Structural Engineering at Aalborg University, Denmark, started using time domain models for system identification of civil engineering structures. A common feature of the work has been the use of the so-called auto-regressive moving average (ARMA) models for time series modelling. The reason is the ability of these models to provide an accurate estimate of the modal parameters of a structural system on the basis of discretely sampled response. This ability makes them suitable as tool for vibration based inspection, i.e. damage detection. In the past decade the results of this work have been reported in several papers and in three Ph.D. theses. However, the link between the ARMA model and the mathematical description of civil engineering structures has not been addressed to the same extent as mathematical description of dynamic systems in fields such as electrical engineering and econometrics. Therefore, the model has been applied toas a greybox model in the above references. The relation between the auto-regressive part of the model and the modal parameters has been well understood, whereas the understanding of the moving average part has been limited.

In order to obtain a deeper understanding of the ARMA models, and how they are related to the modelling of civil engineering structures and damage detection, the project B.1: *Damage Detection in Structures under Random Loading*, with this as its primary objective, was granted as a part of the Danish Research Council frame programme "Dynamics of Structures". Another objective of the Ph.D. project was to implement the obtained knowledge as, especially designed, time domain software for system identification of civil engineering structures. The results have been reported in several papers and the Ph.D. thesis: *System Identification of Civil Engineering Structures using Vector ARMA Models*. In section 9, a list of references to papers and reports prepared during the project is presented.
This list together with the possibility to download some of these and the thesis can be seen at *http://www.civil.auc.dk/~i6pa*. A short description of the Ph.D. thesis can be seen at *http://www.civil.auc.dk/~i6pa/thesis.htm*.

# 2. PLAN FOR THE PROJECT

The following topics relating to system identification of ambient excited civil engineering structures were planned to be investigated.

1. Relation between system identification using ARMA models and vibration based inspection.
2. ARMA modelling of ambient excited civil engineering structures.
3. Estimation of ARMA models from measured system response.
4. Extraction of modal parameters and estimation of their uncertainties.
5. Software development for system identification using ARMA models.

In section 3, the relation between mathematical modelling and system identification is described. Also described are the relations between non-parametric and parametric system identification, and why it is desirable to apply the ARMA models in relation to vibration based inspection of ambient excited civil engineering structures. Finally, the scope of the work of the Ph.D. project is stated. Section 4 explains how the ambient excited civil engineering structure can be modelled in discrete-time by the ARMA model. In section 5, it is explained how the ARMA model can be estimated from measured system response. The extraction of the modal parameters and the estimation of their uncertainties are the topics of section 6. Section 7 briefly describes the software package developed during the project. Finally, in section 8 conclusions are made.

# 3. SYSTEM IDENTIFICATION OF CIVIL ENGINEERING STRUCTURES USING ARMAV MODELS

In this section the basic concepts of system identification are introduced. Also introduced, are the applications of system identification in civil engineering that are of interest to project B.1.

## 3.1 *System Identification*

A convenient way of describing a dynamic system is by use of mathematical models. These models can either be represented in continuous time as differential equation systems or in discrete-time as difference equation systems. There are in general two ways to construct mathematical models:

- ☞ *Physical modelling.*
- ☞ *System identification.*

In physical modelling the construction of a dynamic model is based on physical knowledge and fundamental laws, such as the Newton 2. law of motion. On the other hand, if the physical knowledge about a dynamic system is limited a model of the input / output behaviour of the system can be obtained through system identification based on calibration of a model using experimental data. If the structure of the calibrated model is chosen without regard to physical knowledge the calibrated model is called a black box model. If some parts of the model are based on physical knowledge the calibrated model is called a grey box model. On the other hand, if the calibrated model is based completely on the physical laws, i.e. if it originates from a physical modelling, then the calibrated model is called a white box model. Thus, system identification should not be thought of as a substitute of physical modelling, since identification can be based on model structures that have physical origin. Basically there are two categories of model structures :

- *Non-parametric model structures.*
- *Parametric model structures.*

In any case, physical modelling will always be linked with parametric model structures. Common to both categories of model structures is that they depend on the applied excitation, which may be one of the following

- *Instantaneous excitation.*
- *Periodic excitation.*
- *Pseudo-random periodic excitation.*
- *Stochastic excitation.*

In the case of instantaneous excitation, the system is either given an impulse or step excitation and the system is the left vibrating on its own. The excitation may or may not be measured. It is also possible to excite the system with a known periodic excitation, such as sinusoidal, or several periodic signals mixed to obtain a pseudo-random periodic excitation. Finally, as an alternative to the deterministic excitation, the excitation might also be a stationary stochastic process with either known or unknown statistical properties. In any case, the dynamic behaviour can be conceptually described as in figure 1.

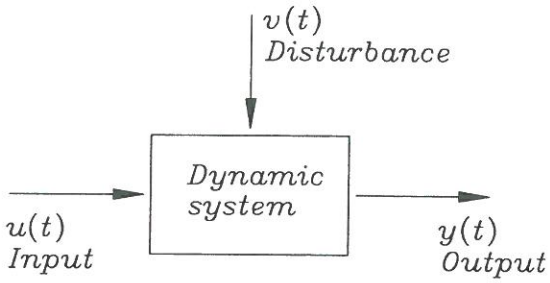


Figure 1: A dynamic system with input $u(t)$, output $y(t)$ and disturbance $v(t)$.

The system is driven by input $u(t)$ and affected by disturbance $v(t)$. In some cases the user can control the input $u(t)$ but not the disturbance $v(t)$. It might also be that the actual input is unknown and therefore uncontrollable in some applications. The output $y(t)$ describes how the system reacts or responds to the applied input and disturbance. Therefore, the output will be a mixture of dynamic response of the system and characteristics of the input and disturbance as well. In general, the input at previous time instances will also affect the current output. In other words, the dynamic system has memory.

### 3.1.1 *Non-Parametric Model Structures*

The non-parametric models are described by curves, functional relationships or tables. These analysis methods are :

- *Transient analysis.*
- *Frequency analysis.*
- *Correlation analysis.*
- *Spectral analysis.*

Transient analysis is applied when the system response is transient, i.e. generated on the basis of impulse or step excitation. The dynamic behaviour of the system is then identified on the basis of the

impulse or step response. Frequency analysis is applied when the excitation is deterministic and either periodic, or pseudo-random and periodic. The measured excitation and the corresponding system response are transformed to frequency domain, and the frequency response function is obtained as the ratio of the transformed response and excitation. Correlation and spectral analysis are methods that are applied to a stationary stochastically excited system. In these cases, the excitation and the system response can be characterized either by the correlation functions in time domain or the spectral densities in frequency domain. Having estimated the correlation functions of the excitation and the response the impulse response function of the system can be obtained. On the other hand, if the spectral densities of the excitation and response are estimated instead, it is possible to obtain the frequency response function.

The traditional non-parametric system identification techniques are primarily based on the Fast Fourier Transform (FFT) techniques. However, the FFT has some limitations. The most obvious limitation is that the FFT assumes periodic data, which is certainly not the case for sampled response from stochastically excited structures. In principle, the Fourier transform assumes that the amount of data is infinite. In this case the frequency response functions or the spectral densities will have an infinite frequency resolution. However, in practice the available data records have a finite length, resulting in a finite frequency resolution. Since sampled stochastic signals in general exhibit non-periodicity, leakage errors will certainly be introduced. Further, in the case of closely spaced modes, it might be impossible to separate these if one of the resonance frequencies has a small amplitude compared to the other. In this case the resonance frequency with the smallest energy content may be masked completely by the resonance frequency with highest energy content. The leakage errors are compensated by windowing the data before the FFT is applied, to secure periodicity of the data by damping the discontinuities at the ends of the data record. The problem of windowing is, that it introduces an extra damping into the system, and thus creates its own leakage problem.

### 3.1.2 *Parametric Model Structures*

Parametric models are characterized by the assumption of a mathematical model constructed from a set of parameters. These parameters are then estimated during the system identification. The mathematical model of a linear and time-invariant continuous-time system is usually in the form of a differential equation system. The equivalent discrete-time parametric model is a difference equation system. In figure 1 an input / output system affected by noise was shown. The appearance of the discrete-time parametric model that describes such a system depends on whether the input is measured or not. If the input is measured, then the associated parametric model will have a deterministic term as well as a stochastic term that describes the unknown disturbance. If the actual input is unknown, it is treated stochastically. In this case the description of input and disturbance will be described by a single stochastic term.

*Model Structures using Deterministic Input*

The general input / output model structure used for modelling of linear and time-invariant dynamic systems excited by deterministic input, is Auto-Regressive Moving Average with eXternal input (ARMAX)

$$\boldsymbol{y}(t) = \boldsymbol{G}(q)\boldsymbol{u}(t) + \boldsymbol{H}(q)\boldsymbol{e}(t) \qquad (1)$$

where $\boldsymbol{G}(q)$ and $\boldsymbol{H}(q)$ are the transfer functions of the deterministic part and the stochastic part. The

stochastic input $\boldsymbol{e}(t)$ are the innovations, which are an equivalent process of the noise and prediction errors. If $\boldsymbol{H}(q) = \boldsymbol{I}$ (1) is called an output error (OE) model. In any case the dynamic properties of the system are modelled by $\boldsymbol{G}(q)$. A parametric model structure is called multivariable when it includes several variables. If there are several outputs, it is characterized as a multivariate model structure. If it only has one output, it is termed a univariate model structure.

*Model Structures using Stochastic Input*

If the input is an unmeasurable stationary stochastic process, the ARMAX model is no longer the correct model structure to use. In this case an Auto-Regressive Moving Average (ARMA) model should be applied

$$\boldsymbol{y}(t) = \boldsymbol{H}(q)\boldsymbol{e}(t) \tag{2}$$

The dynamical properties as well as the noise are now modelled by the same transfer function $\boldsymbol{H}(q)$. In the multivariate case the model structure is called an Auto-Regressive Moving Average Vector (ARMAV) model. As observed the choice of model structure depends on whether the input is deterministic or stochastic, i.e. whether the excitation of the structural system is known and measured or unknown. It also depends on whether the system is stationarily excited, or excited by an impulse or step excitation.

## 3.2 *Applications of System Identification of Civil Engineering Structures*

In the field of civil engineering, system identification might be applied for several reasons. However, the following two areas have attracted much attention in the recent years

- *Modal analysis.*
- *Vibration based inspection.*

Modal analysis covers a variety of applications all based on the analysis of modal parameters. These parameters describe specific dynamic characteristics of the structure. One of the applications that uses the modal parameters as basis is vibration based inspection.

### 3.2.1 *Modal Analysis*

Modal analysis is based on the determination of modal parameters of a structural system. These parameters represent an optimal model, or basis, which can be used to describe the dynamics of a structural system. The modal parameters can be divided into the following four categories:

- *Modal frequencies.*
- *Modal damping.*
- *Modal vectors.*
- *Modal scaling.*

The modal frequencies are more explicitly eigenvalues, or angular or natural eigenfrequencies. Modal damping is characterized by the damping ratios, and modal vectors by the eigenvectors or mode shapes. Finally, modal masses and residues are typical parameters used to characterize modal scaling. Since the modal parameters are directly related to the impulse and frequency response functions, as well as the

correlation functions and spectral densities, they can be extracted from the non-parametric system identification methods by applying different curve fitting procedures. In case of parametric system identification methods there are direct mathematical relationships between the modal parameters and the estimated model parameters.

### 3.2.2 *Vibration Based Inspection*

The accumulation of damages in a civil engineering structure will cause a change in the dynamic characteristics of the structure. The basic idea in Vibration Based Inspection (VBI) is to measure these dynamic characteristics during the lifetime of the structure and use them as a basis for identification of structural damages. Typically, a VBI programme uses the modal parameters to describe the dynamic characteristics of a structure. A synonym for the dynamic characteristics used as basis for the VBI programme is damage indicators. In other words:

☞ *A damage indicator is a dynamic quantity, which can be used to identify the existence of damage in a structure.*

Often VBI has at random been referred to as damage detection. VBI can be divided into the following four levels:

☞ *Level 1 - Detection.*
☞ *Level 2 - Localization.*
☞ *Level 3 - Assessment.*
☞ *Level 4 - Consequence.*

Methods of the first level give a qualitative indication that a structure might be damaged. Level two methods give information about the probable location of the damage as well. Methods of the third level provide information about the size of the damage, and finally the level four methods give information about the actual safety of the structure given a certain damage state. The use of a damage indicator primarily gives a qualitative indication of the existence of damage, and should therefore be characterized as a level 1 method. However, some of the damage indicators will in some cases give rough estimates for the locations of damage, which is equivalent to a primitive level 2 method. Changes in natural eigenfrequencies are no doubt the most used damage indicators. One of the reasons for this is that the natural eigenfrequencies are rather easy to determine with a high level of accuracy. Another reason is that they are sensitive to both global and local damages. So comparison of estimates of natural eigenfrequencies is usually an effective level 1 method. A local damage will cause changes in the derivatives of the mode shapes at the position of the damage. This means that a mode shape having many coordinates or measurement points will be a fast way to locate the approximate position of a damage. They can therefore be characterized as a simple level 2 method. The introduction of damage in a structure will usually cause changes in the damping capacity of the structure. It has been shown that the damping ratios are extremely sensitive to the introduction of even small cracks in a cantilever beam. However, dealing with real structures, the estimation of the damping ratios of the individual modes is highly sensitive to time-varying and non-physical sources. Thus, a satisfactory accuracy of the estimates of the damping ratios will in general be impossible to obtain. Therefore, the damping is applicable as a damage indicator, but it cannot and should not be used as the only damage indicator.

As explained, all modal parameters are in principle applicable as damage indicators. This means that they can be used at least for detection of damage, and as such be characterized as level 1 methods. However, the key to a successful VBI is the use of unbiased and low-variance modal parameter

estimates as damage indicators. If the estimates are biased they might cause a false alarm, i.e. indicate a damage that does not exist. If the estimation inaccuracies are too dominant, it might be impossible to detect any significant changes. Thus, the existence of a damage might be hidden.

So in conclusion :

☞ *Successful VBI based on modal parameters requires accurate and unbiased modal parameter estimates.*

In this context the computational effort spent in obtaining reliable estimates is not so important. Further, the limitations and systematic errors of the traditional FFT-based non-parametric system identification techniques motivates the use of other techniques.

This motivation can be stated as:

☞ *The need for a more accurate estimation of the modal parameters from sampled data, compared to what traditional FFT-based non-parametric techniques can provide.*

This need is basically the reason for using the parametric models in the system identification, since the physical knowledge about a dynamic system in this way is incorporated into the system identification process.

### 3.2.3 *Excitation of Civil Engineering Structures*

In the case of civil engineering structures there will most likely be a natural excitation of the structure such as wind or waves. These natural forms of excitation are commonly called ambient excitation and the vibrations of the structure caused by them are called ambient vibrations. System identification of structural dynamics on the basis of ambient excitation is also referred to as ambient testing. From an experimental point of view, the simplest approach to measure the dynamic parameters of a structure is to detect the response due to ambient excitation. In the case of very large structures this approach is the only practical way of performing dynamic tests, it is simply impossible to excite such structures artificially.

The ambient excitation is stochastic in nature. Therefore, it cannot be described by an explicit time-dependent function, but must be characterized by certain statistical parameters, such as its mean and covariance function. Since the structural system can be seen as a linear transformation of the applied input, this means that the response will also be stochastic, and may as such also be represented by its statistical characteristics. Several researches have shown that ambient excitation provides a quick, inexpensive and reliable way for testing of large civil engineering structures, such as buildings and offshore structures. It has been concluded that parameter estimates obtained by ambient excitation are as good as parameter estimates obtained by external excitation. This conclusion is based on a study of several published results of ambient versus forced vibration tests of high-rise structures in the USA. Because of the nature of dynamic testing under ambient excitation conditions this method has advantages over others, such as the impulse and periodic excitation. Ambient excitation has a broad frequency range, and thus theoretically excites all relevant modes of a structure. Also, the use of ambient excitation in dynamic testing does not disturb the normal functioning of a structure and no excitation equipment is required for ambient testing. However, the disadvantage of ambient excitation is that its characteristics cannot be controlled and measured directly.

Since ambient excitation cannot be measured directly, it can be constructed from other measurements such as the surface elevation if system identification of an offshore structure is considered. From these measurements, sea state characteristics such as significant wave height and average zero-upcrossing period, can be estimated. These characteristics can then be used as input to models, which have been developed to describe the waves either as time series or spectral densities. The connection between the theoretical description of the waves and the forces on the structure is established using a load model, which could e.g. be the Morrison equation. In the case where the ambient excitation is generated by fluctuating wind pressure forces, numerous measurement projects have shown that the fluctuations may be described by a stationary ergodic Gaussian stochastic process with regard to short-term conditions.

## 3.3 *Scope of the Ph.D. Thesis*

From the above the following can be stated concerning system identification of civil engineering structures :

- ☞ *The dynamic behaviour of a civil engineering structure is usually modelled by a linear and time-invariant model.*
- ☞ *The excitation of civil engineering structures is typically unknown ambient excitation.*
- ☞ *If this unknown ambient excitation is e.g. the wind, it is often modelled as a stationary Gaussian stochastic process.*
- ☞ *For applications such as VBI a high degree of estimation accuracy of the modal parameters is required.*
- ☞ *Adequate parametric model structures are not limited by frequency resolution, and can as such be more accurate than FFT-based non-parametric model structures.*

These statements imply that the parametric models are applicable to system identification of civil engineering structures when a high degree of accuracy is needed. Therefore, the main aim of this thesis has been to investigate how to represent ambient excited civil engineering structural systems by stochastic time-domain models, and how to estimate these on the basis of sampled structural response data. Since measurements of the true ambient excitation are not available, system identification using standard multivariate input / output ARMAX model cannot be applied. Therefore, the focus has been put on the use of stochastic models of the Auto-Regressive Moving Average Vector (ARMAV) type. Particular emphasis has been be put on computationally accurate system identification methods, since the intention is to provide a more accurate alternative to the traditional non-parametric system identification methods typically applied in the field of civil engineering. A secondary purpose of the thesis has been to make the theory of system identification using stochastic time domain models more accessible to civil engineers. Since system identification is a relatively new field for civil engineers, it has been natural to search for applicable theory and methods within disciplines that are at the research front, such as automatic control engineering, mathematical system theory, econometrics, and aerospace engineering. It is shown how an ARMAV model equivalent to the continuous-time mathematical model of a stochastically excited structural system arises. In this context, an explanation of the purpose of the moving average is emphasized. It has also been shown how to account for the presence of disturbance, and how ARMAV models are directly related to the so-called stochastic state space systems. Since modal analysis is one of the main reasons for system identification of civil engineering structures, a thorough treatment of the modal decomposition and extraction of modal parameters has been given together with guidelines for estimation of the uncertainties of the estimated modal parameters will be given. During the Ph.D. project emphasis has been put on the practical implementation of user-friendly system identification software.

# 4. CONTINUOUS-TIME STRUCTURAL SYSTEMS

Structures can be regarded as distributed parameter systems characterized by the distribution of the mass, damping and stiffness properties. However, parameter identification of such systems is in general not easy. Thus, with a few exceptions, in most of the literature on testing of structures, the data are analysed based on the assumption that the system is described by one or more linear ordinary differential equations. Because of their simplicity the linear time-invariant lumped parameter models are the most widely used models in structural identification. More complex models such as the linear continuous parameter models and non-linear models are used only when the lumped parameter model cannot be used to provide an adequate representation of the structural behaviour. In general, system identification concerns the determination of modal parameters. If the excitation of a structure e.g. is the wind, then the only available information about the dynamic behaviour of a structure is the measured vibrations of it. As will be shown later, system identification using ARMAV models is in these situations capable of providing good estimates of the modal parameters of the structure. However, it is necessary to obtain some kind of understanding of how the discrete-time ARMAV model relates to the modal parameters, i.e. how it relates to the continuous-time lumped parameter model. It is the purpose of this section to provide this understanding. This chapter is restricted to the continuous-time modelling of civil engineering structures.

## 4.1 *ARMAV Modelling of Ambient Excited Structural Systems*

Experience has led to the following mathematical mass-spring-dashpot lumped parameter model for a structure subjected to external loading

$$\boldsymbol{M}\ddot{\boldsymbol{y}}(t) + \boldsymbol{C}\dot{\boldsymbol{y}}(t) + \boldsymbol{K}\boldsymbol{y}(t) = \boldsymbol{f}(t) \tag{3}$$

$\boldsymbol{M}$, $\boldsymbol{C}$ and $\boldsymbol{K}$ are the mass, damping and stiffness matrices all of dimensions $p \times p$. $\boldsymbol{y}(t)$ and $\boldsymbol{f}(t)$ are the $p \times 1$ displacement and $p \times 1$ force vectors at the mass points, respectively. From a system identification point of view a generalization of the mathematical model is necessary, since the number of measurement channels is usually less than the number of identified modes. A generalized multivariate model can be formulated as, Andersen [1]

$$D^s\boldsymbol{y}(t) + \boldsymbol{A}_{y,s-1}D^{s-1}\boldsymbol{y}(t) + \ldots + \boldsymbol{A}_{y,0}\boldsymbol{y}(t) = \boldsymbol{B}_{f,s-2}D^{s-2}\boldsymbol{f}(t) + \ldots + \boldsymbol{B}_{f,0}\boldsymbol{f}(t) \tag{4}$$

where $D$ is a differential operator. The matrices $\boldsymbol{A}_{y,i}$ and $\boldsymbol{B}_{f,i}$ are all of the dimension $p \times p$. The displacement vector $\boldsymbol{y}(t)$ and its derivatives are all of the dimension $p \times 1$. The $p \times 1$ vector $\boldsymbol{f}(t)$ describes the forces applied to the system. The modes of a structural system will typically be underdamped, which implies that each mode is described by a pair of complex conjugated eigenvalues. In this situation the order $s$ will be defined as $s = \frac{2N}{}$ with $N$ being the number of underdamped modes. It is often assumed that the ambient excitation $\boldsymbol{f}(t)$ is given as the output of a linear time-invariant shaping filter subjected to Gaussian white noise. Due to the Gaussian assumption, it is implicitly assumed that the true ambient excitation is at least weakly stationary. If the ambient excitation can be described by filtered white noise, it is possible to derive a model for it. Assume that the excitation $\boldsymbol{f}(t)$ of the structural system is obtained as the output of an $m$th-order $p$-variate linear time-invariant continuous-time shaping filter

$$D^m f(t) + A_{f,m-1} D^{m-1} f(t) + \ \ldots \ + A_{f,0} f(t) = w(t) \tag{5}$$

For simplicity, it is assumed that $f(t)$ and $w(t)$ have the same dimensions as $z(t)$. This implies that the matrices $A_{f,i}$ all have the dimension $p \times p$. The stochastic process $w(t)$ is a zero-mean Gaussian white noise, fully described by its covariance function. This covariance function is defined in terms of the $p \times p$ intensity matrix $W$ as

$$E[w(t)] = \mathbf{0}, \quad E[w(t) w^T(t-\tau)] = \delta(\tau) W \tag{6}$$

where $\delta(\tau)$ is the Dirac delta function. These statistical properties are abbreviated $NID(\mathbf{0},W)$. It is obvious that the response $y(t)$ of the system will contain a mixture of the dynamic behaviour of the structural system and of the excitation. It is also intuitively clear that during a system identification the dynamic modes of the shaping filter will also be estimated. These modes are, together with any noise modes, called non-physical modes. In this way they can be distinguished from the physical modes of the structural system. The structural system can then be combined with the shaping filter of the excitation by means of convolution into a resulting linear system subjected to a Gaussian white noise. The resulting differential equation system will be of the order $n = s+m$. Such a differential equation system can be represented by the following state space system, Andersen [1]

$$\begin{aligned} \dot{x}(t) &= Fx(t) + Bw(t) \ , \quad w(t) \in NID(\mathbf{0},W) \\ y(t) &= Cx(t) \end{aligned} \tag{7}$$

where $F$ is the $np \times np$ state matrix, $B$ is the $np \times p$ input matrix, and $C$ the $p \times np$ observation matrix. Define a discrete time instance as $t_k = kT$, where $k$ is an integer and $T$ is the sampling interval. A sampling of the solution of (6) then leads to

$$\begin{aligned} x(t_{k+1}) &= Ax(t_k) + \tilde{w}(t_k), \quad \tilde{w}(t_k) \in NID(\mathbf{0},\Omega) \\ y(t_k) &= Cx(t_k) \end{aligned} \tag{8}$$

where the process $\tilde{w}(t_k)$ is a discrete-time Gaussian white noise that is completely described by the covariance matrix $\Omega$, given by

$$\Omega = \int_0^T e^{Ft} B W B^T e^{F^T t} dt \tag{9}$$

The transition matrix $A$ is defined as

$$A = e^{FT} \tag{10}$$

whereas $\boldsymbol{C}$ is unaffected by the sampling. In Andersen [1] and Andersen et al. [7], it is shown how the state space system (6) can be represented in discrete time by a covariance equivalent $p$-variate ARMAV($n$,$n$-1) model, i.e. an ARMAV model with an $n$th order autoregressive part and a moving average part of order $n$-1. However, (7) does not account for the presence of noise which will most certainly always be present. A way to incorporate a noise description into the ARMAV model is to add process and measurement noise to the sampled state space system, Andersen [1] and Andersen et al. [12]

$$\begin{aligned} \boldsymbol{x}(t_{k+1}) &= \boldsymbol{A}\boldsymbol{x}(t_k) + \tilde{\boldsymbol{w}}(t_k) + \boldsymbol{w}(t_k) \\ \boldsymbol{y}(t_k) &= \boldsymbol{C}\boldsymbol{x}(t_k) + \boldsymbol{v}(t_k) \end{aligned} \tag{11}$$

These noise terms are all assumed zero-mean with a joint second-order moment given by

$$E\left[\begin{bmatrix} \tilde{\boldsymbol{w}}(t) \\ \boldsymbol{w}(t) \\ \boldsymbol{v}(t) \end{bmatrix} \begin{bmatrix} \tilde{\boldsymbol{w}}^T(t) & \boldsymbol{w}^T(t) & \boldsymbol{v}^T(t) \end{bmatrix}\right] = \begin{bmatrix} \boldsymbol{\Omega} & \boldsymbol{0} & \boldsymbol{0} \\ \boldsymbol{0} & \boldsymbol{Q} & \boldsymbol{S}^T \\ \boldsymbol{0} & \boldsymbol{S} & \boldsymbol{R} \end{bmatrix} \tag{12}$$

Since external noise is now present in the system the system response at a given time step cannot be calculated explicitly, but only predicted. This prediction is performed by the means of a Kalman filter. From this filter a $p$-variate ARMAV($n$,$n$) model that describes the system dynamics as well as the noise, can be derived, Andersen [1].

$$\begin{aligned} &\boldsymbol{y}(t_k) + \boldsymbol{A}_1\boldsymbol{y}(t_{k-1}) + \ldots + \boldsymbol{A}_n\boldsymbol{y}(t_{k-n}) = \\ &\quad \boldsymbol{e}(t_k) + \boldsymbol{C}_1\boldsymbol{e}(t_{k-1}) + \ldots + \boldsymbol{C}_n\boldsymbol{e}(t_{k-n}), \quad \boldsymbol{e}(t_k) \in NID(\boldsymbol{0},\boldsymbol{\Lambda}) \end{aligned} \tag{13}$$

The left-hand side of this difference equation system is the auto-regressive part that describes the system dynamics. The left-hand side is the moving average part that describes the external noise as well as the white noise excitation, and secures stationarity of the system response. $\boldsymbol{e}(t_k)$ is a stationary zero-mean Gaussian white noise innovation process, described by the covariance matrix $\boldsymbol{\Lambda}$. The matrices $\boldsymbol{A}_i$ and $\boldsymbol{C}_i$ are the auto-regressive and the moving average coefficient matrices, respectively. The auto-regressive coefficient matrices are obtained as

$$\begin{bmatrix} \boldsymbol{A}_n & \boldsymbol{A}_{n-1} & \ldots & \boldsymbol{A}_1 \end{bmatrix} = -\boldsymbol{C}\boldsymbol{A}^n \begin{bmatrix} \boldsymbol{C} \\ \boldsymbol{C}\boldsymbol{A} \\ \vdots \\ \boldsymbol{C}\boldsymbol{A}^{n-1} \end{bmatrix}^{-1} \tag{14}$$

This follows directly from the following relation that links the auto-regressive coefficient matrices to the state space matrices, Andersen [1]

$$CA^n + A_1 CA^{n-1} + \ldots + A_{n-1} CA + A_n C = 0 \tag{15}$$

The conversion from the ARMAV model back to state space is not unique. Several ways to realize the model in state space exist. These realizations can e.g. be balanced or canonical forms, Andersen [1].

## 5. ESTIMATION OF ARMAV MODELS USING THE PREDICTION ERROR METHOD

The parameter estimates, based on $N$ samples, and returned in $\hat{\theta}_N$ can be obtained as the global minimum point of the criterion function

$$V_N(\theta) = det\left(\frac{1}{N}\sum_{k=1}^{N} \varepsilon(t_k,\theta)\varepsilon^T(t_k,\theta)\right) \tag{16}$$

In other words, as $\hat{\theta}_N = arg \min_{\theta} V_N(\theta)$. The model parameter vector $\theta$ is determined so that the prediction error, defined as

$$\varepsilon(t_k,\theta) = y(t_k) - \hat{y}(t_k|t_{k-1};\theta) \tag{17}$$

is as small as possible. $\hat{y}(t_k|t_{k-1};\theta)$ is the one-step ahead predicted system response. The $m \times 1$ parameter vector $\theta$ is organized in the following way

$$\theta = col\left(\left[A_1 \; . \; . \; A_n \; , \; C_1 \; . \; . \; C_n\right]\right) \tag{18}$$

where *col* means stacking of all columns of the argument matrix. The total number of adjustable parameters in $\theta$ is as such $m = 2np^2$. The predictor of the ARMAV($n$,$n$) model is defined as

$$\begin{aligned}\hat{y}(t_k|t_{k-1};\theta) = \\ -A_1(\theta)y(t_{k-1}) - \ldots - A_n(\theta)y(t_{k-n}) + \\ C_1(\theta)\varepsilon(t_{k-1},\theta) + \ldots + C_n(\theta)\varepsilon(t_{k-nc},\theta)\end{aligned} \tag{19}$$

This relation reveals that the predictor of the ARMAV model is non-linear, since the prediction errors themselves depend on the parameter vector $\theta$. This implies that an iterative minimization procedure such as the following Gauss-Newton search scheme has to be applied.

$$\begin{aligned}
\hat{\theta}_N^{i+1} &= \hat{\theta}_N^i + \mu_i \boldsymbol{R}_N^{-1}(\hat{\theta}_N^i)\boldsymbol{F}_N(\hat{\theta}_N^i) \\
\boldsymbol{R}_N(\theta) &= \sum_{k=1}^{N} \psi(t_k,\theta)\boldsymbol{Q}_N^{-1}(\theta)\psi^T(t_k,\theta) \\
\boldsymbol{F}_N(\theta) &= \sum_{k=1}^{N} \psi(t_k,\theta)\boldsymbol{Q}_N^{-1}(\theta)\varepsilon(t_k,\theta) \\
\boldsymbol{Q}_N(\theta) &= \frac{1}{N}\sum_{k=1}^{N} \varepsilon(t_k,\theta)\varepsilon^T(t_k,\theta)
\end{aligned} \tag{20}$$

The dimensions of $\boldsymbol{R}_N(\theta)$ and $\boldsymbol{F}_N(\theta)$ are $m \times m$ and $m \times 1$, respectively. $\mu_i$ is a bisection constant that adjusts the step size. $\psi(t_k,\theta)$ is the gradient of the predictor (19), i.e. the derivative of (19) with respect to each of the adjustable parameters of the ARMAV model. At each time step this gradient forms an $m \times p$ dimensional matrix. The estimate of the parameters of the ARMAV model can as such be calculated by supplying an initial parameter estimate. On the basis of this the prediction errors can be calculated, the matrix $\boldsymbol{R}_N(\theta)$ and the vector $\boldsymbol{F}_N(\theta)$ a can be calculated. An updated estimate can then be calculated using (19). This method is called the prediction error method (PEM) since it is the prediction errors that are minimized.

For Gaussian distributed prediction errors this method is asymptotically efficient. In this case an estimate of the uncertainties of the estimate is provided by the covariance matrix, Andersen [3]

$$\hat{\boldsymbol{P}}(\hat{\theta}_N) = \boldsymbol{R}_N^{-1}(\hat{\theta}_N) \tag{21}$$

When the amount of data is limited the estimator will not be efficient. However, the performance can in this situation be improved by a backward forecasting approach, Andersen et al. [4].

## 6. EXTRACTING MODAL PARAMETERS AND ESTIMATION OF THEIR UNCERTAINTIES

The free vibrations of an ARMAV model realized in state space are described by the deterministic part of (10) as

$$\begin{aligned}
\boldsymbol{x}(t_{k+1}) &= \boldsymbol{A}\boldsymbol{x}(t_k) \\
\boldsymbol{y}(t_k) &= \boldsymbol{C}\boldsymbol{x}(t_k)
\end{aligned} \tag{22}$$

The solution of this system is assumed to be of the form $x(t_k) = \psi\mu^k$, where $\psi$ is an $np \times 1$ complex vector and $\mu$ is a complex constant. Insertion into (21) yields

$$\begin{aligned}
\psi\mu^{k+1} &= \boldsymbol{A}\psi\mu^k \\
\boldsymbol{y}(t_k) &= \boldsymbol{C}\psi\mu^k
\end{aligned} \tag{23}$$

showing that $x(t_k) = \psi\mu^k$ only is a solution if and only if $\psi$ is a solution to the first-order eigenvalue problem

$$(I\mu - A)\psi = 0 \tag{24}$$

This eigenvalue problem only has non-trivial solutions if its characteristic polynomial is satisfied. The order of this real-valued polynomial is *np*. Thus, there will be *np* roots $\mu_j$ that are the eigenvalues of $A$. For each of these eigenvalues there is a non-trivial solution vector $\psi_j$ which is the corresponding eigenvector. The mode shape $\Phi_j$ is then obtained from (22) as

$$\Phi_j = C\psi_j , \quad j = 1, 2, \ldots , np \tag{25}$$

The continuous-time eigenvalues $\lambda_i$, the natural eigen-frequencies $f_i$ and damping ratios $\zeta_i$ can be extracted from the discrete-time eigenvalues as

$$\left.\begin{aligned} \lambda_j &= \frac{\log(\mu_j)}{T} \\ f_j &= \frac{|\lambda_j|}{2\pi} \\ \zeta_j &= -\frac{Re(\lambda_j)}{|\lambda_j|} \end{aligned}\right\} \quad j = 1, 2, \ldots, np \tag{26}$$

Due to the relation (15) these modal parameters are also the modal parameters of the ARMAV model. Above, it was established that the PEM estimator for Gaussian distributed prediction errors would be statistically efficient. A standard for the estimation errors of a statistically efficient estimator is provided by the Cramer-Rao lower bound. This standard was utilized by the model parameter covariance matrix $P_\theta(\hat{\theta}_N) = E[(\theta_0 - \hat{\theta}_N)(\theta_0 - \hat{\theta}_N)^T]$ of the difference between the true parameters $\theta_0$ and estimated parameters $\hat{\theta}_N$ as $N$ tends to infinity. In general, the change of para-meterization from a set of model parameters, given in an $m \times 1$ dimensional vector $\theta$, to another set of physical parameters, given in an $r \times 1$ dimensional vector $\kappa$, can be performed by a known $r$-dimensional functional relation

$$\kappa = f(\theta) \tag{27}$$

Since the number of physical parameters is less than the number of model parameters, obviously the accuracy and thus the sensitivity of $\kappa$ is more significant than that of $\theta$. In addition, the functional relation (27) will in general be non-linear as in the case of the modal decomposition. Thus, to obtain a practically applicable approach, (27) is usually linearized using a first-order generalized Taylor expansion at the operating point $(\hat{\kappa}_N, \hat{\theta}_N)$, Andersen [1]

$$\kappa = \hat{\kappa}_N + \left( \frac{\partial f(\theta)}{\partial \theta} \right)_{|\theta = \hat{\theta}_N} \left(\theta - \hat{\theta}_N\right) = \hat{\kappa}_N + J(\hat{\theta}_N)\left(\theta - \hat{\theta}_N\right) \tag{28}$$

where $\boldsymbol{J}(\hat{\theta}_N)$ is a Jacobian matrix of partial derivatives which should be evaluated at the operating point $\hat{\theta}_N$. The covariance matrix $\boldsymbol{P}_\kappa(\hat{\kappa}_N)$ of the deviation of $\hat{\kappa}_N$ from the true parameters can be estimated by

$$\hat{\boldsymbol{P}}_\kappa(\hat{\kappa}_N) = E\left[\left(\kappa_0 - \hat{\kappa}_N\right)\left(\kappa_0 - \hat{\kappa}_N\right)^T\right] = \boldsymbol{J}(\hat{\theta}_N)\boldsymbol{P}_\theta(\hat{\theta}_N)\boldsymbol{J}^T(\hat{\theta}_N) \tag{29}$$

The estimated covariance matrix $\hat{\boldsymbol{P}}_\theta(\hat{\theta}_N)$ obtained from (20) can then be inserted instead of $\boldsymbol{P}_\theta(\hat{\theta}_N)$. This expression will only be accurate if $\hat{\boldsymbol{P}}_\theta(\hat{\theta}_N)$ is a good estimate of $\boldsymbol{P}_\theta(\hat{\theta}_N)$ and if the error due to the linear approximation is small, Andersen [1]. What remains is to calculate the Jacobian matrix $\boldsymbol{J}(\hat{\theta}_N)$. This is in general impossible to do analytically even for small model structures, when the physical parameters of interest are the modal parameters. It is therefore necessary to rely on numerical differentiation. As an example, the elements of $\hat{\kappa}_N$ can be defined as the estimated natural eigenfrequencies and associated damping ratios of the model.

$$\hat{\kappa}_N = \left[f_1 \;\; \zeta_1 \;\; f_2 \;\; \zeta_2 \;\; \ldots \;\; f_s \;\; \zeta_s\right]^T \tag{30}$$

The functional relationship between these parameters and the model parameters is given by the eigenvalue problem followed by the calculation of the modal parameters given in (26). This means that the resulting functional relation between the model and modal parameters is highly non-linear, and numerical differentiation must be applied. For further information on the practical considerations and the estimation of the uncertainties of the mode shapes, see Andersen [1].

# 7. THE STRUCTURAL TIME DOMAIN IDENTIFICATION TOOLBOX FOR USE WITH MATLAB

As a part of the Ph.D. project, a MATLAB based toolbox for identification of especially ambient excited civil engineering structures using multivariate stochastic time domain models has been developed. The toolbox is called the *Structural Time Domain Identification (STDI) toolbox*. This toolbox has been developed in accordance with the theory and notation of the Ph.D. thesis. It has been the intention to make it completely independent of other official as well as unofficial MATLAB toolboxes. In this section the different routines in the toolbox will briefly be presented. The purpose of the routines can be divided into the following categories that cover all part of a system identification session:

- *Information importing.*
- *Data preprocessing.*
- *Parameter estimation.*
- *Model validation.*
- *Structural mode selection.*
- *Assessment of uncertainties.*
- *Information exporting.*

The presentation of the different routines will include a short description of its purpose. The first step in a system identification session is to set up the bookkeeping involved in the identification process and to acquire data. Table 7.1 shows that the STDI toolbox offers functions for the project management and preprocessing of the geometry of the structure, which is necessary for e.g. animation of mode shapes.

| Information Importing |
| --- |
| Project bookkeeping (Create, load, save....).<br>Structural geometry preprocessing.<br>Data acquisition (Interface to Data Translation plug-in AD-boards, load/save data files acquired in other data acquistion environments). |

Table 7.1: Information importing.

For preprocessing of the data the STDI toolbox contains a whole range of functions, see table 7.2. The goal of such a preprocessing is to make the measured signals suitable for system identification. Further, the preprocessing functions can be used to show and to estimate statistical characteristics of the measured data.

| Preprocessing |
| --- |
| Scaling and trend removal.<br>Show measured data.<br>Show FFT-based spectral densities of the measured data.<br>Low, high or bandpass filtering .<br>Decimation and resampling.<br>Split the data into identification and validation data sets. |

Table 7.2: Preprocessing of the measured data.

For the actual identification the toolbox implements algorithms for identifications of multivariate ARMAV models as well as multivariate stochastic state space systems. The essential algorithms are based on the PEM approach described in section 5. However, several other identification algorithms exist. These can either be used as stand-alone routines or to provide resonable initial estimates for the PEM routines. In the thesis it is shown how to convert an ARMAV model to a stochastic state space realization, and how to convert a stochastic state space realization to an ARMAV model. These conversion schemes make it possible to initialize the ARMAV PEM routine with the parameters of a stochastic state space realization, or to initialize the PEM routine of a stochastic state space realization with initial parameters of an ARMAV model. The different ARMAV estimation routines are listed in table 7.3a, whereas the different stochastic state space realization estimators are listed in table 7.3b.

| Parameter Estimation - ARMAV Models |
| --- |
| Multi-Stage Least-Square estimation of an ARMAV model.<br>Non-linear Least-Square (PEM) estimation of an ARMAV model.<br>Least-Square (PEM) estimation of an ARV model.<br>Estimation of an ARMAV(n,n) model using different stochastic subspace identification algorithms. |

Table 7.3a: Estimation of the parameters of ARMAV related models.

| Parameter Estimation - Stochastic State Space Realizations |
| --- |
| Non-linear Least-Square (PEM) estimation of a stochastic state space realization.<br>Estimation of a stochastic state space realization using different stochastic subspace identification algorithms. |

Table 7.3b: Estimation of the parameters of stochastic state space realizations.

To validate or assess the quality of a set of identified models the toolbox offers several functions, see table 7.4. It is possible to obtain the Akaike Information theoretic Criterion,AIC and the Akaike Final Prediction Error criterion, FPE of the models, plot the spectral densities and correlation functions of the prediction errors, and compare the predicted and measured response. Further, it is also possible to compare the FFT-based spectral densities of the measured response with the spectral densities obtained from the model.

| Model Validation |
| --- |
| FPE / AIC - Akaike's Final Prediction Error / Information theoretic Criterion.<br>Plot spectral densities and correlation functions of prediction errors.<br>Plot measured and predicted response.<br>Plot poles and zeroes and their uncertainty elipsoides.<br>Compare spectral densities of measured response with spectral densities of one or more identified models. |

Table 7.4: Model validation functions.

To select the structural or fundamental modes of an optimal model the toolbox offers different mode selection functions, see table 7.5. One of the simplest ways to identify the structural modes is to compute the modal parameters and compare these with the spectral densities of the model and e.g. the MAC (Modal Assurance Criterion) values of the mode shapes. Another efficient way is to plot stability diagrams with different plotting criteria.

| Structural Mode Selection |
| --- |
| Compute the modal parameters.<br>Compute the Modal Assurance Criterion (MAC).<br>Plot the spectral densities of the model.<br>Plot various stability diagrams. |

Table 7.5: Mode selection functions.

When the optimal model has been selected it is important to be able to quantify the uncertainties of the estimated model and modal parameters, see table 7.8. The estimation of the uncertainties of the modal parameters is performed according to the principles explained in section 6.

| Assessment of Uncertainties |
| --- |
| Return estimated covariance matrix of estimated model parameters.<br>Return estimated standard deviations of estimated modal parameters. |

Table 7.6: Assessment of uncertainties.

Having finished an identification session, the results of it have to be presented and exported. The toolbox offers various functions especially made for these purposes. These functions make tables with all estimated modal parameters and their uncertainties, animate mode shapes, and generate a final report of the identification session, see table 7.7.

| Information Exporting |
| --- |
| Save tables with estimated modal parameters and their uncertainties to a file.<br>Animate the estimated mode shapes<br>Generate a final documentation report of the identification session. |

Table 7.7: Information exporting.

Besides implementing routines that solve the primary tasks presented in the tables the toolbox implements a variety of necessary auxiliary functions. These routines can be divided into the categories shown in table 7.8.

| Auxiliary Functions |
| --- |
| Manipulation of matrix polynomials (Multiplication, modal decomposition, filtering).<br>Manipulation of state space system (Modal decomposition, filtering, balancing , solving Algebraic Riccati and Lyapunov equations etc.).<br>Relating continuous-time to equivalent discrete-time multivariate systems (Zero-order hold and covariance equivalence techniques). |

Table 7.8: Auxiliary functions of the toolbox.

A more comprehensive description of the performance of the routines and how they are used can be found in Andersen [1], Kirkegaard et al. [15], and in the *Structural Time Domain Identification Users Guide*, Andersen et al. [17].

# 8. CONCLUSION

In this Ph.D. project, system identification of civil engineering structures using parametric stochastic models has been considered. It has been shown that if the structural system can be assumed to be a linear and time-invariant lumped parameter system, and if the excitation can be assumed generated by a linear and time-invariant shaping filter subjected to Gaussian white noise, then the ARMAV model will be an adequate model.

The relation between the combined continuous-time system and the ARMAV model has been derived by assuming a covariance equivalence of the response of the continuous-time system and the ARMAV model for all discrete time steps. If the measured response of a linear and time-invariant structural

system is Gaussian distributed and if the excitation is unknown, then the covariance equivalence technique results in a discrete-time model correctly describing the dynamic properties of the structural system as well as the statistical properties of the response.

For an *n*th order multivariate continuous-time system subjected to Gaussian white noise and affected by external noise the covariance equivalent discrete-time model is an ARMAV($n$,$n$) model. In other words, a model that is constructed from an *n*th order auto-regressive matrix polynomial and an *n*th order moving average matrix polynomial. It is shown that an ARMAV($n$,$n$) model reduces to an ARMAV($n$,$n$-1) model when no noise is present. In this project the accuracy of an estimated ARMAV model has been emphasized. For this reason the applied estimation technique is the Prediction Error Method (PEM). The advantage of this estimation technique is that it is asymptotically unbiased and efficient if the prediction errors are Gaussian distributed and if the true system is contained in the estimated model. The use of the PEM estimator has made it possible to estimate the standard deviations associated with the modal parameter estimates.

So to recapitulate the results of the project. The ARMAV model estimated using the PEM should be applied in modal analysis if :

- ☞ *The structural system is linear and time-invariant.*
- ☞ *The excitation is unknown.*
- ☞ *The measured response is stationary and can be assumed Gaussian distributed.*
- ☞ *Uncertainty estimates of the modal parameters are needed.*

For a large variety of practical system identification problems in civil engineering, the assumptions concerning linearity, Gaussianity and stationarity are fulfilled. In these cases, system identification using ARMAV models can serve as a reliable and valuable alternative to the traditional non-parametric system identification techniques.

# 9. REFERENCES

[1] Andersen, P.: *Identification of Civil Engineering Structures using Vector ARMA Models*. Ph.D.-Thesis, Aalborg University, Denmark, ISSN 1395-7953 R9724, 1997.

[2] Brincker, R., P.H. Kirkegaard, P. Andersen & M.E. Martinez: *Damage Detection in an Offshore Structure*. Proceedings of the 13th International Modal Analysis Conference, Nashville, Tennessee, USA, 1995.

[3] Brincker, R., P. Andersen, P.H. Kirkegaard & J.P. Ulfkjær: *Damage Detection in Laboratory Concrete Beams*. Proceedings of the 13th International Modal Analysis Conference, Nashville, Tennessee, USA, 1995.

[4] Andersen, P., R. Brincker & P.H. Kirkegaard: *On the Uncertainties of Identification of Civil Engineering Structures using ARMA Models*. Proceedings of the 13th International Modal Analysis Conference, Nashville, Tennessee, USA, 1995.

[5] Kirkegaard, P.H., J.C. Asmussen, P. Andersen & R. Brincker: *An Experimental Study of an Offshore Platform.* Fracture & Dynamics No. 60, Aalborg University, ISSN 0902-7513 R9441, 1994.

[6] Kirkegaard, P.H., P. Andersen & R. Brincker: *Identification of an Equivalent Linear Model for a Non-Linear Time-Variant RC-Structure.* Proceedings of the International Workshop on Structural Damage Assessment using Advanced Signal Processing Procedures, Pescara, Italien, 1995.

[7] Andersen, P., R. Brincker & P.H. Kirkegaard: *Theory of Covariance Equivalent ARMAV Models of Civil Engineering Structures.* Proceedings of the 14th International Modal Analysis Conference, Dearborn, Michigan, USA, 1996.

[8] Brincker, R., P. Andersen, M.E. Martinez & F. Tallavó : *Modal Analysis of an Offshore Platform using Two Different ARMA Approaches*. Proceedings of the 14th International Modal Analysis Conference, Dearborn, Michigan, USA, 1996.

[9] Kirkegaard, P.H., P. Andersen & R. Brincker: *Identification of the Skirt Piled Gullfaks C Gravity Platform using ARMAV Models.* Proceedings of the 14th International Modal Analysis Conference, Dearborn, Michigan, USA, 1996.

[10] Kirkegaard, P.H., P. Andersen & R. Brincker: *Identification of Civil Engineering Structures using Multivariate ARMAV and RARMAV Models.* Proceedings of the International Conference of Engineering Systems, Swansea, Wales, 1996.

[11] Asmussen, J.C., P. Andersen, R. Brincker & G.C. Manos: *Identification of the EURO-SEIS Test Structure*. Fracture & Dynamics No. 76, Aalborg University, ISSN 1395-7953 R9612, 1996.

[12] Andersen, P., P.H. Kirkegaard & R. Brincker: *System Identification of Civil Engineering Structures using State Space and ARMAV Models.* Proceedings of the 21. International Seminar on Modal Analysis, Leuven, Belgium, 1996.

[13] Kirkegaard, P.H., P.S. Skjærbæk & P. Andersen: *Identification of Time-varying Civil Engineering Structures Using Multivariate Recursive Time Domain Models*. Proceedings of the 21. International Seminar on Modal Analysis, Leuven, Belgium, 1996.

[14] Andersen, P., P.H. Kirkegaard & R, Brincker: *Filtering Out Environmental Effects in Damage Detection of Civil Engineering Structures*. Proceedings of the 15th International Modal Analysis Conference, Orlando, Florida, USA, 1997.

[15] Kirkegaard, P.H., P. Andersen & Brincker: *Structural Time Domain Identification (STDI) Toolbox for use with MATLAB*. Proceedings of the 15th International Modal Analysis Conference, Orlando, Florida, USA, 1997.

[16] Kirkegaard, P.H. & P. Andersen: *State Space Identification of Civil Engineering Structures From Output Measurements*. Proceedings of the 15th International Modal Analysis Conference, Orlando, Florida, USA, 1997.

[17] Andersen P., P.H. Kirkegaard & R, Brincker: *Structural Time Domain Identification Toolbox User's Guide.* Fracture & Dynamics No. 97, Aalborg University, ISSN 1395-7953 R9701, 1997.

[18] Andersen, P. & P.H. Kirkegaard: *Statistical Damage Detection of Civil Engineering Structures using ARMAV* Models. Proceedings of the 16th International Modal Analysis Conference, Santa Barbara, California, USA, 1998.

[19] Kirkegaard, P.H. & P. Andersen: *Use of Statistical Information for Damage Assessment of Civil Engineering Structures*. Proceedings of the 16th International Modal Analysis Conference, Santa Barbara, California, USA, 1998.

**B.2**

# MODAL ANALYSIS BASED ON THE RANDOM DECREMENT TECHNIQUE

-

# APPLICATION TO CIVIL ENGINEERING STRUCTURES

J.C. Asmussen & R. Brincker
Department of Building Technology and Structural Engineering
Aalborg University, Sohngaardsholmsvej 57, DK-9000 Aalborg, Denmark

## Abstract

*This article describes the work carried out within the project: Modal Analysis Based on the Random Decrement Technique - Application to Civil Engineering Structures. The project is part of the research programme Dynamics of Structures sponsored by the Danish Technical Research Council. The planned contents and the requirement for the project prior to its start are described together with the results obtained during the 3 year period of the project. The project was mainly carried out as a Ph.D.-project by the first author from September 1994 to August 1997 in cooperation with associate professor Rune Brincker from the above department. During the project there has been intensive cooperation with professor Sam Ibrahim, Old Dominion University, Virginia, USA. The article is finished with a reference list of the papers and reports prepared during the project. A short description together with the possibility to download papers and reports can be seen at http://www.civil.auc.dk/~i6jca*

# 1 Introduction

The project *Modal Analysis Based on the Random Decrement Technique* has mainly been carried out as a Ph.D.-project by the first author. An explanation for the need of investigating the topics of this project can be given by considering the overall topic *Identification of Civil Engineering Structures.* The assignment of identifying civil engineering structures can be solved using several different methods. One of these methods, the ARMAV-model has been investigated as another project within this framework. This method is a very accurate but also a very time consuming method. The Random Decrement (RD) technique is expected to be perhaps the fastest technique of all but less accurate compared to the ARMAV model. So by investigating ARMAV-models and the RD technique both ends of a time/accuracy scale characterizing identification of civil engineering structures have been investigated. Furthermore, the RD technique has been investigated intensively during the late 1980s and early 1990s at the above department mainly by prof. Brincker. The theory of the technique was improved and the practical application of the technique was considered. From the obtained knowledge it was natural to formulate a project concerning the RD technique at Aalborg University in order to take advantage of and finish earlier work.

During this project cooperation with different persons from universities and companies besides prof. Ibrahim have been carried out. The Queensborough bridge, Vancouver, Canada has been identified from ambient data. The data were collected by prof. Ventura and Dr. Felber from

University of Vancouver, Canada. The results from different researchers applying different algorithms to the data were presented and compared at the 14th International Modal Analysis Conference, Dearborn, Michigan, USA, 1996. The author has spent 4 months at the Aristotle University of Thessaloniki, Greece as part of this project. Furthermore, the initial part of a demonstration project concerning the application of vibration based inspection of bridges has been carried out in cooperation with RAMBOLL, Nørresundby, Denmark and the Danish Road Directorate.

# 2 Plan for the Project

The following topics for the project were described prior to its start.

- Implementation of the RD technique.
- Investigation of the estimation of frequency response functions.
- Investigation of the theoretical background.
- Implementation of modal parameter extraction procedures.

In the next sections it will be pointed out how the different topics and problems have been investigated. It is not the intention to give a detailed mathematical description in this paper. Only the problem, the assumptions, the results and the consequences are described. A detailed report is given in Asmussen [1].

Section 3 contains a short description of the modelling of the vibrations of civil engineering structures and the modelling of the loads of civil engineering structures. Furthermore methods to extract modal parameters from free decays or correlation functions are mentioned. Section 4 gives a brieg description of the RD technique as wll as the progress made during the project. Section 5 describes the Vector Random Decrement technique developed during this project. Section 6 describes a new method to predict the variance of RD functions. Section 7 contains a comparison of the RD and the FFT algorithm for estimation of frequency response functions. The diffent structures and the analysis of the structures using the RD technique are described in section 8 . The implementations performed during this project are described in section 9 and the paper is finished with a conclusion.

# 3 Civil Engineering Structures

If the aim of a vibration test of a structure is to identify the dynamic characteristics of the structure, the following three processes should all be carried out with high accuracy in order to make the test successful.

- The mathematical modelling of the structural vibrations.
- Measurements of the vibrations.
- Data analysis of the measurements.

These three processes are in practice coherent, so that a separation followed by an individual solution and performance is not possible. This is illustrated by fig. 1, where it is indicated that

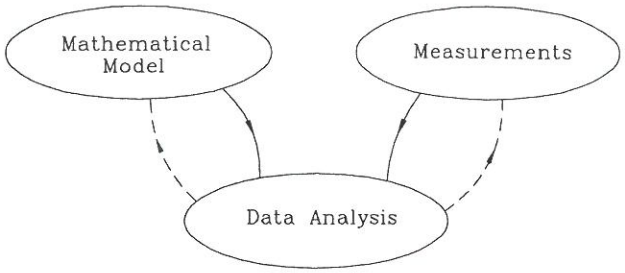


Figure 1: *Illustration of the processes in vibration testing. The data analysis may result in a reformulation of the mathematical model or a change in the experimental setup.*

results of the data analysis could lead to a change of the mathematical model or a change in the experimental setup.

This project deals with the data analysis procedure in vibration testing. This is the process where the measurements of the vibrations of a structure are used to calibrate or identify the parameters of the mathematical model of the structure. The parameters of the mathematical model describe the dynamic characteristics of the structure. Collecting the measurements of the vibrating structure is the fundamental basis for a succesful test. If the measurements are not collected carefully, it is impossible to obtain satisfactorily accurate dynamic characteristics of the structure, regardless of the mathematical modelling and data analysis.

Civil engineering structures are continuous or distributed systems. The mass, damping and stiffness properties are distributed throughout the spatial definition of the structure. In this project the mathematical model used to describe the vibrations of a structure is a discrete model: The linear lumped mass parameter model. The damping forces, which model all energy dissipation from the structure, are assumed to be proportional to the velocity of the lumped masses, and the stiffness forces are assumed to be proportional to the displacements of the lumped masses. The principle is illustrated in fig. 2.

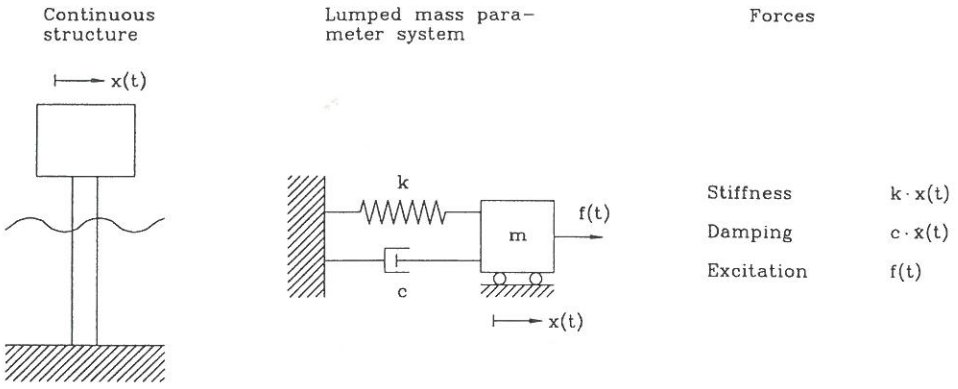


Figure 2: *Example of a continuous structure modelled by a lumped mass parameter system. The displacements at the top of the monopile offshore platform are modelled by a lumped mass parameter system. The loads on the structure, wind and waves, are modelled by $f(t)$, the damping forces are modelled by $c \cdot \dot{x}(t)$ and the stiffness forces are modelled by $k \cdot x(t)$.*

In principle any material point of the continuous structure has a mass, damping and stiffness property attached. So a structure should intuitively have infinitely many of such dynamic degrees of freedom. Since the structure is assumed to be linear, the properties of the dynamic degrees of freedom, which are local properties, can be converted to the dynamic characteristics called modal parameters, which are global parameters of the structure. The modal parameters consist of eigenfrequencies, damping ratios and mode shape vectors. Sometimes the term structural mode or just mode is used. A structural mode is described by an eigenfrequency, damping ratio and a mode shape vector, which belongs together. An eigenfrequency can be interpreted as a frequency where the structure will have a high response level to a harmonic force with that frequency. The eigenfrequencies of a structure are therefore sometimes also denoted resonant frequencies. A damping ratio gives information about how fast the vibrations of the structure at the corresponding eigenfrequency dissipate. The mode shape vectors describe the relative displacements of the material points of the structure at the corresponding eigenfrequency. These properties make the modal parameters global parameters.

Theoretically structures have infinitely many modes and thereby inifinitely many modal parameters. In vibration testing the number of modes, that can be identified, are limited by the force. The forces work in a limited frequency area, so only structural modes with an eigenfrequency within that frequency area are brought into vibration and can therefore be identified. This also means that the lumped mass parameter model of the structure can also be limited. It does not have to contain an infinite number of degrees of freedom. These are the arguments for using the linear lumped mass parameter model with a finite number of masses and thereby finite number of degrees of freedom. This is the mathematical model used to describe the vibrations of the structures considered in the present thesis.

The above assumptions of the mathematical modelling of the structure might seem very restrictive. But it is a very general mathematical model and has been used to model various structures from large civil engineering structures such as high-rise buildings, bridges, offshore platforms to small mechanical systems. It is important that the mathematical model assumes the dynamic characteristics of the structures to be time-invariant during the measurement period. This is also widely assumed. The loads of the structure are assumed to be stationary and Gaussian distributed.

For a general $n$ DOF system the equations of motion become

$$\begin{aligned} &\mathbf{M}\ddot{\mathbf{x}}(t) + \mathbf{C}\dot{\mathbf{x}}(t) + \mathbf{K}\mathbf{x}(t) = \mathbf{f}(t) \\ &\mathbf{x}(0) = \mathbf{x}_0, \quad \dot{\mathbf{x}}(0) = \dot{\mathbf{x}}_0 \end{aligned} \tag{1}$$

This expresses a force equilibrium between external and internal forces. All matrices have the dimension $n \times n$ and the response vectors and force vector have the dimension $n \times 1$, where $n$ is the number of DOFs. $\mathbf{M}$ is a diagonal and positive definite mass matrix. The stiffness matrix, $\mathbf{K}$, is symmetric and positive definite. The dissipation of energy is modelled by the symmetric and positive semi-definite damping matrix $\mathbf{C}$. As indicated in eq. (1) the system is assumed time-invariant, since $\mathbf{M}$, $\mathbf{C}$ and $\mathbf{K}$ do not depend on time. The acceleration, velocity and displacement response are denoted $\ddot{\mathbf{x}}$, $\dot{\mathbf{x}}$ and $\mathbf{x}$, respectively.

The displacements, velocity and acceleration response of the lumped mass parameter system to initial conditions become

$$\mathbf{x}(t) = \Phi e^{\Lambda t}\mathbf{q}_0 \tag{2}$$

$$\dot{\mathbf{x}}(t) = \mathbf{\Phi} e^{\mathbf{\Lambda} t} \mathbf{\Lambda} \mathbf{q}_0 \tag{3}$$

$$\ddot{\mathbf{x}}(t) = \mathbf{\Phi} e^{\mathbf{\Lambda} t} \mathbf{\Lambda}^2 \mathbf{q}_0 \tag{4}$$

where $\mathbf{\Phi}$ are the mode shapes and $\mathbf{\Lambda}$ contains the eigenvalues from which the eigenfrequencies, $f$, and damping ratios, $\zeta$, of the system can be extracted, and $\mathbf{q}_0$ contains the initial conditions. As seen, the difference between the free decay displacement response, velocity response and acceleration response is only a complex scaling factor in the form of the eigenvalue matrix, $\mathbf{\Lambda}$. This scaling factor changes the amplitude and the phase of the exponentially damped sinusoidal free decay response. The relations are important, since the modal parameters can be extracted from all free decay responses in eqs. (2) - (4) using algorithms like Ibrahim Time Domain or Polyreference Time Domain, which have been implemented as part of this project.

The load which excites the lumped mass parameter system is assumed to be a stationary zero mean Gaussian distributed vector process. In order to generalize the load process it is assumed that the load process can be described as a white noise vector process passed through a linear shaping filter. This is an extension of the traditional white noise assumption. The idea behind this approach and the theory are presented in Ibrahim et al. [4], where the filter is referred to as a pseudo-force filter. The principle is shown in figure 3.

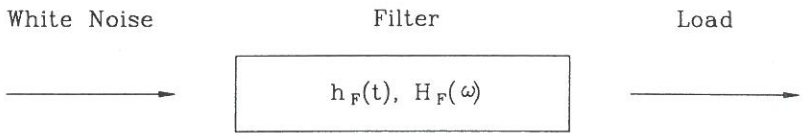


Figure 3: *Outline diagram for modelling of loads using a shaping filter. $h(t)$ and $H(\omega)$ are the impulse response and frequency response matrix, respectively.*

The correlation functions of a stationary stochastic vector process are defined as

$$\mathbf{R}_{\mathbf{XX}}(\tau) = E[\mathbf{X}(t+\tau)\mathbf{X}^T(t)] \tag{5}$$

From this definition and if the above modelling of the structure and the loads is assumed any column in the correlation matrix of $\mathbf{X}$, $\dot{\mathbf{X}}$ or $\ddot{\mathbf{X}}$ can be written as

$$\mathbf{R}^i_{\mathbf{XX}}(\tau) = \tilde{\mathbf{\Phi}} e^{\mathbf{\Lambda}\tau} \tilde{\mathbf{m}}^{-1} \tilde{\mathbf{q}}_i \tag{6}$$

$$R^i_{\dot{\mathbf{X}}\dot{\mathbf{X}}}(\tau) = -\tilde{\mathbf{\Phi}} e^{\mathbf{\Lambda}\tau} \mathbf{\Lambda}^2 \mathbf{c}_i \tag{7}$$

$$R^i_{\ddot{\mathbf{X}}\ddot{\mathbf{X}}}(\tau) = \tilde{\mathbf{\Phi}} e^{\mathbf{\Lambda}\tau} \mathbf{\Lambda}^4 \mathbf{c}_i \tag{8}$$

where $\mathbf{R}^i_{\mathbf{XX}}$ is an abbreviation of the $i$th column in the correlation matrix and the scaling constant $\tilde{\mathbf{q}}_i$ is the $i$th column of the matrix $\tilde{\mathbf{c}}$. Equations (6) - (8) correspond exactly to eqs. (2) - (4), so in the modal parameter extraction procedure there is no reason to distinguish between the correlation functions of the displacements, velocities or the accelerations of the structure or free decays.

# 4 The Random Decrement Technique

Four major contributions to the theory and application of the RD technique have been prepared

- Generalization of the RD technique by introduction of the general applied triggering condition.
- Introduction of a new concept: Quality assessment.
- Optimal choice of triggering level.
- Comparison of the RD technique with other unbiased methods for estimation of correlation functions.

In the following sections these three topics will be briefly described.

## 4 .1 The General Applied Triggering condition

The RD technique is a method which transforms the stochastic processes *X(t)* and *Y(t)* into RD functions. It is assumed that $X(t)$ and $Y(t)$ are stationary and Gaussian distributed processes with zero mean. The index $t$ is interpreted as time. The RD functions are defined as the mean value of a stochastic process, $Y(t)$ on condition, $T_{X(t)}$

$$D_{YX}(\tau) = E[Y(t+\tau)|T_{X(t)}] \tag{9}$$

An RD function is referred to as e.g. $D_{YX}(\tau)$. The first subscript refers to the process from which the mean value is calculated and the second subscript refers to the process where the condition is fulfilled. The condition $T_{X(t)}$ is denoted triggering condition.

In practical applications of the RD technique only a single realization of the stochastic process is available. Or in other words, usually only a single measurement at each chosen location of a vibrating structure is collected. In order to estimate the conditional mean value correctly from a single observation it is necessary to assume that the stochastic process is not only stationary but also ergodic. In this case the RD functions can be estimated as the empirical conditional mean value from a single realization

$$\hat{D}_{YX}(\tau) = \frac{1}{N} \cdot \sum_{i=1}^{N} y(t_i+\tau)|T_{x(t_i)} \tag{10}$$

where $N$ is the number of points in the process which fulfils the triggering condition and $y(t)$ and $x(t)$ are realizations of $X(t)$ and $Y(t)$. The absolute decisive variable in estimation of RD functions is the number of triggering points, $N$. $N$ has to be large enough to ensure that eq. (10) has converged sufficiently towards eq. (9).

During this project the triggering condition has been generalized to the applied general triggering condition, $T^{G_A}_{X(t)}$

$$T^{G_A}_{X(t)} = \{a_1 \leq X(t) < a_2, b_1 \leq \dot{X}(t) < b_2\} \tag{11}$$

Using this general triggering condition the RD functions become a weighted sum of the correlation function and the time derivative of the correlation functions

$$D_{YX}(\tau) = \frac{R_{YX}(\tau)}{\sigma^2_X} \cdot \tilde{a} - \frac{R'_{YX}(\tau)}{\sigma^2_{\dot{X}}} \cdot \tilde{b} \tag{12}$$

$$\tilde{a} = \frac{\int_{a_1}^{a_2} x p_X(x) dx}{\int_{a_1}^{a_2} p_X(x) dx} \qquad \tilde{b} = \frac{\int_{b_1}^{b_2} \dot{x} p_{\dot{X}}(\dot{x}) d\dot{x}}{\int_{b_1}^{b_2} p_{\dot{X}}(\dot{x}) d\dot{x}} \tag{13}$$

where the triggering levels $\tilde{a}$ and $\tilde{b}$ are functions of the triggering bounds and the density functions, $p$. Equation (12) illustrates how versatile the RD technique is. By adjusting the triggering bounds $a_1, a_2$ and/or $b_1, b_2$ the contribution of the correlation functions and the time derivative of the correlation functions to the resulting RD functions can be changed. In the limit by choosing one of the triggering level sets, $[a_1\ a_2]$ or $[b_1\ b_2]$, to $[-\infty\ \infty]$ or $[0\ 0]$ the resulting RD functions become proportional to either the correlation functions or their time derivatives.

In application of the RD technique only special formulations of the applied general triggering condition is used. The most common are: Level crossing, $T^L_{X(t)}$, local extremum, $T^E_{X(t)}$, positive point, $T^P_{X(t)}$, zero crossing, $T^Z_{X(t)}$,

$$T^L_{X(t)} = \{X(t) = a\} \tag{14}$$

$$T^E_{X(t)} = \{a_1 \leq X(t) < a_2, \dot{X}(t) = 0\} \tag{15}$$

$$T^P_{X(t)} = \{a_1 \leq X(t) < a_2\} \tag{16}$$

$$T^Z_{X(t)} = \{X(t) = 0, \dot{X}(t) > 0\} \tag{17}$$

The link between the RD functions and the correlation functions can be established directly from the result of eqs. (12) and (13) by inserting the triggering levels. This illustrates the importance of $T^{G_A}_{X(t)}$. The derivation is given in Asmussen [1].

## 4 .2 Quality Assessment

In application of the RD technique it is an advantage to have some standard methods to assess the quality of the estimated RD functions. The advantage of standard methods is that valuable experience with this technique can be transferred between different data sets obtained from different physical systems. The purpose of quality assessment of RD functions is to answer the following questions.

- Has the empirical mean value converged sufficiently towards the true mean value (or: Is the number of triggering points adequate)?
- How many points in the RD functions are estimated with sufficient accuracy?

Two different types of tests or investigations are suggested as standard methods for quality assessment of RD functions: Shape invariance test and symmetry test.

Testing the shape invariance of RD functions is based on several different estimations of a correlation function using different triggering levels for the same triggering condition

$$R^1_{YX}(\tau) = \frac{D_{YX}(\tau)}{a_1}\sigma_X^2 \ , \quad R^2_{YX}(\tau) = \frac{D_{YX}(\tau)}{a_2}\sigma_X^2 \ , \quad \ldots \tag{18}$$

where superscripts $1, 2, \ldots$ refer to the different choice of triggering levels. These correlation functions can be compared graphically or the correlation functions between them could be calculated. Any correlation which differs significantly from the others is estimated with erroneous triggering levels.

The second approach suggested for quality assessment of the RD functions is based on the symmetry relations for correlation functions of stationary stochastic processes. This approach generally assumes that all possible RD functions are estimated, corresponding to estimating the full correlation matrix of the measurements at each time step. The approach can still be used if only a part of the correlation matrix is estimated, but this is considered to be a special case. The symmetry relation is

$$R_{YX}(\tau) = R_{XY}(-\tau) \tag{19}$$

From this symmetry relation an average and an error RD function can be calculated by subtraction and addition. From these functions different error functions can be calculated and used as indicator of the optimal choice of triggering level.

Examples and a detailed description are given in Asmussen [1] and Asmussen et al. [15].

## 4 .3 Optimal Choice of Triggering Level

One of the difficulties in applications of the RD technique is how to choose the triggering levels $[a_1\ a_2]$ for a given triggering condition. From a user point of view it is important to know how to choose a proper triggering level and to know how sensitive the results are to the choice of triggering level. The optimal choice of triggering level is defined as the choice which minimizes the variance of the RD functions normalized to be equal to the correlation functions

$$\min(\mathrm{Var}[\frac{\hat{D}_{XX}(\tau)}{\tilde{a}} \cdot \sigma_X^2]) \rightarrow [a_1\ a_2] \tag{20}$$

For the level triggering condition eq. (20) has been solved. The solution is a triggering level of $a = \sqrt{2}\sigma_X$. The assumptions are that the processes are stationary zero mean Gaussian distributed and that the time segments used in the averaging process are independent. The latter assumption is of course violated in some sense. However the above result is considered a good basis for selecting the triggering level for the level crossing triggering condition.

For the local extremum triggering condition eq. (20) has been investigated for an SDOF system. The optimal triggering levels are shown in fig. 4.

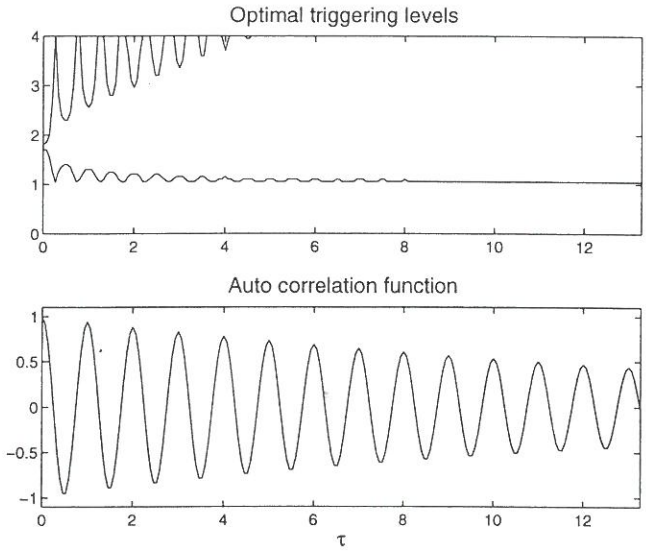


Figure 4: *Theoretically predicted optimal lower and upper triggering level ($\times\sigma_X$) for an SDOF system using local extremum triggering and the corresponding correlation function.*

Figure 4 illustrates a new result. The optimal choice of triggering levels is not always those which maximize the number of triggering points. Theoretically, it is predicted that the triggering levels should be chosen as $[a_1\ a_2] = [\sigma_X\ \infty]$. The above result can only be a guideline to the user, since the result is dependent on the correlation function. Other triggering conditions have been investigated and the general result was that the triggering points between 0 and $\sigma_X$ should not be used. The work is presented in Asmussen [1] and Asmussen [14].

### 4 .4 Unbiased Estimation of Correlation Functions

The purpose of this investigation is to compare the RD technique with two other unbiased methods for estimation of correlation functions: The direct approach and an FFT-IFFT approach. The results are presented in Asmussen et al. [6] and Asmussen [1]. The comparison of the different techniques is based on simulations of the displacement response of a 2DOF system loaded by independent white noise at each mass.

The result was that the RD technique is clearly the fastest technique for short correlation functions and as accurate as the FFT-IFFT approach. This indicates that the RD technique can replace the FFT-IFFT technique with advantage.

## 5 The Vector Random Decrement Technique

A new concept is introduced: Vector triggering Random Decrement (VRD). The argumentation for developing this technique is that experience has discovered some problems with the RD technique applied to a large number of measurements (e.g. >4) collected simultaneously. This is often the situation in ambient testing of bridges.

- If all measurements are used as the reference measurement, which will result in the maximum number of RD functions (full correlation matrix estimated), the estimation time will increase proportionally to the number of measurements compared to the situation

where only a single measurement is used as reference measurement. Since the speed is one of the main advantages of this technique a decision of estimating all possible RD setups should be reconsidered. On the other hand, if not all possible RD functions are estimated, valuable information can be lost.

- If only some of the RD setups are estimated, how should the actual reference measurements be chosen. By assuming the signal-to-noise ratio to be highest at the measurements with highest standard deviation, the standard deviation could be used as a criterion. But this is only a guideline, not a full solution.

- Usually the uncertainty of the cross RD functions is higher than the uncertainty of the auto RD functions. So auto RD functions should only be used for modal parameter estimation. But this excludes the possibility to estimate mode shapes.

The above problems are the motivation for developing the VRD technique. The target is somehow to estimate equivalent auto RD functions, which contains phase information and thus the possibility to estimate mode shapes, in contrast to auto RD functions only. The solution is to apply a vector triggering condition instead of a scalar triggering condition. The VRD concept is first presented in Ibrahim et al. [9], [11] and Asmussen et al. [9].

Consider an $n$-dimensional stochastic vector process, $\mathbf{X}(t)$. The VRD functions are defined equivalently to traditional RD functions

$$\mathbf{D}_{\mathbf{X}}(\tau) = E[\mathbf{X}(t+\tau)|T^{v}_{\mathbf{X}(t+\boldsymbol{\Delta t})}] \tag{21}$$

where the vector triggering condition, $T^{v}_{\mathbf{X}(t+\boldsymbol{\Delta t})}$, is defined as

$$T^{v}_{\mathbf{X}(t+\boldsymbol{\Delta t})} = T^{v}_{X_1(t+\Delta t_1),X_2(t+\Delta t_2),...,X_m(t+\Delta t_m)}\ , \quad 2 \leq m \leq n \tag{22}$$

The size of the vector triggering condition has to be in between 2 and $n$. If the condition is scalar, a traditional RD triggering condition is formulated. A triggering point is detected if several of the elements ($m$) in the stochastic vector process fulfil individually formulated triggering conditions at any time $t$ plus the individual time shifts $\Delta t_i$, $\boldsymbol{\Delta t} = [\Delta t_1, \Delta t_2, ..., \Delta t_m]$.

The VRD functions are estimated as the empirical mean by assuming the processes to be ergodic

$$\hat{\mathbf{D}}_{\mathbf{X}}(\tau) = \frac{1}{N}\sum_{i=1}^{N}\mathbf{X}(t_i+\tau)|T^{v}_{\mathbf{X}(t_i+\boldsymbol{\Delta t})} \tag{23}$$

Estimation of the VRD functions using eq. (23) provides unbiased estimates, corresponding to the RD technique.

Consider an $n \times 1$-dimensional stochastic vector process, $\mathbf{X}(t)$

$$\mathbf{X}(t) = [X_1(t),\ X_2(t),\ \ldots\ , X_n(t)]^T \tag{24}$$

The vector positive point triggering condition is

$$T^{v}_{\mathbf{X}(t+\boldsymbol{\Delta t})} = \{a_1 \leq X_1(t+\Delta t_1) < b_1,\ \ldots \{a_m \leq X_m(t+\Delta t_m) < b_m\} \tag{25}$$

The VRD functions of the process using the vector positive point triggering condition become

$$D^v_{\mathbf{X}}(\tau) = \mathbf{R}_{X_1}(\tau - \Delta t_1) \cdot \tilde{a}_1 + \ldots \mathbf{R}_{X_m}(\tau - \Delta t_m) \cdot \tilde{a}_m \tag{26}$$

where the triggering level $\tilde{\mathbf{a}}$ is now defined as

$$\tilde{\mathbf{a}} = \frac{\mathbf{R}^{-1}_{\mathbf{Y}_v \mathbf{Y}_v}}{k_1} \int_{\mathbf{a}}^{\mathbf{b}} \mathbf{y}_v \cdot p(\mathbf{y}_v) d\mathbf{y}_v \; k_1 = \int_{\mathbf{a}}^{\mathbf{b}} p_{\mathbf{Y}_v}(\mathbf{y}_v) d\mathbf{y}_v \; \mathbf{Y}_v = [X_1(t) \ldots X_m(t)] \tag{27}$$

and $\mathbf{R}_{X_i}$ is the $i$th column of the correlation matrix of $\mathbf{X}$. Only the weights, $\tilde{a}_i$, of the correlation functions have changed. In practice only the vector positive point triggering condition is of interest, since this is the only triggering condition, which results in a reasonable number of triggering points.

In conclusion the VRD functions are a sum of a number of correlation functions corresponding to the size of the vector condition. In Ibrahim et al. [8], [10] and Asmussen [9] the technique is validated and the theory is derived in Asmussen [1].

# 6 Variance of Random Decrement Functions

A new method for estimating the variance of the RD functions is introduced. It will be assumed that the measurements are realizations of stationary zero mean Gaussian distributed processes. A new method should fulfil the following demands.

- The method should be valid for all triggering conditions. This means that the correlation between the time segments should be taken into account and that the method is independent of the chosen triggering condition.
- The method should be accurate and consistent. Consistent means that the accuracy of the method should be independent of the physical system describing the measured responses.
- The method should be fast, otherwise the absolute main advantage of the RD technique is wasted and the method will only have theoretical interest.
- The requirement for the speed of the method is fulfilled if the variance can be predicted by the RD functions only.

In the following a new method is proposed and it is investigated if it fulfils the above demands. Only cross RD functions and the variance of the estimated cross RD functions are considered, in order to simplify the derivations and still preserve generality.

$$\begin{aligned} \mathrm{Var}[\hat{D}_{YX}(\tau)] = \frac{1}{N^2} \cdot \Bigg( & \sum_{i=1}^{N} \mathrm{Cov}[Y(t+\tau)|T^{G_T}_{X(t)}; Y(t+\tau)|T^{G_T}_{X(t)}] \\ & + \sum_{j=1}^{m} N_j \mathrm{Cov}[Y(t+\tau)|T^{G_T}_{X(t)}; Y(t+j\Delta T+\tau)|T^{G_T}_{X(t+j\Delta T)}] \\ & + \sum_{j=1}^{m} N_j \mathrm{Cov}[Y(t+j\Delta T+\tau)|T^{G_T}_{X(t+j\Delta T)}; Y(t+\tau)|T^{G_T}_{X(t)}] \Bigg) \end{aligned} \tag{28}$$

where $T^{G_T}_{X(t)}$ is of the same form as the theoretical general triggering condition.

$$T^{G_T}_{X(t)} = \{X(t) = a, \dot{X}(t) = b\} \tag{29}$$

The major problem is to calculate the general covariance between $Y(t+\tau)|T^{G_T}_{X(t)}$ and $Y(t+j\Delta T+\tau)|T^{G_T}_{X(t+j\Delta T)}$. Consider the following two Gaussian distributed stochastic vector processes.

$$\mathbf{X}_1 = [Y(t+\tau)\ Y(t+t_1+\tau)]^T \tag{30}$$

$$\mathbf{X}_2 = [X(t)\ X(t+t_1)\ \dot{X}(t)\ \dot{X}(t+t_1)]^T \tag{31}$$

The covariance of $\mathbf{X}_1$ on condition of $\mathbf{X}_2$ is

$$Cov[\mathbf{X}_1|\mathbf{X}_2] = \mathbf{R}_{\mathbf{X}_1\mathbf{X}_1} - \mathbf{R}_{\mathbf{X}_1\mathbf{X}_2}\mathbf{R}^{-1}_{\mathbf{X}_2\mathbf{X}_2}\mathbf{R}^T_{\mathbf{X}_1\mathbf{X}_2} \tag{32}$$

Using the definition of the correlation functions in eq. (5) the correlation matrices in (32) can be calculated from eqs. (29) - (30) ($\mathbf{X}$ and $\mathbf{Y}$ are assumed to have zero mean value).

The estimate of the variance of the RD functions involves the following computational steps.

- Sampling the time for each triggering point in estimation of the RD functions.
- Sorting the time differences between the triggering points.
- Numerical (two-time) differentiation of the RD functions (scaled to be the correlation functions).
- Calculating the variance estimate according to eq. (28).

None of these computational steps are extremely time consuming. The sampling of the time points for each triggering point is free, since these time points are identified in the estimation process of the RD functions.

Different simulation studies have been performed and the new approach is superior with respect to accuracy compared to the traditional methods. The method is introduced in Asmussen [1] and Asmussen et al. [2].

# 7 Estimation of Frequency Response Functions

A new method for estimating FRF has been tested. The method is based on the RD functions of the load to and the response from a linear system. It is assumed that the input is stochastic and stationary. Traditionally the measured response of and load on a linear system have been analysed using the FFT algorithm in order to obtain the FRFs. As described in the introduction to this thesis such an approach will in general always result in biased estimates of the FRM. Using the RD technique as basis a for the estimation of the FRFs bias can under the right circumstances be removed. This is an important feature of the RD technique. This method was first tested in Brincker et al. [8] and Asmussen et al. [3].

By introducing the Fourier transform of an RD function as $Z_{XY}(\omega)$ defined as

$$Z_{XY}(\omega) = \frac{1}{2\pi}\int_{-\infty}^{\infty} e^{-i\omega\tau} D_{XY}(\tau) d\tau \tag{33}$$

the following frequency domain relation can be proven

$$Z_{YX}(\omega) = H(\omega)Z_{XX}(\omega) \tag{34}$$

and

$$Z_{YY}(\omega) = H(\omega)Z_{XY}(\omega) \tag{35}$$

These two equations constitute a basis for estimating $H(\omega)$. The approach in eq. (34) is denoted $H_1^{RD}$ and the approach in eq. (35) is denoted $H_2^{RD}$

$$H(\omega) = H_1^{RD} = \frac{Z_{YX}(\omega)}{Z_{XX}(\omega)} \tag{36}$$

$$H(\omega) = H_2^{RD} = \frac{Z_{YY}(\omega)}{Z_{XY}(\omega)} \tag{37}$$

The main advantage of this approach compared to the traditional approach based on pure FFT is that the natural decay of the RD functions makes it possible to avoid bias or leakage.

This is illustrated in fig. 5, where a theoretical FRF of an SDOF system is plotted together with an FFT based estimate and an RD-FFT based estimate. The advantage of unbiased estimates is obvious.

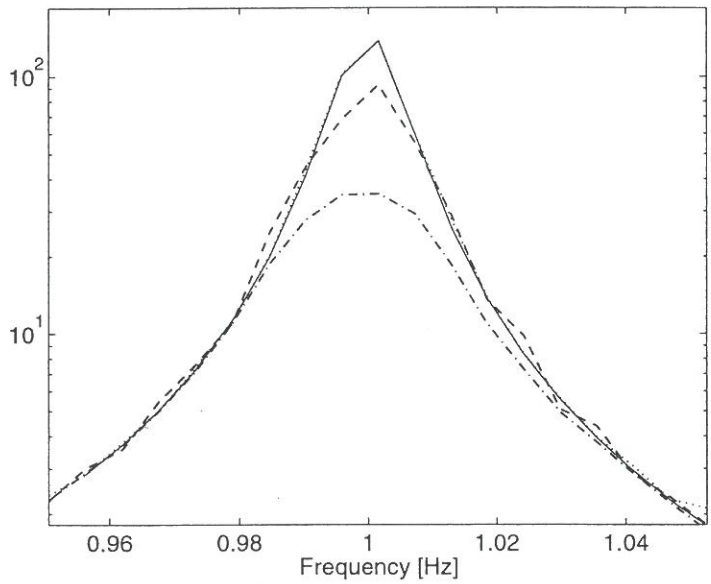


Figure 5: *Zoom of absolute value of the FRFs. [——]: Theoretical. [- - - - ]: FFT Hanning window, $H_1$. [· · · · ]: RD-FFT, No windowing, $H_1^{RD}$. [· – · – ·]: RDD-FFT, exponential window, $H_1^{RD}$.*

# 8 Application of the Random Decrement Technique to Civil Engineering Structures

The main advantages of the RD technique is the low estimation time and the simple estimation algorithm. The advantage of a low estimation time can be utilized in identification of large

structures, where the response of the structure is collected at many locations. In general this is the situation in ambient testing of bridges. Ambient testing of bridges refers to measurements of the vibrations of bridges due to ambient loads such as traffic, wind, waves and micro tremors.

During this project three different bridges have been analysed: The Queensborough bridge, a laboratory bridge model and the Vestvej bridge.

The Queensborough bridge crosses the Fraser river near Vancouver B.C., Canada. The bridge has a length of 200 m and has 3 spans. An outline draft of the bridge is shown in figure 6.

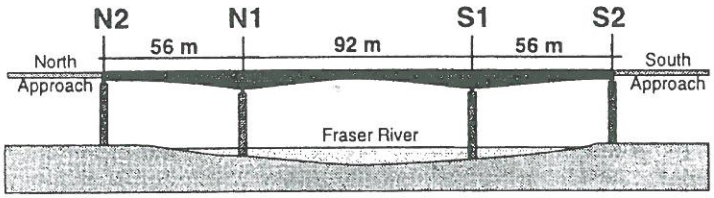


Figure 6: *Outline draft of the Queensborough bridge.*

The analysis of the Queensborough bridge is presented in Asmussen et al. [5].

The purpose of analysing the laboratory bridge model is to make the final development and documentation of the VRD technique. The bridge model is a 3-span simply supported 0.01 m thick steel plate with a total length of 3 m and a width of 0.35 m. Figure 7 illustrates the laboratory bridge model.

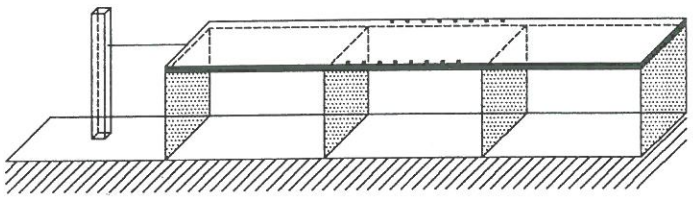

Figure 7: *Laboratory bridge model and sensor locations.*

The analysis of the bridge model is presented in Asmussen et al. [10].

The ambient vibration study of the Vestvej bridge forms the initial part of a demonstration project concerning the application of vibration based inspection to bridges. The Vestvej bridge is shown in fig. 8. The project is carried out with RAMBOLL and the Danish Road Directorate.

Figure 8: *The Vestvej bridge.*

The analysis of the Vestvej bridge is presented in Asmussen et al. [12], [13], [14] and [15]. The measuremenents of the Vestvej bridge were collected using a bridge measurement system developed as a part of this project.

# 9 Implementation of the Random Decrement Technique

During the project period different functions have been programmed in MATLAB. These functions are currently being improved and generalized in MATLAB. A Graphical User Interface is under construction.

The programming is expected finished at the end of 1997. A user manual is going to be published with the examples of identification of civil engineering structures performed during this project. The finished program will be presented at the adress http://www.civil.auc.dk/ i6jca.

# 10 Conclusions

During this project identification of civil engineering structures using the Random Decrement technique has been performed. The theory of the Random Decrement has been extended by the following developments

- Introduction of the general applied triggering condition including the derivation of the relation between the RD functions and correlation functions.
- Introduction of the Vector triggering Random Decrement technique. Derivation of the theoretical background of this approach in terms of correlation functions and validation of the technique by simulation and experimental studies.
- Introduction of the idea, theory and validation of a new approach for predicting the variance of Random Decrement functions.

The practical application of the Random Decrement has also been improved by

- Introduction of a new concept: Quality assessment.
- New guidelines for the choice of triggering levels.
- Comparison with other unbiased estimators of correlation functions.

The technique has been tested on several different structures:

- The Queensborough bridge.
- A laboratory bridge model.
- The Vestvej bridge.

Furthermore, a bridge measurement system has been developed as a part of this project and a MATLAB graphical user interface for identification of ambient excited structures is going to be finished 1/1 1998.

It is concluded that the project more than fulfils the expectations prior to the start of the project.

# References

[1] Asmussen, J.C. *Modal Analysis Based on the Random Decrement Technique - Application to Civil Engineering Structures* Ph.D.-Thesis, Aalborg University, Denmark, ISSN

[2] P.H. Kirkegaard, J.C. Asmussen, P. Andersen & R. Brincker. *An Experimental Study of an Offshore Platform.* Fracture and Dynamics paper No. 72, Aalborg University 1994.

[3] Asmussen, J.C. & Brincker, R. *Estimation of Frequency Response Functions by Random Decrement.* Proc. 14th International Modal Analysis Conference, Dearborn, Michigan, USA, February 1996, Vol I, pp. 246-252.

[4] Ibrahim, S.R., Asmussen, J.C. & Brincker, R. *Modal Parameter Identification from Responses of General Unkonwn Random Inputs.* Proc. 14th International Modal Analysis Conference, Dearborn, Michigan, USA, February 1996, Vol I, pp. 446-452.

[5] Asmussen, J.C., Ibrahim, S.R. & Brincker, R. *Random Decrement and Regression Analysis of Traffic Responses of Bridges.* Proc. 14th International Modal Analysis Conference, Dearborn, Michigan, USA, February 1996, Vol I, pp. 453-458.

[6] Asmussen, J.C. & Brincker, R. *Estimation of Correlation Functions by Random Decrement.* Proc. ISMA21 - Noise and Vibration Engineering, Leuven, Belgium, September 18-20 1996, Vol II, pp. 1215-1224.

[7] Asmussen, J.C., Andersen, P., Brincker, R. & Manos, G.C. *Identification of the Euro-Seis Test Structure.* Fracture and Dynamics Paper No. 76, Aalborg University, March 1996.

[8] Brincker, R. & Asmussen, J.C. *Random Decrement Based FRF Estimation.* Proc. 15th International Modal Analysis Conference, Orlando, Florida, USA, February 3-6 1997, Vol. II, pp. 1571-1576.

[9] Ibrahim, S.R., Asmussen, J.C. & Brincker, R. *Theory of Vector Triggering Random Decrement.* Proc. 15th International Modal Analysis Conference, Orlando, Florida, USA, February 3-6 1997, Vol. I, pp. 502-509.

[10] Asmussen, J.C., Ibrahim, S.R. & Brincker, R. *Application of Vector Triggering Random Decrement.* Proc. 15th International Modal Analysis Conference, Orlando, Florida, USA, February 3-6 1997, Vol. II pp. 1165-1171.

[11] Ibrahim, S.R., Asmussen, J.C. & Brincker, R. *Vector Triggering Random Decrement for High Identification Accuracy.* Accepted for publication in Journal of Vibration and Acoustics.

[12] Asmussen, J.C., Brincker, R. & Rytter, A. *Ambient Vibration Testing of the Vestvej Bridge - Full Virgin Measurements: 1st Study.* Report to the Danish Road Directorate and RAMBOLL, April 1997.

[13] Asmussen, J.C., Brincker, R. & Rytter, A. *Ambient Vibration Testing of the Vestvej Bridge - Full Virgin Measurements: 2nd Study.* Report to the Danish Road Directorate and RAMBOLL, June 1997.

[14] Asmussen, J.C., Brincker, R. & Rytter, A. *Ambient Vibration Testing of the Vestvej Bridge - Full Virgin Measurements: 3rd Study.* Report to the Danish Road Directorate and RAMBOLL, October 1997.

[15] Asmussen, J.C., Ibrahim, S.R. & Brincker, R. *Random Decrement: Application to Identification of Ambient Excited Structures.* To be presented at the 16th International Modal Analysis Conference, Santa Barbara, California, USA, February 2-5 1998.

[16] Asmussen, J.C. & Brincker, R. *A New Approach for Predicting the Variance of Random Decrement Functions.* To be presented at the 16th International Modal Analysis Conference, Santa Barbara, California, USA, February 2-5 1998.

[17] Asmussen, J.C., Rytter, A. & Brincker, R. *Ambient Testing of the Vestvej Bridge Using Random Decrement.* To be presented at the 16th International Modal Analysis Conference, Santa Barbara, California, USA, February 2-5 1998.

[18] Asmussen, J.C. & R. Brincker. *A New Approach for Predicting the Variance of Random Decrement Functions.* Submitted to Journal of Mechanical Systems and Signal Processing.

[19] Asmussen, J.C., Ibrahim, S.R. & Brincker, R. *Statistical Theory of the Vector Random Decrement Technique.* Submitted to Journal of Sound and Vibration.

# PROJECT B3

# Fatigue and crack propagation

Project B3 deals with a newly developed crack growth model based on an energy criterion. The model is able to predict crack propagation in ductile as well as brittle materials.

The crack propagation formula is a first order differential equation. The energy changes required may be determined using simple linear elastic finite element methods. The non linearity is taken into account using Irwins crack length correction.

The theory is compared with experimental results with three point bending test on concrete beams. It is shown that the theory is able to predict size effects.

Furthermore the theory is compared with tests on fatigue loaded high strength steel and aluminium. The relation between the stress intensity factor $K_I$ and the critical stress intensity factor $K_{IC}$ is the main issue. Tests determining $K_{IC}$ as a function of $K_I$ have been performed. It is shown that $K_{IC}$ is not a constant, but clearly depends on $K_I$.

The theory has been compared with test results on welded connection. The effect from residual stresses and crack closure is taking into account.

The results are presented in 4 reports, which are shortly described including the main conclusions in the following.

## Fatigue and crack propagation

### Abstract

The main purpose of this paper is to test a new theory of crack propagation by comparing its results with test results. The advantage of the new theory is that crack propagation may be predicted on the basis of knowledge of well-known material parameters, contrary to the empirical formulas, the parameters of which must be determined by time consuming fatigue tests.
The paper is divided into three main parts:

- Presentation of the new theory (chapter 2)
- Presentation of test results (chapter 3-5)
- Calculation of the crack propagation using the new theory, and comparing test results with calculated results. (chapter 6)

The theory is based on an energy balance criterion. This leads to a formula, which is a first order differential equation to be solved numerically. The method chosen to solve the equation is the Runge Kutta method.

To test the theory three types of tests have been performed. Firstly a simple tension test to determine the yield strength and the true fracture strength and the modulus of elasticity (chapter 3). Secondly a standard $K_{IC}$ test to determine the critical stress intensity factor $K_{IC}$, and to show the dependency of $K_{IC}$ upon the stress intensity factor $K_I$ (chapter 4). Finally a fatigue test was performed (chapter 5). All the tests were done on three different materials. The chosen materials are two high strength aluminiums (Al2024 and Al7075) and one high strength steel (Hardox400).

The results from the three tests are analysed in chapter 6, and the crack propagation behavior is calculated on the basis of the test results from chapter 3 and 4, and is finally compared with the fatigue tests from chapter 5.

**Main conclusions**

The main purpose of this paper is to support the newly developed theory for predicting crack propagation behavior under fatigue loading by comparing the calculated results with test results.

The two main topics discussed throughout the paper are the size effect on the ultimate stresses and the relation between the stress intensity factor $K_I$ and the critical stress intensity factor $K_{IC}$.

The most important result of the investigation performed is that in order to make reliable predictions about crack growth two important issues must be considered.

First it must be taken into account, that the critical value of the stress intensity factor or the fracture energy varies with the stress intensity level. Relations have been measured for three materials and they clearly exhibit such a relationship.

Second it must be taken into account, that the ultimate stresses at the crack tip are much higher than the usual values obtained by standard laboratory measurements. To calculate the enhanced values is extremely difficult, and has never to the authors opinion been done before. In the paper it has been suggested to base the calculation on Weibulls theory of size effects. However it turned out that the size range, which can be obtained in the laboratory, is far too small to get reliable results. To remedy this situation, it has been suggested to base the calculation of the Weibull parameters on the Orowan estimate of the atomic strength, i.e. the strength of a perfect crystal free of dislocations, grain boundaries, foreign particles etc.
The solution presented of the two basic problems in deriving a theoretical formula for crack growth was shown to give good estimates of the crack growth, far better than the results obtained by other theoretical crack growth formulas.

However much more work is necessary to cover the whole range of relevant materials and to cover the relevant strength range for the individual materials.

## Fatigue in high strength steel

### Abstract

The main purpose of this paper is to present some tests with high strength steel. The paper is a follow-up of the work on fatigue and crack propagation, see above. It is the purpose to further evaluate the new theory of crack propagation by comparing its results with test results.

The paper is divided into four main parts:
- Fracture toughness standard tests (chapter 2)
- Fatigue tests (chapter 3)
- Prediction of crack propagation using the new theory, and comparing the theory with test results (chapter 4)

The relation between the stress intensity factor $K_I$ and the critical stress intensity factor $K_{IC}$ is the main issue. Tests determining $K_{IC}$ as a function of $K_I$ have been performed. It is shown that $K_{IC}$ is not a constant, but clearly depends on $K_I$. The results are used to predict fatigue behaviour of high strength steel using the Energy Crack Propagation Formula (ECP).

### Main conclusion

This paper is a follow-up on the work described in Fatigue and crack propagation, see above. The main purpose has been to further evaluate the basic concepts of the Energy Crack Propagation Formula (ECP), and to examine the capability of ECP to predict crack propagation behaviour.

As a main conclusion it has been verified that the critical stress intensity factor $K_{IC}$ varies with the stress intensity level. It has been shown that this dependency may be used to calculate the slope of the da/dN-$\Delta K_I$ curve, which means that it is possible to calculate the Paris m value.

The level of crack propagation rate is highly dependent on the ultimate strength and the critical stress intensity factor $K_{IC}$. It has been shown, that for the steel tested, ECP can not estimate the level of the crack propagation rate in its present form. Several parameters influence the fracture mechanical parameters, such as microstructure, size effects, hardening of the material etc. It is necessary to perform further research in these areas in order to understand the effect on the fracture mechanical parameters.

The effect of crack closure has been investigated. It was shown that to some extent this may explain the delay in fatigue crack growth, but much more research is needed in this field before any final conclusion may be drawn.

The Energy Crack Propagation formula (ECP) has been shown to be able to predict crack propagation in different metals in this and the earlier work, when the correct fracture mechanical parameters are used. Therefore the model can be recommended for future research to understand the mechanisms of fatigue and crack propagation. Even more research is needed before it can be used for practical applications.

## Fatigue in welded connections

### Abstract

In this paper the theory is compared with two types of welded test specimens, using the da/dN-$K_I$ and the S-N concept respectively.

Firstly a tests series performed by Glinka is chosen because it very clearly shows how the crack velocity da/dN depends on the type of weld in the plates. The test specimen is a standard Welded Center Cracked testspecimen (WCCT) welded together in different directions compared to the crack propagation direction. This results in different residual stress fields in the specimens and the capability of the crack propagation formula to predict the effect from this examined. Secondly a test series with welded joints (WJT) performed by Ibsø is investigated.The test series has been chosen because the welded joint plates are very similar to those used in real structures, as for example off shore structures. It is examined whether the crack propagation formula is able to predict the crack propagation and determine the fatigue life of the specimens.

The report touches upon subjects like residual stresses, the so-called R-ratio and crack closure when evaluating the new theory.

### Main Conclusions

In the present investigation, the fatigue life of welded connections under constant amplitude loading has been studied. It has been the main purpose to examine the capability of the Energy Crack Propagation Formula (ECP) to predict crack propagation. Two tests series influenced by different parameters, such as residual stresses, the stress ratio R and crack closure are examined.

The overall conclusion is that ECP is able to predict crack propagation in welded connections and estimate the fatigue life very well.

A new method to take the influence of the R ratio into account has been derived. The method showed better results than those found by Forman's equation. Still a comparison with more tests has to be carried out before a final conclusion regarding the validity of the method can be made.

In the investigation of the WCCT specimen a large influence of the residual stress field was observed. In the paper an approximate method to take the residual stresses into account was introduced. Very

good results were obtained both in the tension and in the compression residual stress field range. It was shown that ECP was able to predict the change of the crack propagation rate very precisely, when the minimum stress including the residual stress was less than zero. This might encourage to investigate the capability of ECP when applied to specimens with $R<0$ and, using a similar procedure.

The method is simple and may be used for practical applications, but more tests must be evaluated to ensure the general validity of the method.

It was shown that crack closure could be taken into account using a very simple empirical equation. Although the empirical relation is based on a large theoretical investigation the result can not be considered as a general way to describe the effect from crack closure. However, the method used does indicate that crack closure might be determined solely on the basis of the maximum stress level including the residual stress, and on the assumption that the minimum stress is less than the crack opening stress.

To fully understand the effect of residual stresses, R-ratio and crack closure, more research is still needed. It has been the purpose of this paper to present a new theory, to evaluate it, and hopefully to encourage the reader to apply it to other test conditions and thereby getting closer to the understanding of the behaviour of crack propagation in welded connections.

## Fracture and crack growth in concrete

### Abstract

This paper examines the crack propagation formulas capability to predict crack propagation in concrete.

A parametric study of the crack propagation formula has been carried out, in order to evaluate the consistency of the theory. It is shown that the theory is able to predict size effects and crack propagation in ductile as well as brittle materials.

In order to investigate the capability of the model a comparison carried out between theory and experimental results is obtained with three point bending tests on plain concrete.

Full load - deflection curves for three point bending tests where material properties of concrete such as compressive strength and maximum aggregate size together with beam dimensions are varied, are compared with theoretical results.

The crack propagation formula presented is able to predict the peak value and part of the descending branch of the load - deflection curve for different strength levels, notch height ratios and maximum aggregate sizes.

## Main conclusions

The main purpose of this report has been to support the newly developed theory for predicting crack propagation behaviour under static load conditions, applied to concrete structures, by comparing the calculated results with test results.

Furthermore it has been the aim to investigate the crack propagation formulas capability to predict crack propagation under static loading condition upon both ductile and brittle materials in general, and to examine the models capability of predicting the size effect.

The important part of the investigation is that it has been shown that the process zone or the crack length correction $l_e$ varies with the the fracture energy $G_F$, meaning that the theory do solve the basically fracture mechanics problems when applied to any material, ductile or brittle. This results in the fact that the crack propagation formula is able to predict the size effect.

The model has been compared with experimental results of three point bending tests of plain concrete beams. The main conclusions are that the theory presented is able to predict the peak value and part of the descending branch of the load - deflection curve for different strength levels, variation of notch depth ratios and maximum aggregate sizes. It may be concluded that the theory is applicable to concrete.

The model has not been able to predict the fully descending part. The reason is that the process zone or more precise Irwins crack length correction $l_e$ is determined on the basis of the stress concentration factor of the first term, which only is valid for small values of $l_e$ compared to the crack length a. The solution gives increasing $l_e$ for increasing a. It has presently been shown that by taking account for the linear second term of the stress concentration factor, $l_e$ will decrease for large values of a, which results in a determination of the fully descending part of the load-deflection curve. However much more work is necessary to fully understand the theoretical behavior of the crack correction length $l_e$, if the theory shall be able to predict the fully descending part of the load deflection curve.

However it may be concluded that with this newly developed theory it is possible, with very simple calculations, to predict crack propagation, load and deflection in any material subjected to statical loading.

## References

[1] Fatigue and crack propagation, BKM, Technical University of Denmark, Report no 316, T.C.Hansen, 1994

[2] Fatigue in high strengths steel, BKM, Technical University of Denmark, Report no 9, T.C.Hansen, 1996

[3] Fatigue in welded connections, BKM, Technical University of Denmark, Report no 10, T.C.Hansen, 1996

[4] Fracture and crack growth in concrete, BKM, Technical University of Denmark, Report no 11, T.C.Hansen and D.H.Olsen, 1996

# C1 Behaviour of Soil Subjected to Dynamic Loads

Lars Bødker
*Aalborg University, Aalborg, Denmark*

SYNOPSIS: Many geotechnical problems involve design of dynamically loaded foundations. The design criterion for dynamically loaded foundations is often described in terms of limiting values for the displacements. The displacements in the soil are normally very small when dealing with dynamically loaded foundations, and hence it is necessary to know the deformation properties for the soil at very low strain level. The main topic of the project is to increase the knowledge of the behaviour of Danish soils at small strain levels and to extend the laboratory facilities to deal with testing at small strains. The soil behaviour at very small strain levels is non-linear, and the most common testing technique for this situation is the resonant column technique. One of the aims of this project is to install, check, get familiar with and perform tests on different kinds of Danish soils in a new Drnevich Longitudinal-Torsional Resonant Column apparatus placed at the Soil Mechanics Laboratory at Aalborg University. Another, but quite new technique for small strain testing to determine the maximum shear modulus, $G_{max}$, is the bender element technique, and as part of the project this technique has also been introduced in the laboratory.

## 1 INTRODUCTION.

Very often geotechnical problems involve design of foundations to resist dynamic loading. Dynamic loading is characterised by the magnitude of the load fluctuating with time and the deformations of the soil consist of both recoverable and permanent displacements. Problems associated with dynamic loading are normally connected to the following design situations:

- machine foundations
- off shore structures exposed to wind- and wave loading
- on shore structures e.g. windmills
- structures exposed to traffic loading
- structures exposed to vibrations from earthquakes
- structures exposed to blasting

Foundations exposed to dynamic loading must normally fulfil both a static and a dynamic design criterion. The static criterion normally requires both safety against failure and acceptable permanent displacements of the structure. The dynamic criterion also requires safety against failure, acceptable level of permanent displacements caused by consolidation from excess pore pressure generated by the dynamic loading, acceptable variable displacements of the foundation and safety against liquefaction. Very often the final design of foundations exposed to dynamic loading is determined by the established criteria to the variable deformations of the foundation.

Normally the design criterion for dynamically loaded foundations is described in terms of limiting values of accelerations, velocities or displacements. The limits are determined based on comfort requirements and the use of the structure. Figure 1 illustrates some general criteria depending on the actual use of the structure. The criteria presented in the figure are only intended as guidelines and they are

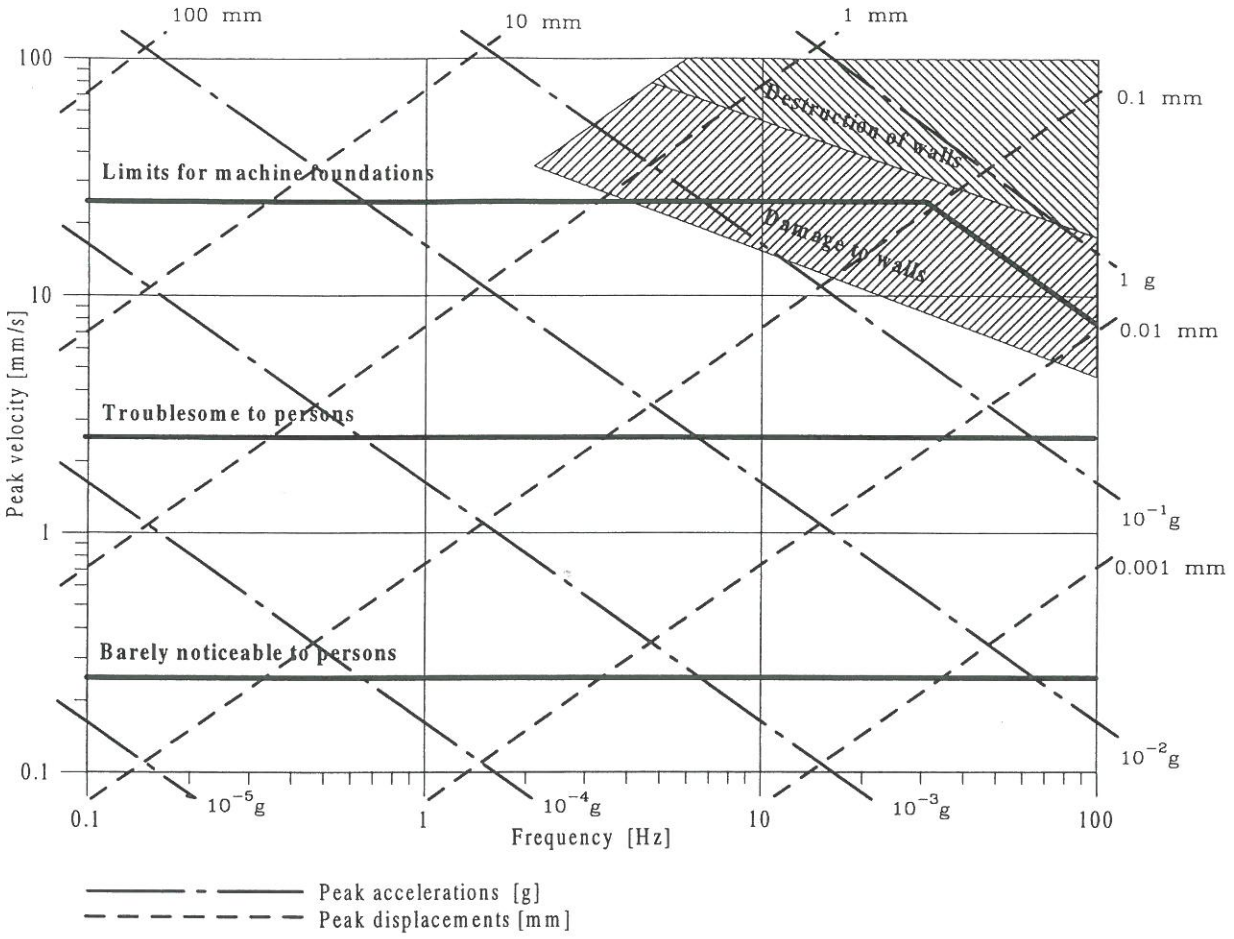


*Fig. 1 Criteria for displacements, velocities and accelerations of foundations due to dynamic loading (after Richart, Hall & Wood, 1970). The criteria presented in the figure are only intended as guidelines.*

based on motions of structures caused by blasting.

The criteria illustrated in Figure 1 are not unique as it may appear from the figure. First of all the limits are established due to tests with blasting. Therefore the persons and structures involved in the study are only exposed to a few cycles of vibrations. Secondly, the sound from the blasting may affect the way the persons perceive the vibrations. Thirdly, noise from the structures due to the vibrations will influence the limits for persons. Finally, distinction between secondary - such as windows and doors - and primary part of structures have to be made. Often seriously damage is observed on the secondary parts while the primary parts are intact.

From Figure 1 it appears that the sensitivity of persons often are the crucial factor when designing structures exposed to dynamic loading. Even at very low levels of vibration persons notice the movements and feel it troublesome.

During the last decades extensive work has been put into developing new and more accurate models to predict the behaviour of dynamically loaded foundations. Depending on the design situation the models both involve wave propagation through the soil strata and half space theories, where foundations are assumed to rest on a half space, which in general will be modelled using spring and damping elements. Common to the models is that values for the stiffness and damping of the soil are required.

Because the behaviour of soil is very non-linear also for very small strain levels, the deformation parameters for the soil has to be determined at the stress and strain level for the actual design situation. The deformations due to the dynamic loading are normally very

small, and hence the behaviour of the soil has to be investigated at very small strain levels.

Behaviour of soils is a mixture of elastic and plastic behaviour. The elastic properties of the soil structure are primarily due to the behaviour of the individual grain and the contact between the grains, while the plastic behaviour is related to rearrangement of the grains or chemical/electrical bindings between the grains. At very low strain levels the soil exhibit elastic, albeit clearly non-linear, behaviour. Hence, it is essential to obtain reliable estimates of the elastic deformation parameters of soil, in particular at small strain levels for dynamically loaded foundations.

In Denmark no laboratory equipment for measuring the properties of soil at very low strain levels were present at the beginning of the work, and this fact initiated the content of the current project. Concurrently with development of new and more accurate models to describe the behaviour of soil the need for determination of the parameters at low strain levels for Danish soils also increases.

*1.1 Content of project*

The current project deals with determination of the elastic properties, such as Young's modulus, the shear modulus, Poisson's ratio, and damping of both frictional soils and cohesive soils. These parameters typically form part of the analyses of foundations exposed to dynamic loading. The parameters can be determined experimentally by performing tests where the testing condition comply with the dynamic loading situation. The tests can be performed either in the field or in the laboratory. The present work is aimed at measuring and analysing the elastic deformation parameters determined only in the laboratory for different kinds of soils exhibited to dynamic loading. At small strain levels traditional laboratory tests, such as e.g. triaxial tests and simple shear tests, are not capable of describing the behaviour of soils for the mentioned conditions. Alternative tests have to be performed. The most common laboratory tests are resonant column tests and tests using piezocheramic bender elements. The resonant column testing technique was introduced in the 1940s and has been used in earnest since the 1950s, while the technique with bender elements is quite new in connection with soil testing.

In the current project the work has concentrated on introducing and developing new techniques for testing soil at low strain levels in the Soil Mechanics Laboratory at Aalborg University, AAU. At the beginning of the project a simple longitudinal resonant column apparatus was present at the laboratory, but the apparatus was limited to operate with stress states in the range of 0-100 kPa. In the project the facilities at the laboratory have been extended both with a longitudinal-torsional resonant column apparatus and introduction of bender elements in test set-ups.

The advantage of the resonant column device is that it is possible to control the strain level applied to the specimen during the dynamic testing. This facilitates the study of the non-linearity also at very low strain levels. In the tests using bender elements it is not possible to control the strain level, but instead the elements can be fitted into many conventional geotechnical testing equipment's.

By necessity, the main focus of the project had to be shifted from production terms to proof terms of the behaviour of the equipment and development and evaluation of interpretation techniques. To this end a number of tests on different kinds of clay and sand have been carried out in the new devices.

Besides the described content of the current project, some co-operative projects has been carried out during the research period.

Firstly, a co-operative project was carried out with the EU-founded LITASEIS project which is an international and interdisciplinary project. This project is dealing with field- and laboratory measurements of the dynamic properties of soils.

Secondly, as a result of a research period of 4 month at the Norwegian Geotechnical Institute in Oslo, Norway in the beginning of 1995, a co-operative project with the company was initiated and carried out concerning execution and interpretation of results from bender element tests.

## 2 RESONANT COLUMN EQUIPMENT

The most common testing technique to determine the elastic parameters for soil is the resonant column testing. Several different kinds of apparatus are available today. However, the general testing technique is to apply a sinusoidal force, and then adjust the frequency of the force until resonance in the soil column is established. For the different apparatuses the main difference is in the boundary conditions.

The most common configurations of the apparatus are sketched in Figure 2. Commonly, the configuration of the apparatus are based on the "fixed-free" model. The three models require slightly different driving equipment and methods of data interpretation. Model a) in Figure 2 is the true "fixed-free, while model b) is slightly changed by adding a rigid mass at the top. This configuration is used in the Drnevich type apparatus. The last model is known as the Hardin type. This apparatus was developed in order to allow application of anisotropic stress states to the soil specimen. The other two configurations only allow isotropic stress states.

The resonant column method consists of applying a sinusoidal axial force or torque to a cylindrical soil specimen, which can either be solid or hollow. The applied force or torque generate either compression or shear waves that propagate through the specimen and are reflected at the other end of the specimen. The frequency of the applied force/torque is adjusted until resonance is established, and the moduli and damping ratio can be calculated. The main concern in interpretation of the measurements when doing resonant column test is, how the configuration of the apparatus is modelled and therefore how the performance of the apparatus fits the model. Especially, it is very important that the modelled and actual boundary conditions are in agreement. Mostly, a single degree of freedom model is supposed. Here one end of the specimen is supposed totally fixed, and at the other end a totally rigid mass is attached.

The apparatus that has been installed at the laboratory as part of the project is of the Drnevich type. The advantage of this type of device is, that it is capable of applying both longitudinal and torsional motions to the soil specimen and therefore allow both determination of Young's modulus, shear modulus and damping ratio at low strain levels. Applying both longitudinal and torsional motions also enables determination of Poisson's ratio, which is a key parameter in most numerical models.

The apparatus is more or less constructed as a conventional triaxial cell and accommodates cylindrical specimens. The diameter of the specimens can be either 35.7 or 71.1 mm and height to diameter ratio of 2. The top and bottom caps are rough platens mounted with large filter stones. The rough platens are necessary to ensure total contact between the soil and platen during rotational motions. The void space of the specimen may be filled with air, partially saturated or fully saturated with water. To enhance the degree of saturation application of back pressure has been enabled.

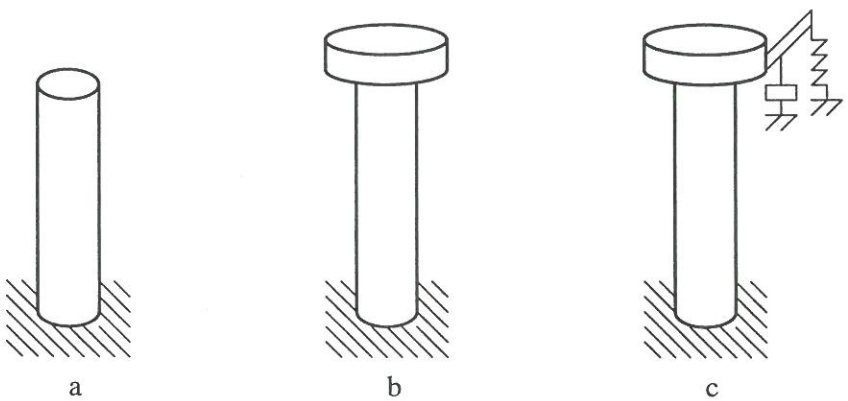


*Fig. 2 Principle of the most common configuration of the resonant column apparatus.*

The original device enabled drainage only as one-way or radial drainage. Construction of new top and bottom platens enables both one-way, two-way and/or radial drainage during the consolidation process. This reduces the consolidation time and the distribution of the pore pressure during consolidation is more uniform. The specimen is encapsulated in a latex membrane and surrounded by deaired water pressurised by means of regulated compressed air. The limit of the confining pressure for the apparatus is 700 kPa, and as mentioned before only isotropic stress states can be applied. The apparatus located at Aalborg University is shown in Figure 3.

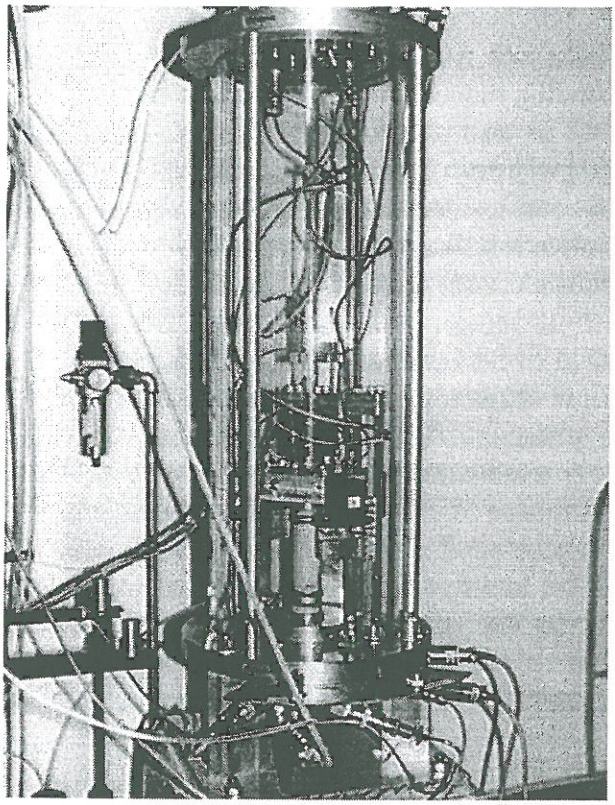

*Fig. 3 The Drnevich longitudinal-torsional resonant column device located at the Soil Mechanics Laboratory at Aalborg University.*

The force or torque is applied at the top of the specimen, while the bottom is supposed to be totally fixed. The force or torque is applied by means of coils and magnets. A sinusoidal voltage is applied to the coils, which in reaction with the magnets makes the top move. The movements are measured by means of

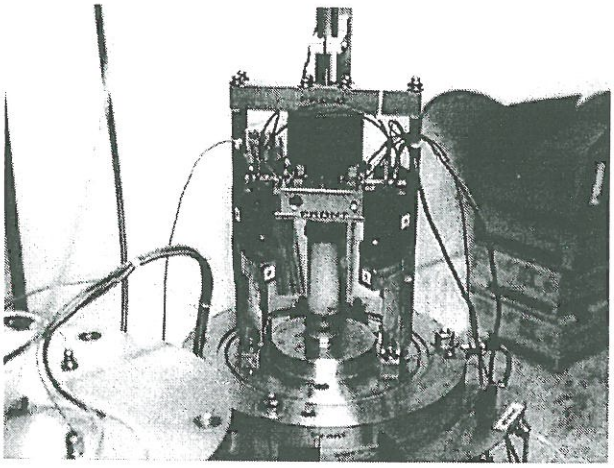

*Fig. 4 Detail of the loading system in resonant column device. Supporting frame for the magnets and coils and the top part is shown.*

accelerometers build into the top part. By adjusting the applied voltage the deformation level an therefore the strain can be adjusted. A detail of the system is shown in Figure 4.

The manufacturer of the apparatus prescribes how the apparatus must be installed to ensure proper performance when testing soil specimen. The apparatus is primarily made of steel and aluminium parts which are assembled with nuts. The cell is resting on three pedestals made of aluminium, which are bolted to an aluminium plate. The plate is connected to a block of concrete. The prescribed mass of the block is 140 kg. This should ensure fixity at the bottom of the specimen.

The installation of the apparatus was finished during spring 1996, and tests series on several different kinds of soils have been performed. The tested soils are both clay and sand.

As part of the project a four month research period at Norwegian Geotechnical Institute, NGI was included. The main purpose was to get familiar with the resonant column testing technique, and to perform some test in their resonant column device for duplication in the apparatus installed at AAU. By reproducing the tests, it is possible to see how the new apparatus behave compared with an old, well-tested apparatus. The apparatus at NGI is of the Hardin type, where only torsional motions are possible, and the results from the study

were presented in Bødker (1996). During the stay a lot of work was put into calibration and modelling of the apparatus, and five tests were performed. The soils used in the study were two kinds of clay, two kinds of sand and one silty soil. The soils were chosen to cover a large range of shear moduli.

A single degree fixed-free model, where the bottom of the soil specimen is supposed to be totally fixed, is used for interpretation of the measurements from the tests in the two apparatuses. The calculated shear moduli from the tests are shown in Figure 5. In the figure the corresponding results from the device located at AAU are plotted against the shear modulus calculated from the tests in the NGI device.

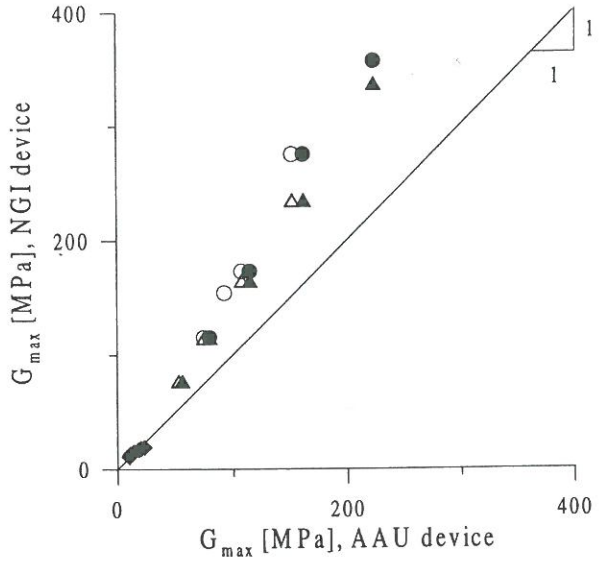


*Fig. 5 $G_{max}$ determined in the NGI and the AAU resonant column device.*

As seen from Figure 5 the results obtained in the AAU resonant column device deviate from the results from the NGI device. Therefore, the apparatus located at AAU has been thoroughly checked by placing accelerometers at different locations around the apparatus to observe the behaviour of the configuration when making a frequency sweep for both longitudinal and torsional motions. The response of the accelerometers showed, that the fixed boundary condition was not fulfilled. Therefore, the configuration of the apparatus has been changed. The mass of the concrete base has been increased and the stiffness of the bottom of the apparatus has been increased by removing the aluminium pedestals and the aluminium plate and replacing some of the connections.

To check the new configuration a hollow specimen of plastic with well known material properties and dimensions has been produced. The vertical and torsional stiffness of the constructed specimen has been matched to the stiffness of a soil specimen with a shear modulus of 100 MPa and a Young's modulus of 300 MPa. A new frequency sweep was applied and the response showed that the new configuration behaves better. But still the condition of fixity is not totally fulfilled and several resonance frequencies are observed. By placing accelerometers at each corner of the top part resting on the specimen it is seen that the different frequencies measured matches resonance for one translation mode and two bending modes.

The test with the plastic specimen shows that when performing tests and interpreting the measurements from the resonant column device installed at AAU several things have to be improved. First of all three accelerometers for torsional motions and three for translation have to be installed in the top part. By using three accelerometers for each measurement, it is possible to see whether the response is due to a translation resonance mode or a bending resonance mode. Secondly, a new model has to be developed in which the boundary condition is not totally fixed, but reflects reality. In this model the stiffness and mass of the moving part of the bottom has to be determined and modelled. By the proposed improvements the testing method and model will be more complicated, but the amount and quality of information obtained from the tests will be increased.

## 3 BENDER ELEMENT EQUIPMENT

The behaviour of soil is non-linear, but at strain levels below approximately $10^{-3}$ % the modulus, E or G, seems to be constant. Increasing the strain level above this limit the modulus decreases. The limiting or maximum value are normally termed $E_{max}$ and $G_{max}$.

A very straightforward method to determine the modulus at very low strain levels is obtained by using wave propagation, either by compression or shear waves. While compression wave velocity is influenced by the degree of saturation of the void space, the shear wave velocity is almost unaffected. A new testing method based on the wave propagation theory is the bender element technique (Dyvik and Madshus, 1985). Using a set of piezocheramic bender elements as transmitter and receiver a shear wave is generated and propagated through a soil specimen.

The earliest work concerning transducers to generate and measure shear waves involved shear plates made of piezoelectric material such as quartz crystal or piezoelectric ceramic. A piezoelectric material is a material that can convert electric voltage into mechanical motion and vice versa.

The earliest type of transducer using shear plates is not suitable for measuring the shear wave velocity in soil specimens. The main problem with the transducer is the mismatch between the impedance of the element and the soil skeleton. The mechanical motion that is transferred from the element to the soil specimen is small because the element exhibits a small movement with a large force, while the soil exhibits a large movement with a small force (Shirley and Hampton, 1978).

One way to overcome the mismatch between the mechanical performance of the element and the soil is to use piezoceramic bender elements. Piezoceramic bender elements consist of two thin piezoceramic plates cemented rigidly together. The polarization of the ceramic material in the plates and the electrical connection results in elongation and shortening of the two platens respectively when a driving voltage is applied to the element (Shirley and Hampton, 1978; and Shirley, 1978). The performance of an single bimorph element is sketched in Figure 6.

The aim of the work performed by Shirley and Hampton (1978), was to make a system to determine the wave velocity in-situ. The scope was to make an apparatus which during coring could measure both compression and shear wave velocities. After development of the new piezoceramic bender element transducer,

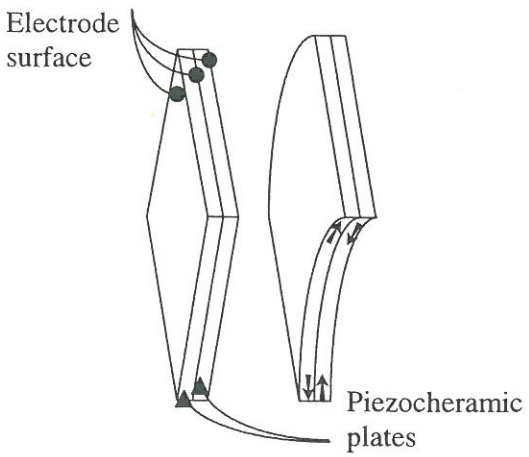


*Fig. 6 Principle of single bimorph piezoceramic bender element. Relaxed element at left and excited element at right.*

which was made of several bimorph elements Shirley and Hampton performed some tests on Kaolin clay in the laboratory using a transducer consisting of three bimorph elements fixed together. The results were very promising but because of the relatively high stiffness of the elements and therefor the small deflection the range of application is limited to high stiffness sediments. The noise sensitivity was also significant.

In Dyvik and Madshus (1985), a comprehensive work concerning construction of piezoceramic bender elements and implementation of these into conventional soil testing laboratory equipment is presented. They presented a bender element consisting of only a single bimorph element by which the stiffness of the bender element decreases significantly compared to the one used by Shirley and Hampton. Because of the small physical dimension of the bender elements it is easy to mount them in existing apparatuses. The advantages of incorporating the bender elements into existing laboratory equipment are that more information are obtained from standard laboratory tests. At the same time the need to run parallel resonant column tests to determine $G_{max}$ is eliminated and $G_{max}$ in itself can be a very useful guide during the consolidation process. These obvious advantages of using bender elements in existing laboratory equipment have increased the use considerably during the last decade.

Application of the bender element technique to determine the shear wave velocity and from this the shear modulus, is very simple if it is possible to generate and recognise the transmitted shear waves in the soil specimen.

The elements developed by Dyvik and Madshus seem to be suitable to generate and measure shear waves, and in 1985 they presented the comprehensive work carried out on specimens of clay, with shear modulus in the range of 10 - 100 MPa. In the paper they describe how to mount the elements in existing apparatuses and how to operate and interpret the results obtained from the elements. The equipment, they used, was the resonant column device fitted with bender elements. The advantage of using this apparatus is that the shear modulus is determined by two different and independent techniques but still on the same soil specimen. Hence, the calculated values for the modulus can be compared directly. The agreement between the moduli determined by the two methods was very good in the range of the testing.

Because of the promising results it was decided to introduce the technique at AAU as part of this project. The research in the project has been focused on two main subjects, namely comparison of shear moduli obtained by resonant column and bender element tests performed in the same device for a larger range of shear moduli and soil types, and

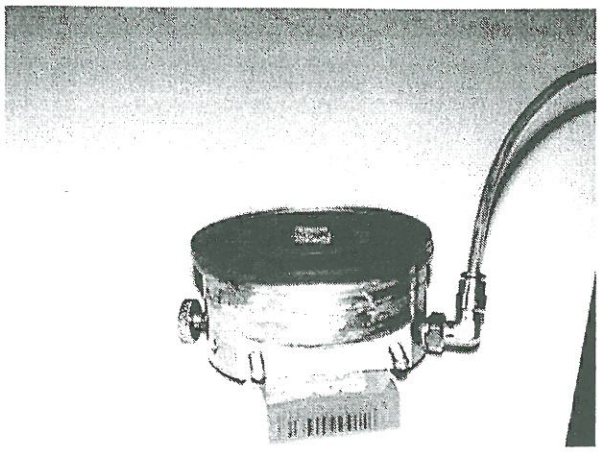

*Fig. 7 Bottom cap used in triaxial test fitted with bender element.*

development and performance of bender element tests in triaxial cells.

The first part has been carried out in the resonant column device located at NGI. The device is the Hardin type in which the platens have been fitted with bender elements. This enables concurrent resonant column and bender element tests on the same specimen.

The development of new equipment at the Soil Mechanics Laboratory at AAU has been concentrated on fitting the bender element technique to the triaxial test set-up. A bender element fitted into the bottom platen is shown in Figure 7 and the developed set-up is shown in Figure 8. Fitting the elements in the triaxial equipment makes the testing as flexible as the conventional triaxial test regarding the stress

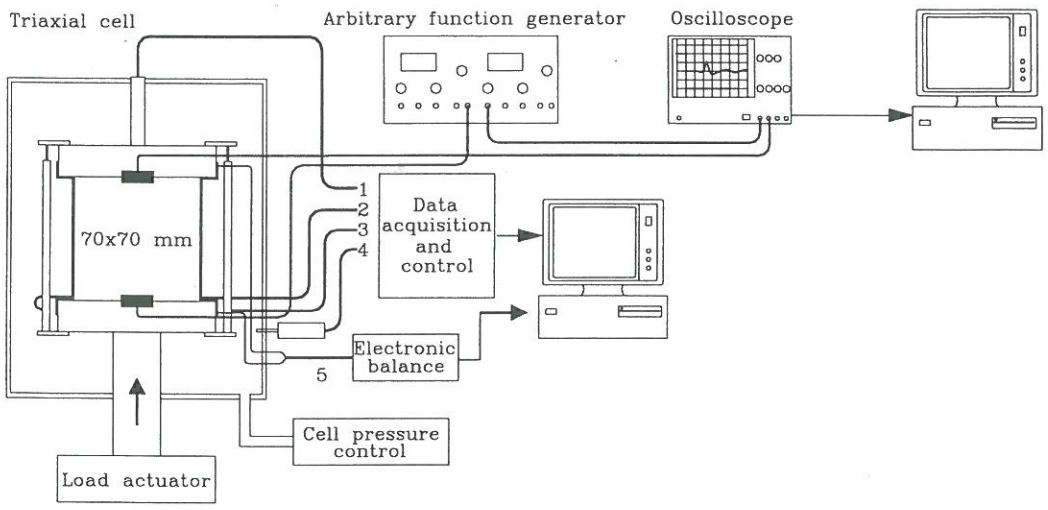


*Fig. 8 Principle of test set-up for bender element tests in triaxial cell.*

states. The elements are fitted into the same type of top and bottom platens as usually used in triaxial test, and both radial and vertical drainage is enabled and the platens are maintained as smooth. The dimensions of the element are HxBxD = 16x12x3 mm.

The developed set-up shown in Figure 8 allows testing of both cohesive and frictional soils, and isotropic as well as anisotropic stress states may be applied to the soil specimen. The results from the tests such as stresses, deformations and wave propagation's are all stored on a computer for mathematical analyses of the response of the soil.

*3.1 Testing technique.*

In the method developed by Dyvik and Madshus an electric pulse is applied to one of the elements to generate the shear wave. By use of an oscilloscope also connected to the element placed at the other end of the specimen, the trace of the generated and received shear wave is measured. By knowing the exact time of generating and receiving the wave, the travel time is determined. Combining this with the travel length, defined as height of specimen less the protrusion length of the elements into the specimen, the shear wave velocity may be calculated. Assuming elastic behaviour the shear modulus is calculated as $G = \rho v_s^2$, where $\rho$ is the density of the specimen, and $v_s$ is the shear wave velocity.

The driving signal used by Dyvik and Madshus (1985), was a square wave. This choice is due to the fact that the time at which the wave is generated and sent is well-defined and unique. The arrival of the wave is then defined as the first clear inversion of the received signal. A typical example of a recorded trace is shown in Figure 9 where the arrival definition according to Dyvik and Madshus is marked. The disadvantage of the method using a square wave as driving signal is that the interpretation procedure is very difficult to automate because the elements is very sensitive to electrical noise which may interfere the signals, and hence make it difficult to define the first inversion.

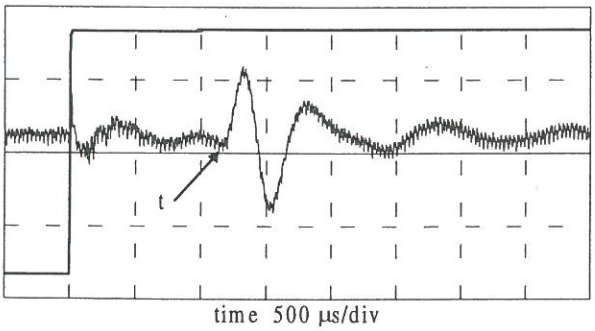


*Fig. 9 Typical trace of square wave and receiver signal. The arrival time according to the definition by Dyvik and Madshus is marked with t. The result is from a test on a clay with a shear modulus in the range of 50 MPa.*

A lot of workers have performed different kinds of tests using the bender elements. Dyvik and Madshus (1985), presented results from tests performed on five different kinds of clay, Langø (1991) presented results from tests on three different clays, Brignoli and Gotti (1992) performed tests on Kaolin clay, Suoto et al (1994) performed isotropically consolidated tests on road pavement materials such as sand and gravel, Viggiani and Atkinson (1995) performed a series of anisotropic consolidated tests on London clay and Bødker (1996) compared results from resonant column tests and bender elements for two kinds of sand, two kinds of clay and one silt.

The listed tests are all interpreted as described in Dyvik and Madshus (1985) using the single square wave as driving signal. The testing produce was developed in connection with tests on clay, and the range of shear moduli were quite limited. Extending the method to other materials and higher stiffnesses shows that very often it is hard to define the exact time of arrival of the shear wave (Bødker, 1996), see Figure 10.

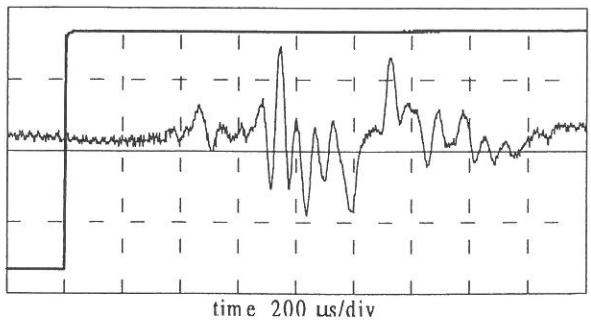


*Fig. 10 Driving and receiving signal for test on sand. Definition of arrival time is not unique.*

The stiffness determined by the bender element method in these tests is typically larger than the stiffness determined by the resonant column method when testing stiff materials. This can be due to the so-called near field effect, which is a small amplitude compression wave that is generated as the shear propagates through the soil. This compression wave will be observed a little time before the arrival of the shear wave, and therefore it will blurr the definition of the correct arrival time of the shear wave.

The fact that problems occur when testing stiffer materials and the want of developing a procedure to automate the interpretation, has initiated an extensive study of the behaviour when using other driving signals than the square wave. The study has been a co-operative project with NGI, and it has concerned sine waves and the so-called Ricker wavelet. The mathematical description of the wavelet is given as $g(t) = (1 - 2\pi^2 f^2 t^2) e^{-\pi^2 f^2 t^2}$, where f is the frequency at peak in the power-spectrum and t is the time. The driving signals which have been used in the study are sketched in Figure 11.

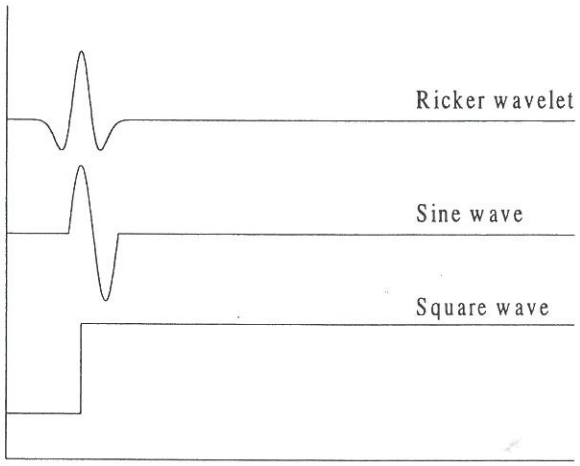


*Fig. 11 Driving signal used in co-operation project with NGI concerning automation of bender element test.*

The reason for using these waves is that it is possible to perform spectral analyses for both transmitted and received signals, and that the characteristic of the waves may minimise the effect of the near field compression wave. By using spectral analysis it is possible to mathematically calculate the travel time.

In the study of the effect of the type of driving signal applied to the transmitter both test on sand specimens and two different clays have been performed. The apparatus used is the NGI resonant column apparatus, which were installed at AAU for a period of two months. The set-up is in principle the same as shown for the triaxial cell in Figure 8. The time signals are all stored on the computer for further mathematical analysis.

The rationale for using the sine wave or Ricker wavelet is that it is possible to identify the transmitted signal in the received signal. The travel time is then calculated in two different ways. The travel time is determined by calculation of the cross-correlation between the driving and receiving signal, and by calculation of the slope of the frequency-phase diagram of the cross-spectrum.

To study the behaviour of the elements when excited, tests are performed where the elements are placed tip-to-tip. By placing the elements tip-to-tip the influence from the wave propagation through the soil skeleton is eliminated. The behaviour is studied both when the elements are surrounded by air and by different types of soil. When surrounding the elements by soil a thin slice of soil is placed between the elements in such a way that the tips just are in physical contact. The set-up with elements placed in air is shown in Figure 12.

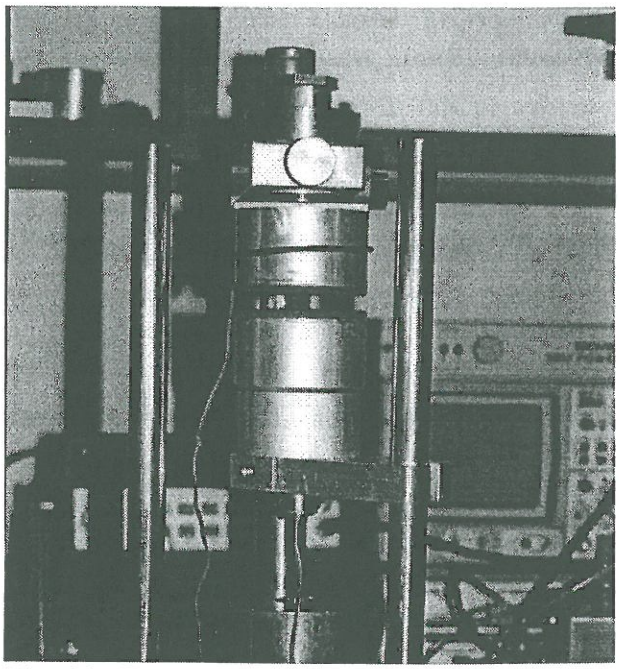

*Fig. 12 Test set-up when testing elements tip-to-tip in air.*

The response depending on the frequency of the driving signal of the elements is studied for the different types of waves. The frequency range tested for the sine wave and Ricker wavelet is 1 to 30 kHz.

The analysis shows, that when using a square wave as driving signal the deflection of the receiver placed in air is almost immediate and the peak of the deflection is delayed approximately 80 μs. Calculation of the power-spectrum for the receiver shows that the recorded time signal consist of waves with frequencies of 5 and 50 kHz. Analysing the response when elements are placed in soil shows that the deflection is also almost immediate. When placed in sand the response looks like when placed in air, while the 5 kHz wave disappears when placed in clay.

Tests using the sine wave or Ricker wavelet show, that a time lag between the transmitter and receiver is introduced and the time lag changes depending on the frequency of the driving signal. Testing with elements placed in air and sand shows that for frequencies less than 3 kHz, i.e. less than the first natural frequency observed at 5 kHz, the response of the receiver is identical to the signal applied to the transmitter.

Increasing the frequency results in a lot of vibrations and the response is not at all looking like the driving signal which consists of only a single wave. In the mathematical analysis problems arise when receiving more than one single wave because the transmitted signal must be uniquely identified in the received signal.

Testing with elements placed in clay shows that the amplitude of the received signal is very small, but the response is not as "dynamic" as when placed in sand or air. Only when applying signals with the high frequencies more than one deflection is observed.

Generally, the tests with elements placed tip-to-tip show that the cross-correlation method give applicable results when using frequencies well below the limit at which the response changes and becomes dynamic and completely different from the signal applied to the element used as transmitter. But mostly, when using sine wave or Ricker wavelet a time lag between transmitted and received signal is observed. This has to be taken into consideration when calculating the shear wave velocity in real tests.

The time lag for the tested materials with elements placed tip-to-tip is in the range of 0 to 30 μs. The analysis of the time lag determined by calculation of the phase shows results with large scatter. The slope of the frequency-phase line is very sensitive to the range of frequencies at which the fit of the slope is carried out.

Both Ricker wavelet and sine wave signals generate vibrations with smaller amplitudes compared to the square wave. This fact is very important when using the elements in real specimens because of the material and geometric damping. The amplitude of the shear wave can disappear in electric noise if the amplitude is too small. This fact is observed in some of the tests performed on specimens with a height from 70 to 140 mm, where it is almost impossible to observe the shear wave at some stress levels. When increasing the frequency the amplitude increases but the tendency for generating near field waves also increases and often the signal becomes "dynamic", i.e. a lot of vibrations of the receiver is observed. If the response of the receiver does not fit the transmitted signal the mathematical analysis gives uncertain results.

Because of the described problems and uncertainties in the method using the cross-correlation to determine the travel time of the shear wave it is not at this moment possible to automate the testing technique. The response and behaviour seem to depend on several factors such as soil type and stress level. At this moment the traditional method using the square wave can not be rejected, and the problems with the near-field waves have to be studied more closely in the future.

REFERENCES

Souto, A., Hartikainen, J. & Özüdogru, K. (1994). Measurement of dynamic parameters of road pavement materials by the bender element and resonant column tests. *Geotechnique,* vol. 44, No. 3, pp. 519-526.

Viggiani, G. & Atkinson, J. H. (1995). Stiffness of fine-grained soil at very small strains. *Geotechnique,* Vol. 45, No. 2, pp. 249-265.

Bødker, L. (1996). $G_{max}$ determined by bender element at anisotropic stress states, *Nordiskt Geoteknikermøde, NGM-96*, Reykjavik, 26-28 June 1996, pp. 93 - 98.

Richart, F. E., Hall, Jr. & Woods, R. D., (1970). *Vibrations of soil and foundations.* Prentice Hall, Inc., Englewood Cliffs, New Jersey, 1970.

Brignoli, E. & Gotti, M. (1992). Misure di velocità di onde di taglio in laboratorio con l'impiego di transduttori piezoelettrici. *Rivista Italiana di Geotecnica,* Vol. 1, pp. 5-16.

Langø, H. V. (1991). *Cyclic shear modulus of natural intact clays.* Ph.D. Thesis, Norwegian Institute of Technology, Trondheim.

Dyvik, R. & Madshus, C. (1985). Lab. measurements of $G_{max}$ using bender elements. *Advances in the art of testing under cyclic conditions, American Society of Civil Engineers,* pp. 186-192.

Shirley, D. J. (1978). *An Improved Shear Wave Transducer.* Journal of the Acoustical Society of America, 63 (5) May, pp. 1643-1645.

Shirley, D. J. & Hampton, L. D. (1978). *Shear-Wave measurements in Laboratory Sediments.* Journal of the Acoustical Society of America, 63 (2) Feb., pp. 607-613.

## PARTICIPANTS

Lars Bødker, Ph.D. student, Department of Civil Engineering, Aalborg University. Financed by the research program since 1.7.1994.

Lars Bo Ibsen, Assistant Professor, Department of Civil Engineering, Aalborg University.

# C.2 DYNAMIC RESPONSE OF COARSE GRANULAR MATERIALS TO WAVE LOADS

**Steen Krenk**

The theoretical work on the dilatant behavior of granular friction materials like sand has continued. A summary of a simple version of the theory was presented at the IUTAM Symposium on Granular and Porous Materials in Cambridge 1996 (Krenk, 1997a). This version of the model makes use of associated plasticity theory in a simple format that incorporates the dilatant behavior before failure. Theoretical work has continued on the identification of an improved plasic flow potential, and a promising theory has been developed for triaxial shear stress states, (Krenk, 1997b). This theory extends the classical Coulomb theory, by including the possibility of dilation. The friction is thereby divided into two parts - the classical material friction between grains, and a kinematic part due to relative motion of the grains. This theory seems to give qualitative correct behaviour, and avoids some inconsistencies present in previous theories. Furthermore it is in a format, where it can be extended to general stress states by a plausibility argument, thus leading to a general non-associated elasto-plastic theory for granular friction materials. Calibration procedures for this general model are presently being developed, and different ways of introducing hardening to obtain appropriate loading/unloading characteristics are being studied.

Krenk,S.: A characteristic state plasticity model for granular materials, *IUTAM symposium on Granular and Porous Media*, Eds. N.A. Fleck & A.C.F. Cocks, pp. 83-94, Kluwer, Dordrecht, 1997.

Krenk, S.: Friction, dilation and plastic flow potential, *NATO Advanced Study Institute on Physics of Dry Granular Materials*, Cargese, Corsica, September 15-26, 1997.

# C.2 Advanced Numerical Analysis of Caisson Breakwater on Frictional Materials

L.B. Ibsen, Andersen A.T, Madsen E.B, Schaarup-Jensen A.L

*Department of Civil Engineering, Aalborg University*
*DK-9000 Aalborg, Denmark*

The Single Hardening Model was introduced and investigated with the purpose of evaluating its capability of predicting the behaviour of frictional materials. The database, resulting from the work in project C.2.2, has been used for the calibration of the model. Besides providing a solid basis for the parameter study, the triaxial tests serve to elucidate the general behaviour of sand. Among other things, the aim of this work has been to investigate the applicability of the Single Hardening Model for solving geotechnical problems of a more complex nature. In this article a caisson breakwater structure, which has been tested in the centrifuge at Delft Geotechnics, is modelled in ABAQUS by means of the verified material model subroutine containing the Single Hardening Model. The response of the caisson is investigated under drained as well as undrained conditions. The results from the numerical analysis are compared to results obtained from the centrifuge test. Furthermore, an analytical bearing capacity analysis in the shape of an upper bound solution is put forward as a reference for the numerically obtained horizontal bearing capacity. Finally, reference numerical calculations based on the simpler Drucker-Prager Model are brought in for comparison. The performed analysis with the Single Hardening Model and have these analysis are compared, with analytical and the centrifuge test. The work is fully reported in (Andersen et all, 1998.a).

## 1 INTRODUCTION

Traditionally, a general geotechnical problem is divided into two parts which are considered individually. Thus, the bearing capacity of the given structure is calculated by means of the theory of plasticity, with no regard to the deformation taking place. In this bearing capacity analysis, the soil is assumed to behave perfectly plastic. Subsequently, the settlements of the structure in question are considered. In this phase, the response of the soil material beneath the foundation is often assumed to be linear elastic. However, considering the stress-strain curve obtained from e.g. a triaxial test on a soil specimen, it becomes clear that the actual soil response is highly non-linear. This implies that neither the assumption of perfect plasticity, nor the assumption of linear elasticity, fit the experimentally observed behaviour well.

Over the years, the capacity of computers has undergone large developments. Hereby, it has become obvious to bring more complex solution methods into the analysis of geotechnical problems. Thus, when dealing with problems with a complexity, which displays the traditional methods as defective, it is obvious to employ a finite element program as e.g. ABAQUS for the solution. However, in order to obtain reliable results from a finite element analysis, it is essential that the applied constitutive theory is capable of matching the experimentally observed behaviour of the considered material in a satisfactory way. In course of time, several constitutive theories have been proposed in order to provide this fundamental basis for an exact modelling of the response of soil materials. Of these could be mentioned: The Mohr-Coulomb Model, the Drucker-Prager Model, and the Cam Clay Model. However, each of the above mentioned soil models has its limitations as regards to capturing the response of certain soil materials. As an example it could be mentioned that the Cam Clay Model mentioned above is generally considered to be able to capture the response of normally consolidated clay, whereas the constitutive theory defined by this model is insufficient for describing the response of frictional materials.

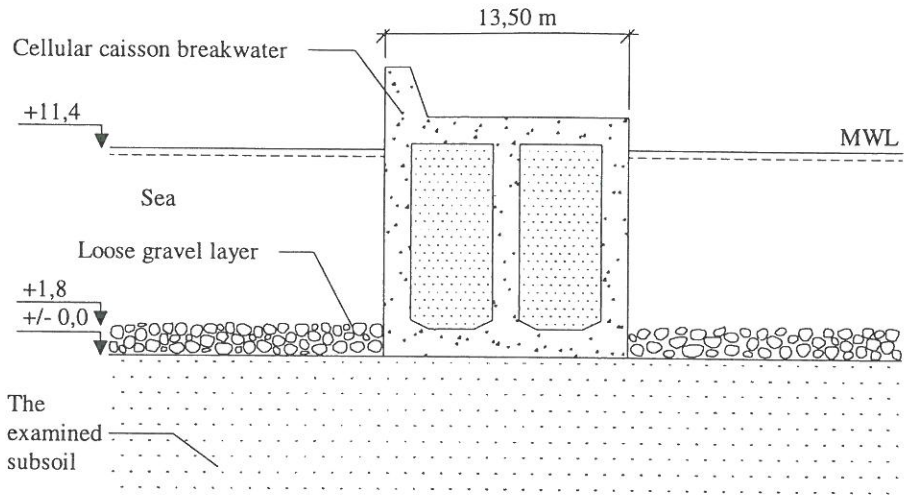


*Figure 1. Section with the prototype of the continuous cellular caisson breakwater.*

In connection with the present research, the Single Hardening Model developed by Poul V. Lade is of particular interest. The Single Hardening Model has been developed with the purpose of describing the response of frictional materials in a more accurate way. Among other things, the aim of this work has been to investigate the applicability of the Single Hardening Model for solving geotechnical problems of a more complex nature. In this article a caisson breakwater structure which has been tested in the centrifuge at Delft Geotechnics, is modelled in ABAQUS by means of the verified material model subroutine containing the Single Hardening Model. In Figure 1. a section with the prototype of the continuous cellular caisson breakwater modeled is shown.

## 2. CALIBRATION OF THE MODEL

On the basis of the results from the performed triaxial tests together with results from the database at the Soil Mechanics Laboratory at Aalborg University, it is possible to calibrate the Single Hardening Model for the two different materials in question, Baskarp Sand No 15 and Eastern Scheldt Sand. In this connection, it should be mentioned that calibration of the Single Hardening Model requires determination of twelve parameters. These parameters are listed below:

Elastic parameters: $\nu$, $\lambda$, $M$
Failure envelope parameters: $\eta_1$, $m$, $a$
Plastic potential parameters: $\psi_2$, $\mu$
Hardening parameters: $C$, $p$
Yield surface parameters: $h$, $q$

The obtained set of calibration parameters at different void ratios have formed the basis for an investigation of a possible void ratio dependency formulation, as shown in (Andersen et all, 1997).

### 2.1 *Observed soil behaviour*

Besides providing a solid basis for the parameter study, the triaxial tests have served to elucidate the general behaviour of sand. In this way, it is stated that tested sand supports the characteristic state theory explained in detail elsewhere, (Ibsen L.B, 1998). Furthermore, the behaviour observed during large stress reversals has been subjected to an analysis. Performing un- and reloading cycles it was observed that plastic strains were present, in contrast with the theory of the Single Hardening Model where purely elastic behaviour during a load cycle is assumed. However, performing un- and reloading cycles down to 50 percent of the maximum shear stress, purely elastic behaviour was indeed observed. This supports the presence of the Bauschinger effect and questions the applicability of the Single Hardening Model, if a precise description of large un- and reloading cycles is wished for. Finally, the assumption of isotropic soil behaviour has been investigated, as this is a fundamental assumption made by the Single Hardening Model. Thus, the slopes of the volumetric strain curves from hydrostatic compression tests have been considered. It was found out that some scatter is present, as the slopes differ slightly from the required slope of 1 in 3. The scatter is put down to experimental uncertainties.

### 2.2 *Parameter calibration*

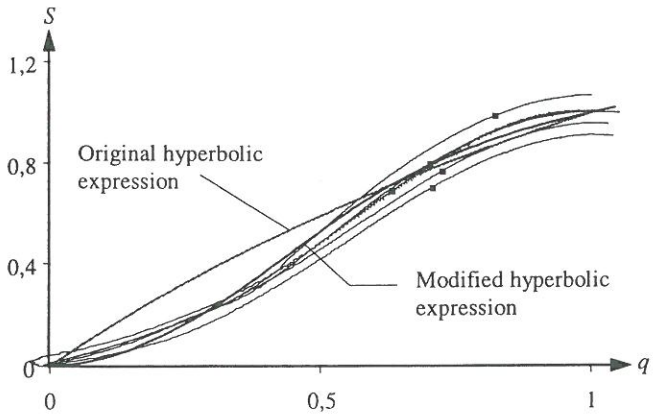


*Figure 2. q,S variations for Baskarp Sand No. 15 e=0,85, approximated by the original hyperbolic expression and the modified hyperbolic expression.*

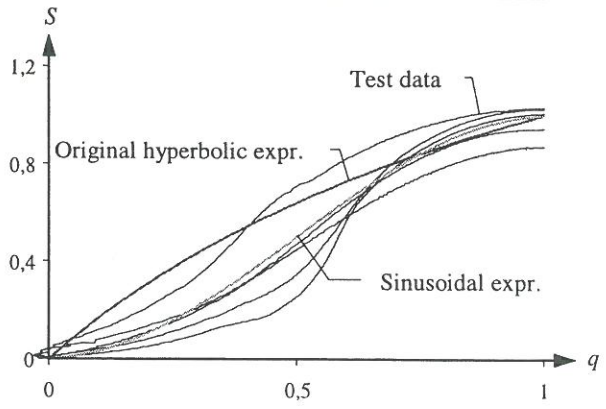


*Figure 4. q,S variations for Baskarp Sand No. 15 with e = 0,70, and $\sigma_3' = 80, 160, 320, 640,$ and 800 kPa. $\zeta = 0{,}502$ and $\upsilon = 0{,}503$.*

Parameter calibrations have been carried out in the same manner as introduced in (Andersen et all ,1997). Similar tendencies were observed, as especially the yield surface parameter, $h$ and the $q,S$ variation are encumbered with some deviation relative to the assumptions of the Single Hardening Model, as shown in Figure 2 and Figure 4. Therefore, initiatives have been taken in order to improve the parameter calibrations in general.

First and foremost, the observed deviation relative to isotropic soil behaviour during hydrostatic compression has been investigated. Thus, a determination of the hardening parameters based on $\varepsilon_1$, only, was carried out. It has turned out that in this way, the variation of the yield surface parameter, $h$ with respect to the confining pressure becomes less pronounced. Thus, a clear improvement of the triaxial test predictions was observed and therefore it has been chosen to base the entire parameter determination on this assumption. Still, the suggested $q,S$ variation has been seen to capture the experienced variations inadequately, which has given rise to the development of alternative proposals for the $q,S$ expression, as shown in Figure 2 and Figure 3. The first attempt resulted in a modified hyperbolic expression calibrated on the basis of the characteristic state, as shown in Figure 2 . However, the modified hyperbolic expression has been seen to be numerically unstable in a general FEM description. As a numerically stable alternative, a sinusoidal expression was developed, whereby a better reconstruction of the $q,S$ variation for all materials is possible, as shown in Figure 4. Some deviations are still experienced for Baskarp Sand No. 15 at the smallest void ratios. It has been concluded that the best predictions are obtained using the sinusoidal expression combined with a reduced value of the initial slope of the softening curve.

The remaining model parameters have been investigated as well, in order to estimate the influence of a change of these parameters to the numerical predictions. In that way it has been concluded that the influence of a change of the elastic parameters is insignificant as long as the parameters are chosen

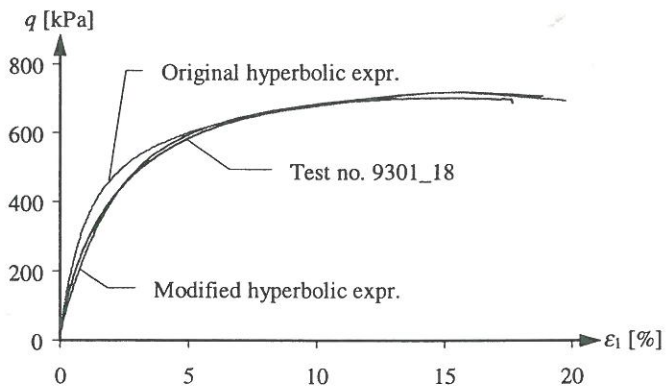


*Figure 3. Predicted and experimental stress-strain curves for Baskarp Sand No. 15 with void ratio, e = 0,85, and $\sigma_3' = 320$ kPa.*

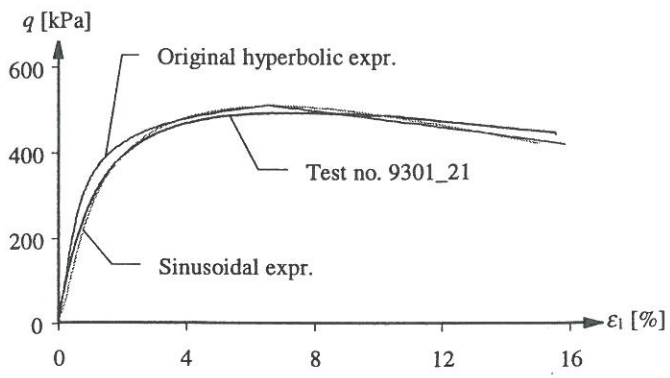


*Figure 5. Predicted and experimental stress-strain curves for Baskarp Sand No. 15 with e = 0,70, and $\sigma_3' = 160$ kPa.*

within a reasonable range. For triaxial test predictions, the same observation is present for the parameter, $\psi_1$, which governs the shape of the plastic potential- and yield surfaces in the octahedral plane. This parameter is determined on the basis of the failure parameter, $m$. The remaining plastic potential parameters, $\psi_2$ and $\mu$ have been seen not to influence the stress-strain behaviour. However, evaluating the predicted volumetric strain curves, the change of these parameters is clearly registered. It should be noted that no attempt has been done in order to modify the failure parameters, as these parameters are generally determined on a firm basis.

Finally, a void ratio dependency formulation has been put forward on the basis of the parameters determined from the tests in the database. As additional reference, data determined for Monterey No. 0 Sand, and Sacramento River Sand have been brought in. On the basis of the limited amount of data it is observed that a coherence between the parameters and the void ratio is present, although quite some scatter is present.

Summing up, it is stated that the below listed issues are considered to be essential in order to achieve numerical predictions of the highest quality:

1. In general, the experimental behaviour of Eastern Scheldt Sand is captured the best by the numerical predictions. One of the significant differences between the tests performed on Baskarp Sand No. 15, and the tests on Eastern Scheldt Sand is a smaller amount of preconsolidation during preparation for Eastern Scheldt Sand. As the development of plastic work is essential to the parameter determination, it is believed that it is important to carry out the preparation of the test specimens at the lowest possible vacuum in order to prevent a high rate of pre-consolidation.

2. Furthermore, it is advised to plan the performance of the triaxial tests in such a manner that the parameter calibration is supported by reliable test results. Thus, a hydrostatic compression test to a high level of confining pressure is an absolute must in order to determine reliable hardening parameters. It has moreover been observed that a hydrostatic un- and reloading cycle supports the determination of the elastic parameters quite well in terms of the bulk modulus.

3. In order to estimate reliable data for Poisson's ratio, it is required that the triaxial tests are performed at constant confining pressure.

4. At least three drained triaxial tests must be performed over a wide range of confining pressures. The tests should include un- and reloading cycles after peak failure.

5. The hardening parameters should be estimated on the basis of the assumption of isotropic soil behaviour.

6. Finally, the newly described sinusoidal expression together with an initial slope of the softening curve equal to 0,8 provide significantly better predictions of the experimentally observed behaviour.

Taking these issues into account it is believed that it is generally possible to optimise the Single Hardening Model in order to provide reliable numerical predictions.

## 3. IMPLEMENTATION

Until this point, the constitutive behaviour defined by the Single Hardening Model has been employed for predictions of triaxial tests, exclusively. For use in a general problem, however, the Single Hardening Model must be linked with a finite element program. Therefore, the constitutive model has been implemented in a subroutine working together with the finite element program ABAQUS.

In order to ensure that reliable results are obtained when using the material model subroutine for actual calculations, the implementation has been verified. During the verification process it was experienced that the implemented version of the model was unable to handle certain situations in a proper manner. Thereby, the necessity of obtaining knowledge regarding the actual implementation arose. In this way, great emphasis has been laid on investigating the material model subroutine in order to solve the problems encountered during the verification process. As a particular interesting issue, the concept of strengthening of a material due to preshearing was investigated. In order to investigate the behaviour of the subroutine in the case of preshearing a triaxial specimen exposed to the following loading scheme has been analysed:

1. Isotropic consolidation to $\sigma_3' = 160$ kPa

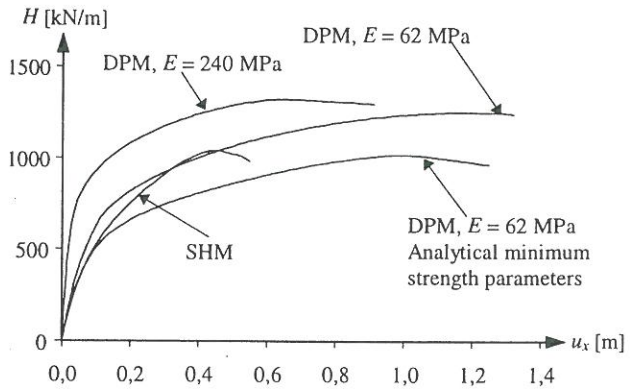


*Figure 6. Appearance of the failure- and yield surface in the case of preshearing.*

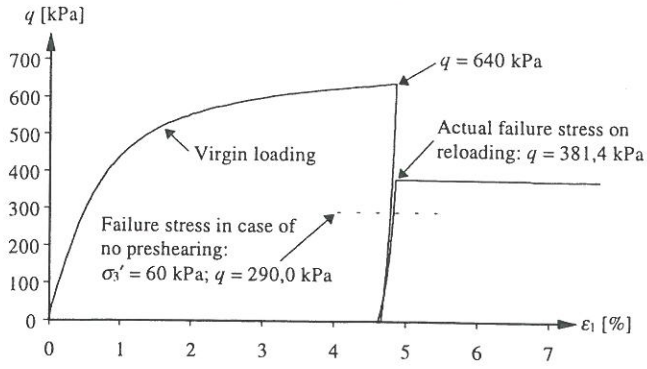


*Figure 7. Stress-strain curve for triaxial specimen exposed to preshearing.*

2. Triaxial compression to $q$ = 640 kPa
3. Unloading to isotropic stress, $\sigma_3'$ = 160 kPa
4. Decreasing confining pressure to $\sigma_3'$ = 60 kPa
5. Reloading until peak failure is reached

The analysis is based on the parameters corresponding to Eastern Scheldt Sand with $e$ = 0,59. Inserting the failure envelope parameters for this material into failure criterion, the peak value of deviator stress can be calculated to be: $q_{failure}$ = 661,2 kPa, meaning that the original failure envelope is not reached during preshearing, as shown in Figure 6. However, the stress of 640 kPa is sufficient to cause the yield surface to be extended beyond the failure envelope, whereby a strengthening of the material when reloading at a lower confining pressure would be expected. In Figure 7 the resulting stress-strain curve from the preshearing analysis is presented.

It appeared that the implemented version of the Single Hardening Model is in fact capable of handling the concept of preshearing, although still some unanswered questions are present.

It has been observed that in the case of preshearing, the consistency condition, which is an essential part of an elasto-plastic formulation is no longer fulfilled. In order to solve this problem, intensive investigations of this particular issue must be carried out in the future.

## 4. ANALYSIS OF CAISSON BREAKWATER

On the basis of the verified version of the material model subroutine, the response of a gravity caisson breakwater has been subjected to a numerical analysis. As one out of several bases for comparison, the results from a centrifuge test performed at Delft Geotechnics have been brought in. In order to ensure reliable use of the test results, emphasis has been laid on acquiring knowledge regarding the special technique of centrifuge testing. The application of the caisson dead load in the caisson is carried out by accelerating the centrifuge to the chosen level of gravitational acceleration. This acceleration process has been compared with a corresponding numerical analysis, based on the Single Hardening Model. An observed deviation between the experimental and numerical behaviour has been put down to experimental uncertainties, together with an uncertain constitutive description at very low stress levels.

### 4.1 *Analytical analysis*

The drained bearing capacity due to horizontal loading of the caisson breakwater as predicted by the Single Hardening Model is compared with the bearing capacity obtained from an analytical analysis based on a kinematically admissible rupture figure. Furthermore, an analysis based on the bearing capacity formulation of Terzaghi has been carried out. A clear resemblance between the bearing capacity obtained on the basis of the Single Hardening Model and the analytically calculated bearing capacities has been experienced.

As an additional reference, predictions of the drained response of the caisson breakwater, based on the much simpler linear Drucker-Prager Model have been carried out. The employed version of the Drucker-Prager Model is the linear elastic, perfectly plastic model. It has been experienced that the response of the caisson is highly dependent of the used input parameters, as quite distinct results can be

obtained, although the chosen parameters are considered to be relevant for the material in question. In this way, it must be stated that if the linear Drucker-Prager Model is to be used at all, it is essential to be able to provide a reasonable estimate on the stress state in the soil in order to apply the correct strength parameters for the analysis in question. The movements of the caisson predicted by the Single Hardening Model, and the Drucker-Prager Model, respectively, have been seen not to coincide. The predictions by the Drucker-Prager Model are considered to describe the situation inadequately, due to the assumption of linear elastic, perfectly plastic soil behaviour.

*Figure 8. Predictions of the horizontal loading, performed by the Single Hardening Model and the Drucker-Prager Model.*

### 4.2 *Numerical analysis*

A simplified section of the cylindrical container elucidates the model of the caisson breakwater used in the centrifuge test is shown in Figure 9.

The response of the caisson when exposed to load cycles of varying magnitude has been investigated by the Single Hardening Model as well. The dependency of the void ratio has been analysed. In both cases, the predicted response is considered reasonable.

During the centrifuge test, the caisson breakwater is exposed to several impact loads of a large magnitude, in order to simulate a storm situation. On the basis of the scaling factors, the impact loads reveals

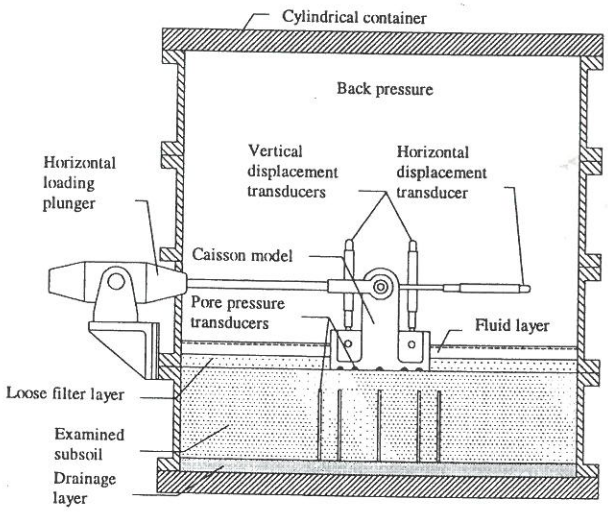


*Figure 9. Section of the cylindrical container containing the test set-up of the gravity caisson breakwater in the centrifuge test. Loading connection and transducers are illustrated.*

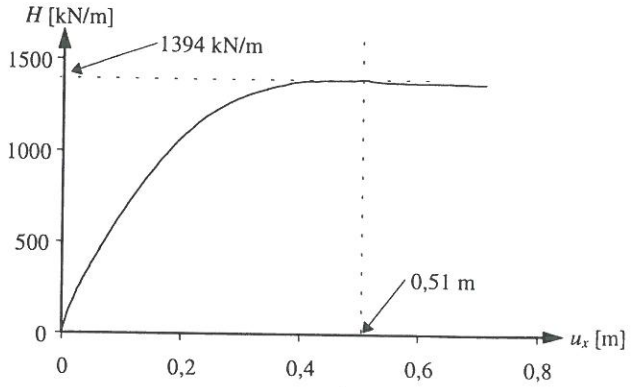


*Figure 10. Performance curve for the undrained response of the caisson, predicted by the Single Hardening Model.*

a wave impact force of H = 1440 kN/m for the prototype structure.

As an estimate on the response of the caisson in this situation, an undrained numerical analysis including the pore fluid response has been carried out by the Single Hardening Model. The Performance curve for the undrained response of the caisson, predicted by the Single Hardening Model is shown in Figure 10.

The horizontal bearing capacity obtained from this analysis is larger than the corresponding drained prediction, which is due to a negative pore pressure build-up in the soil layer. A nice correspondence between the numerically predicted bearing capacity, and the maximum force experienced in the centrifuge test has been observed.

### 4.3 *Failure mechanisms*

The failure mechanisms observed from the respective numerical analyses have formed the basis of a visual comparison. In all cases, a fully developed rupture zone, concentrated around the corner of the caisson, opposite to the load application point, is experienced. This behaviour is in correspondence with the rupture figure considered in connection with the analytical upper bound solution. Furthermore, the numerically predicted displacement fields are similar to the displacement field considered in the analytical analysis.

### 4.4 *Computational efficiency*

Regarding the computational efficiency of the respective numerical analyses, it should be mentioned that large differences have been experienced regarding the time needed for the analyses. In this way, the predictions based on the Single Hardening Model have been observed to require considerably more computational power than the

corresponding Drucker-Prager analyses. It should be kept in mind, however, that due to the linear-elastic, perfectly plastic behaviour assumed by the Drucker-Prager Model, the number of calculations within each increment is small compared to the corresponding Single Hardening Model prediction, as this model includes hardening plasticity. Still, it would be preferable if it was possible to increase the computational efficiency of the subroutine containing the Single Hardening Model. Actually, this is considered to be a necessity if it is desired to be able to model a general three dimensional prototype structure. This statement is based on the fact that during the verification of the material model subroutine, the response of a simple shear test has been predicted by means of three dimensional elements. Even though the number of elements of the model is no higher than 400, the required computational time is extremely extensive. For modelling a general three dimensional structure, the required number of elements would be considerably higher. A possible point of effort regarding an improvement of the efficiency of the routine could be a change of the stress updating procedure, which is currently based on the forward Euler scheme.

## 5. CONCLUSION

Still, it must be emphasised that use of an advanced constitutive model like the Single Hardening Model is bound to require great efforts as regards to the calibration of the model, as well as the computational power needed for the actual analysis. Therefore, the relevance of applying such advanced model for solution of a geotechnical problem must be judged on the basis of the character of the problem considered. Hence, if e.g. only the drained bearing capacity of a given structure is desired, a simple analytical solution is considered to provide sufficiently precise results, meaning that in such cases application of a complex constitutive model is far from necessary. On the other hand, if the actual stress-strain response of the considered material is important to the results, as e.g. when the pore pressure build-up in the soil is essential, the use of a constitutive relation, which is able to capture the actual soil response is indeed relevant. On the basis of the analyses performed throughout this work, it is stated that the Single Hardening Model is at this point ready for application in such types of geotechnical problems.

## 6. REFERENCES

Andersen A. T, Madsen E.B, Schaarup-Jensen A.L, Ibsen L.B. 1997. *Constitutive Modelling of Baskarp Sand.* Research Report by Aalborg University, Geotechnical Engineering Group. *co-sponsored by* Commission of the European Union Directorate General XII MAST contract MAS3 - CT95 - 0041 (1996 - 1999). 200 pages report

Andersen A. T, Madsen E.B, Schaarup-Jensen A.L, Ibsen L.B, Jacobsen 1998.a. *Advanced Numerical Analysis of Caisson Breakwater Founded on Frictional Materials.* Research Report by Aalborg University, Geotechnical Engineering Group. *co- sponsored by* Commission of the European Union Directorate General XII MAST contract MAS3 - CT95 - 0041 (1996 - 1999). 300 pages report.

Andersen A. T, Madsen E.B, Schaarup-Jensen A.L 1998.b. *DATA REPORT 9701 Part 1. Easter Scheldt Sand, Baskarp Sand No.15.* Data Report by Aalborg University, Geotechnical Engineering Group. *co- sponsored by* Commission of the European Union Directorate General XII MAST contract MAS3 - CT95 - 0041 (1996 - 1999).

Ibsen L.B, 1998. *Dynamic Responce of Course Granular Material to Wave load.* Article in this report.

# C.2

# Dynamic Response of Coarse Granular Material to Wave Load

Lars Bo Ibsen
*Department of Civil Engineering, Aalborg University*
*DK-9000 Aalborg, Denmark*

ABSTRACT: The soil beneath vertical breakwaters is subjected to a combination of forces induced by the waves. The forces acting on the soil can be characterized as (1) static load due to submerged weight of the structure, (2) quasi-static forces induced by cyclic wave loading, and (3) wave impact from breaking waves. The stress conditions in the soil below a foundation exposed to these types of loading are very complex. The key to explain and quantify the soil response beneath a vertical breakwater is to understand the role of the volume changes and to be able to model these correctly. It is shown that the volume changes in soil subjected to static and dynamic loading are controlled by the characteristic line. Experiments have been performed to study the factors that influence the location of the characteristic line in drained and undrained tests for various types of sand and various types of loading. These factors include the relative density, the minor principal stress, the intermediate principal stress, the stress path, and the effects of nonhomogeneous and localized strains. The relation of the characteristic line to other features of static, cyclic and dynamic (rate dependent) soil behavior are explained and illustrated with experimental data.

KEYWORDS: characteristic line, confining pressure, cubical triaxial test, cyclic triaxial test, dilatancy, drained behavior, dynamic behavior, phase transformation line, sand, shear test, stress path testing, triaxial test, undrained behavior

## 1 INTRODUCTION

The soil beneath vertical breakwaters is subjected to a combination of forces induced by the waves. These forces can be characterized as (1) static load due to the submerged weight of the structure, (2) quasi-static forces induced by cyclic wave loading, and (3) wave impact from breaking waves on the vertical wall. A detailed explanation of the wave induced forces are given De Groot et al. (1996). The stress conditions in the soil below a foundation exposed to these types of loads are very complex, as illustrated in Figure 1.

The behavior of granular materials can normally be accurately characterized by results from drained tests, since the materials can be considered fully drained in many practical problems. However, if the rate of loading is very high, such as that resulting from impact forces from breaking waves on vertical breakwaters, then essentially undrained conditions can exist. In addition, if the dimensions of the breakwater is large and the permeability of the cohesionless soil is relatively low, significant pore-pressure changes may develop as a result of the quasi-static forces induced by cyclic wave loading.

To model and predict this complex soil-structure interaction, a reliable soil model is required, which describe the basic phenomena related to soil behavior during static, cyclic, and dynamic loading. Laboratory testing makes it possible to study soil behavior in detail under controlled and well known conditions. By studying the basic phenomena in triaxial tests under uniform conditions, it has been discovered that identical phenomena characterize the sand behavior when subjected to static and dynamic loading. The key to explain and quantify the soil response beneath a vertical breakwater is to understand the role of the volume changes and to be able to model these correctly.

Volume changes are important for the behavior of soils whether under drained or undrained conditions and whether exposed to static, cyclic, or dynamic loading. Volume changes can be contractive or expansive in nature. Expansive or dilative volume changes are most pronounced for dense sands at low confining pressures and high stress levels approaching failure. The transition from compressive behavior observed at lower stress levels to dilative behavior at high stress levels occurs along a straight line through the origin of the stress space. For

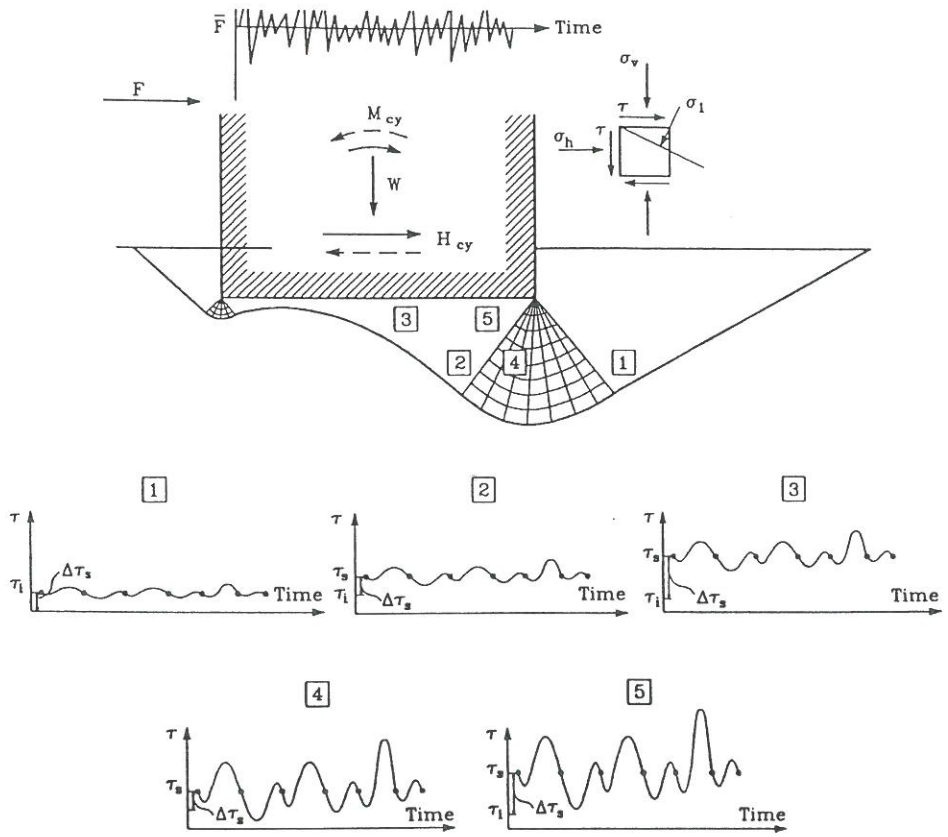


Figure 1. Example of stress conditions for specific elements in the soil below a vertical monolithic structure exposed to static and stochastic non-stationary loads.

drained tests, this line is referred to as the characteristic line.

In elasto-plasticity models the characteristic line, evaluated from $p' = const$ tests, corresponds to the point on the plastic potential surface where the plastic strain increment vector is perpendicular to the $p'$- axis or the hydrostatic axis (Ibsen and Lade 1998). This state is therefore comparable to the similar point on the yield surface at which the normal is perpendicular to the hydrostatic axis. This indicates the point at which sand may become unstable, as explained in detail elsewhere (Lade *1995).* Thus, the characteristic line plays a similarly important role for the plastic potential surface as the instability line plays for the yield surface. Both lines are shown on the diagram in Figure 2. The behavior of soils is greatly influenced by and may be explained in view of the relative locations of these two lines. For sands the two lines are distinctly separate, while for normally consolidated, insensitive clays the two lines coincide, and they also coincide with the critical state or ultimate state line.

Experiments have been performed to study the factors that influence the location of the characteristic line in drained and undrained tests for various types of sand and various types of loading. These factors include the relative density, the minor principal stress, the intermediate principal stress, the stress path, and the effects of nonhomogeneous and localized strains. The relation of the characteristic line to other features of soil behavior during static, cyclic, and dynamic loading are explained and illustrated with experimental data.

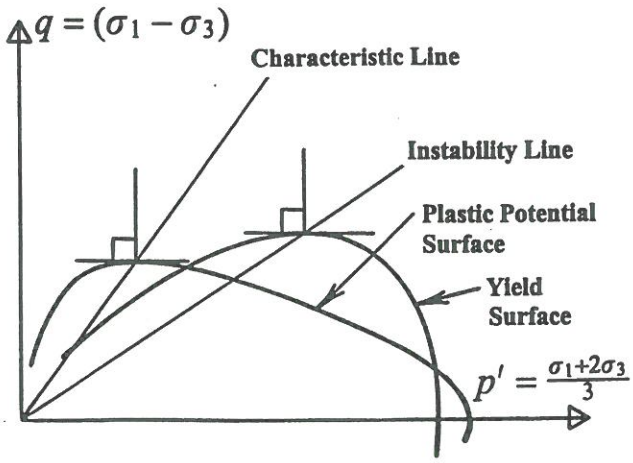


Figure 2. Comparison of characteristic and instability lines.

## 2. TEST PROGRAM

The tests performed in connection which this project were conventional static CD-tests, $CU_{u=0}$-tests, and cyclic and dynamic CU-tests. The cyclic and dynamic CU-tests were performed as undrained tests with pore pressure measurements. The $CU_{u=0}$-tests were carried out by measuring the volume change and controlling the cell pressure in such a way that $\delta\varepsilon_v = 0$ throughout the test. In this way the undrained condition is ensured and the effective stress path is followed throughout the test.

In conventional triaxial tests the loads, deformations, volume changes or pore pressure are measured outside the specimen, and homogeneous conditions must exist inside the specimen to calculate the correct values of stresses, strains and void ratios throughout the test. Although it has been advocated since 1965 that triaxial tests should be performed on specimens with lubricated cap and base (Rowe and Barden 1964), and height equal to diameter (Bishop and Green 1965 Jacobsen 1967, Lade 1982), it is often considered that sufficiently uniform conditions are achieved by using tall specimens with heights greater than or equal to two diameters.

Ibsen (1994) found that specimens with double height developed nonuniformities in strains resulting in measurements of incorrect stress-strain relations of the material. During undrained conditions the nonuniform development in volumetric strains results in inner draining and consequent generation of erroneous pore pressures. Basic phenomena in soils under drained or undrained conditions, must be studied in test performed on specimens with height equal to diameter and with smooth end plates. This is the best way to ensure that the real stress-strain behavior is determined, while properties of soils obtained from tall specimens may reflect test errors.

To ensure homogeneous stress and strain conditions, the tests presented here were performed on cylindrical specimens with a height and diameter equal to 70 mm, and bounded by lubricated caps and bases. The tests were performed in a newly developed version of the Danish Triaxial Apparatus in which control of stress path, measurement, and data analysis is automated (Ibsen 1994).

The static triaxial specimen was loaded by a mechanically controlled piston, while the dynamic test is loaded by a hydraulic piston. The static tests were performed with constant deformation rate of 4 % per hour, and the dynamic tests were conducted with constant deformation rate varying from 40 to 100,000 % per hour. The measuring systems in the two apparatuses were identical and consisted of electronic load, pressure, and deformation transducers. The working principles of triaxial cell is similar to those described by Jacobsen (1970).

The study described in this paper is based on tests performed on two uniform sands: Aalborg University sand No. 1 and Lund sand No 0. The index properties for these sands are shown in the Table 1.

*Table 1. Index Properties.*

| Property | Aalborg University sand No 1 | Lund sand No 0 |
|---|---|---|
| $d_{50\ mm}$ | 0.14 | 0.4 |
| $C_U$ | 1.78 | 1.7 |
| $d_s$ | 2.65 | 2.65 |
| $e_{max}$ | 0.86 | 0.82 |
| $e_{min}$ | 0.55 | 0.55 |

The test specimens were prepared by a pluvial deposition and carefully saturated in total vacuum (approx. -98 kPa). This causes all specimens to be pre-consolidated to approximated 100 kPa during the preparation process. This technique ensures homogeneous and totally saturated specimens. The triaxial test series was performed on isotropically consolidated specimens with relative densities as shown in Table 2. The test results are reported by Ibsen (1990), Ibsen and Bødker (1994), Jacobsen and Simonsen (1994), and Ibsen and Jacobsen (1996).

*Table 2. Relative densities for sand specimens in static triaxial tests.*

| | Relative densities |
|---|---|
| Aalborg University sand No. 1 | 0.10, 0.51, 0.80, 1.00 |
| Lund sand No. 0 | 0.48, 0.78, 0.93, 1.00 |

The parameters that describe the state of the soil under axisymmetrical stress conditions, are calculated from the measurements taken during the tests. These parameters are:

the cell pressure $\sigma_3'$
the mean normal stress $p' = \frac{1}{3}(\sigma_1' + 2\sigma_3')$
the deviator stress $q' = \sigma_1' - \sigma_3'$
the volumetric strain $\varepsilon_v$
the deviator strain $\varepsilon_q = \frac{2}{3}(\varepsilon_1 - \varepsilon_3)$

where $\sigma_1'$ is the vertical and $\sigma_3'$ the horizontal principal stresses. The stresses are effective and $\varepsilon_1$ and $\varepsilon_3$ are the principal strains.

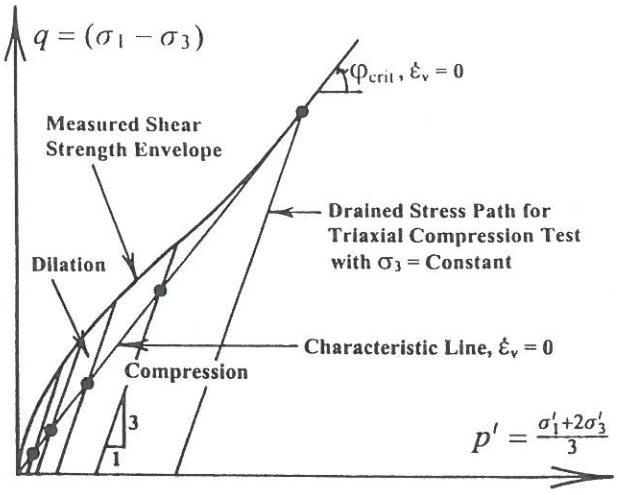


Figure 3. Variation of drained shear strength envelope for sand with constant confining pressure (Lade and Ibsen 1997).

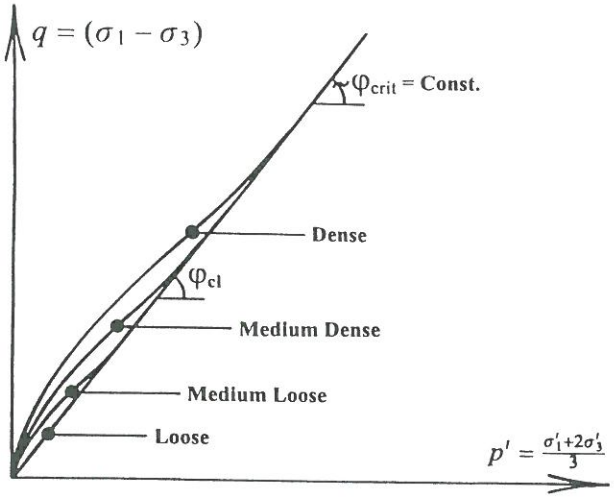


Figure 4. Variation of drained shear strength envelope for sand with relative density. (Lade and Ibsen 1997).

## 3 DRAINED SHEAR STRENGTH OF SAND

The typical variation of drained shear strength of sand with mean effective stress is illustrated schematically in Figure 3. For a sand with a given initial density, the peak friction angle, $\varphi'_{peak}$, consists of two components. One from the basic friction between sand particles modified for contributions from rearrangement of particles at constant volume. The resulting friction angle is referred to as the critical friction angle, $\varphi_{cr}$. The second component derives from the dilation of the sand during shear, $\psi_{peak}$. This relation can be expressed as:

$$\varphi'_{peak} = \varphi'_{cr} + \psi_{peak} \qquad (1)$$

The dilation is suppressed at higher pressures due to crushing, and the resulting strength component therefore reduces to zero at very high pressures.

Thus, a curved failure surface is observed. Experiments on sands have shown that both the contribution from dilation and the range of confining pressures in which dilation occurs reduce with decreasing relative density, as shown schematically in Figure 4.

## 4. THE CHARACTERISTIC STATE

Figure 5 shows the results of four CD-tests. The tests are performed with different cell pressures, $\sigma'_3$, which are held constant throughout each test. Failure is seen to be well defined as the state in which the deviator stress $q'$ is a maximum, as shown in Figure 5b. In this diagram the stress-strain curves are normalized on $\sigma'_3$. This causes the curve with the smallest confining pressure to be located at the top. Laboratory tests on several sands have shown that a characteristic threshold exists in granular materials which is defined as the stress state where the volume

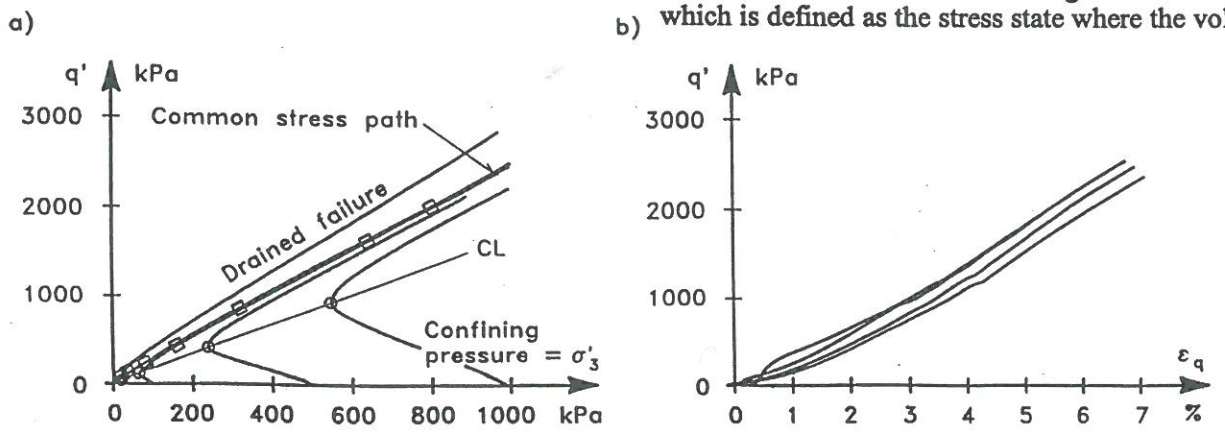


**Figure 5. Diagram illustrating the development of stress-strain behavior in CD-tests on dense sand performed with different confining pressures on specimens with equal height and diameter.**

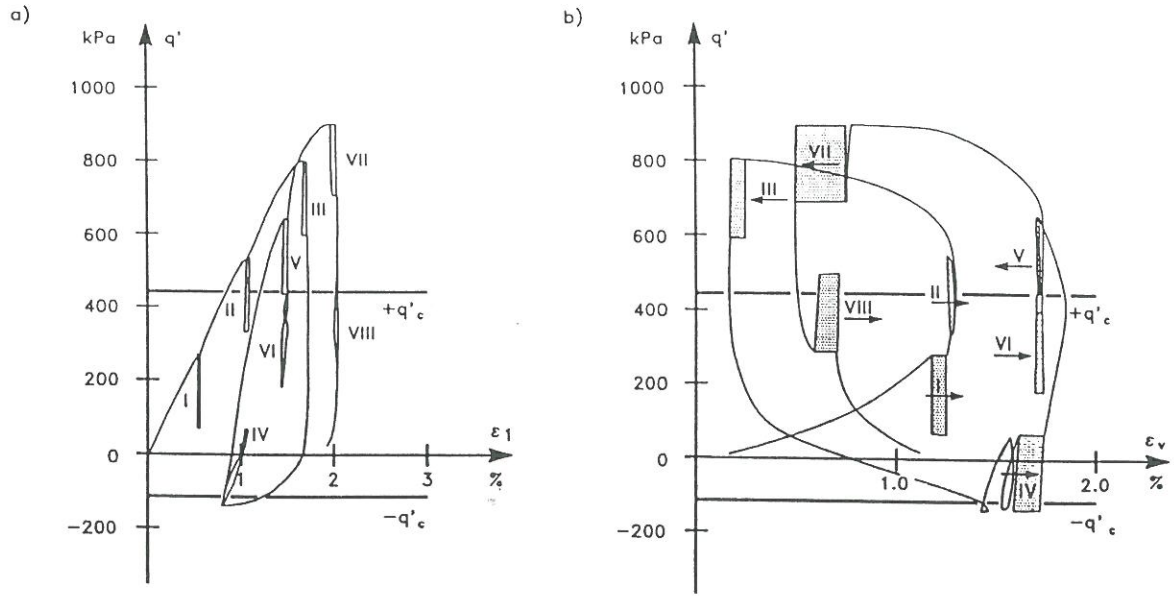


Figure 6. Cyclic loading under constant confinement condition $\sigma'_3$ = 200 kPa performed on Fountainbleau sand $I_D$ = 0.64 (Luong 1982).

change goes from contraction to dilation. On the $\varepsilon_1 - \varepsilon_v$ curve, Figure 5c, the characteristic threshold is marked by open circles at the point where the specimen has minimum volume. The stress state characterized by ($p_{cl}$, $q_{cl}$) where $\delta\varepsilon_v/\delta\varepsilon_1 = 0$ is defined and described as the *Characteristic State,* (Luong 1982). Characteristic states occur at the transition from contraction to dilation, and these states are located on a line, the *Characteristic Line cl*, through the stress origin. The slope of the characteristic line may be described by an angle, $\varphi_{cl}$. The characteristic state and the critical state are very similar, as discussed by (Luong 1982). For loose sand and sand at high confining pressure, $\delta\varepsilon_v/\delta\varepsilon_1 = 0$ is reached at the critical state. The critical state is therefore the same as the characteristic state, and it occurs at failure for sand that compresses during shear. For dense sand or sand at low confining pressure, the characteristic state is reached at small strain magnitudes, as indicated by open circles in Figure 5b, while the critical state is reached at large strains.

The characteristic line divides the stress space into two subspaces in which the stress combinations lead to different deformation mechanisms.

> Below the characteristic line the stress combinations lead to contraction, i.e. $\delta\varepsilon_v > 0$.
> Above the line the stress combinations lead to dilation, i.e. $\delta\varepsilon_v < 0$.

Below the characteristic line the resistance to deformation is governed by sliding friction due to microscopic interlocking depending upon surface roughness of the particles or interlocking friction between particles. According to (Luong 1982), the resistance is due to pure friction and the characteristic state describes an intrinsic parameter which defines a characteristic angel $\varphi_{cl}$ for a given sand. In the subspace situated between the failure envelope and the characteristic line the resistance to deformation is governed by disrupture of the interlocking and volumetric dilation.

In Figure 6 cycling sequences are carried out at different deviator stress levels under drained conditions and at constant confinement, $\sigma'_3 = 200$ kPa. Each cycling sequence consists of 20 cycles with a amplitude of 100 kPa. The diagram shows very clearly that the contracting behavior of the soil is obtained when the mean deviator stress level is lower than the characteristic level. The dilation behavior of the soil during load cycling is evident when the mean deviator stress level becomes higher than the characteristic threshold, $q'_{cl}$.

Loung (1982) has observed that the contraction decreases when the characteristic threshold is approached and dilation increases when deviator stresses increase further. The contraction effect is more pronounced for extension loading having $q' < 0$.

### *4.1 Effects of Relative Density and Minor Principal Stress*

The characteristic angles for drained triaxial compression tests on Aalborg University sand No.1 and Lund sand No.0 at four relative densities, $I_D$, are shown in Figures 7 and 8. The experiments in these two tests series, in which the relative density varied from 0.01 to 1.0, show that the characteristic angle $\varphi_{cl}$ is constant and independent of (1) relative density for a given sand, and (2) confining pressure or minor

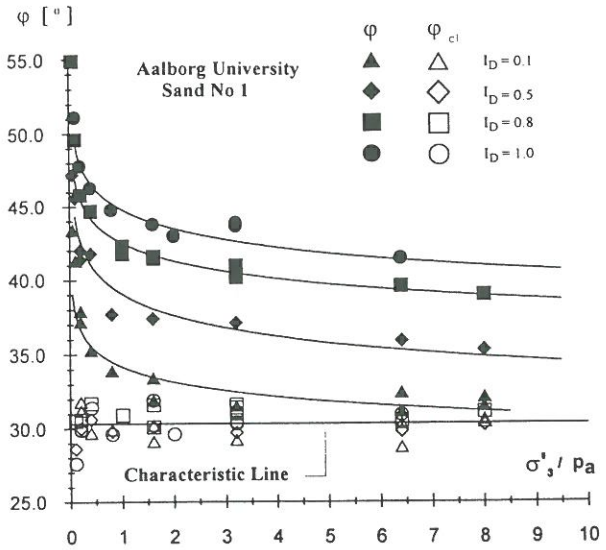


Figure 7. Characteristic angles obtained from triaxial compression tests on Aalborg University Sand No. 1.

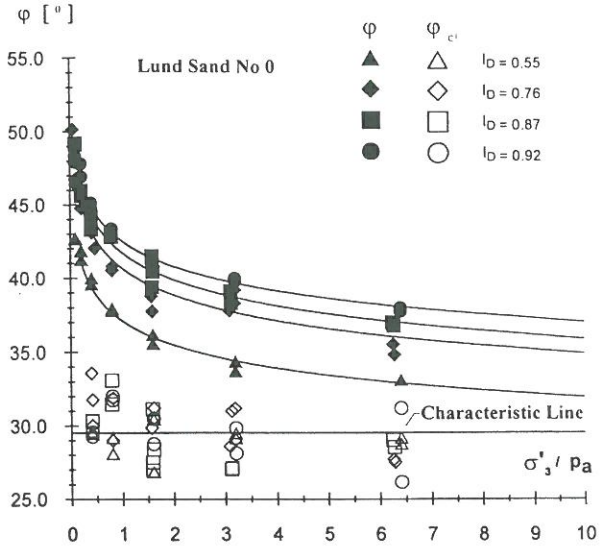


Figure 8. Characteristic angles obtained from triaxial compression tests on Lund No. 0.

principal stress. These observations were also made by Loung (1982).

As discussed in connection with Figure 17, the determination of the stress state at which $\delta\varepsilon_v = 0$ is not necessarily very accurate, because the volume change curve is relatively flat near the characteristic state, while the stress state varies considerably. Therefore, the determination of the characteristic stress points shows some scatter. The characteristic angle for Aalborg University sand No. 1 is found to be $\varphi_{cl} = 30.3^0$ and for Lund sand No.0 it is $\varphi_{cl} = 29.5^0$ These angles are determined according the definition used by Luong (1982).

### *4.2 Effects of Specimen H/D-Ratio*

The characteristic stress states corresponding to $\delta\varepsilon_v = 0$ for triaxial compression tests on Santa Monica Beach sand at four relative densities (Lade and Prabucki 1995) are shown in Figure 9. These experiments were performed on specimens with height-to-diameter ratio $H/D = 2.65$ and with lubricated ends. They also show that the characteristic angle, $\varphi_{cl}$, is independent of relative density for a given sand, but due to the development of nonuniformities in strains, the angle is found to vary slightly with the minor principal stress.

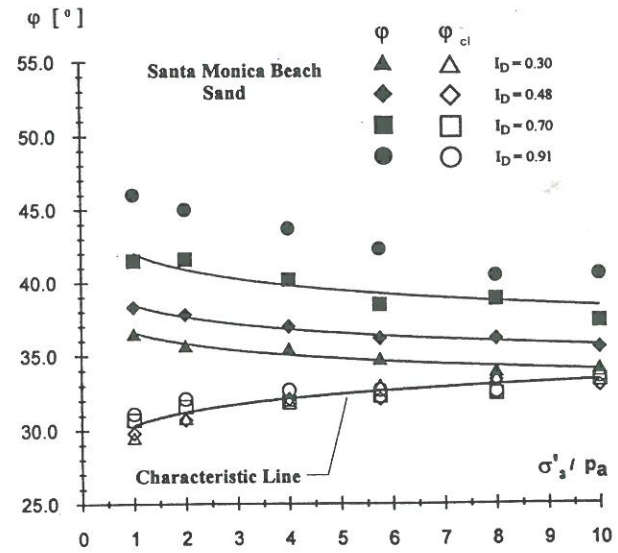


Figure. 9 Characteristic states obtained from triaxial compression tests on Santa Monica Beach Sand.

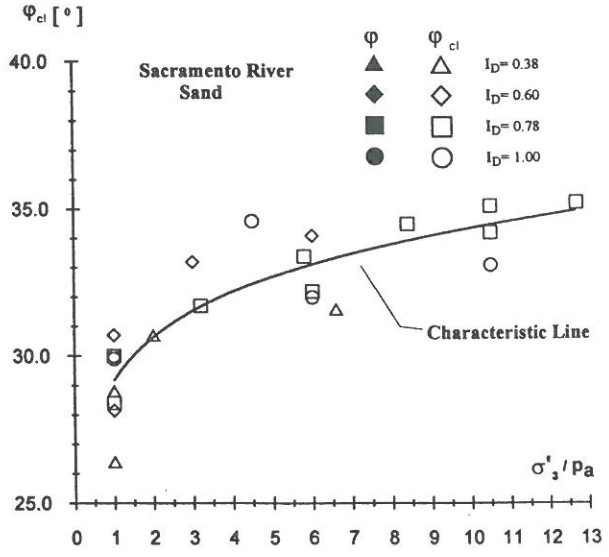


Figure. 10 Characteristic states obtained from triaxial compression tests on Sacramento River Sand.

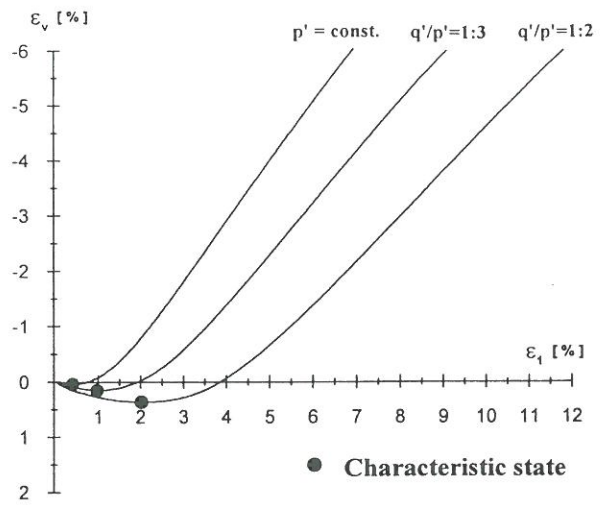


Figure 11. Volumetric curves obtained by stress path tests on Aalborg University sand No. 1, $I_D$ = 1.00. Isotropic consolidated to $\sigma'_3$ = 20 kPa before shearing.

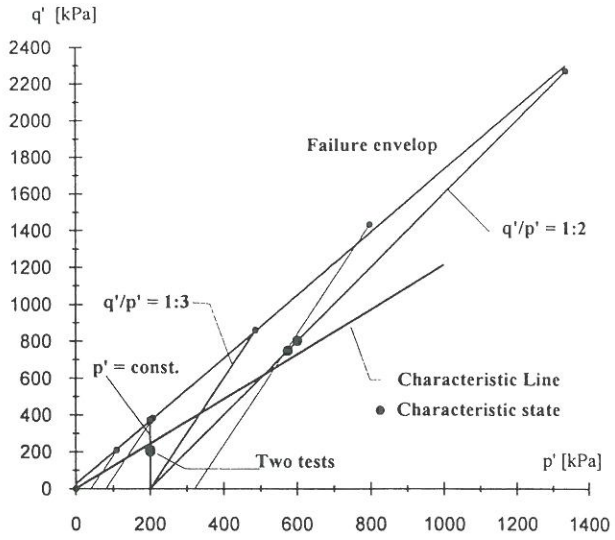


Figure 12. Stress path tests obtained from triaxial compression tests on Aalborg University sand No. 1, $I_D$ = 1.00.

The characteristic angles for drained triaxial compression tests on Sacramento River sand (Lee 1965, Lee and Seed 1967) were also determined for four different relative densities, and they are shown in Figure 10. These tests were performed on specimens with $D$ = 3.56 cm and $H/D$ = 2.43, and without lubricated ends. The data for Sacramento River sand shows more scatter than the other test series. Still, the tests indicate that the characteristic angle is independent of relative density. Due to the more pronounced nonuniformities in stress and strains caused by rough end plates, the characteristic angles vary more with confining pressure than the data for Santa Monica Beach sand. It is therefore important to realize that the nonuniform deformations, which develop at very small strains, influence the measured characteristic angles and therefore the conclusions regarding the effect of the minor principal stress.

### *4.3 Effects of stress path testing*

The characteristic stress state discussed above is that observed in conventional triaxial compression tests in which the stress path corresponds to constant confining pressure and $\delta q'/\delta p' = 1/3$. The volumetric strain curves from three triaxial test on Aalborg University sand No. 1 conducted with different stress path are shown in Figure 11. The tests were all performed on specimens with $I_D$ = 1.00 and consolidated to a mean normal stress of $\sigma'_3$ = 200 kPa before shearing. The corresponding stress paths $\delta p' = const$, $\delta q'/\delta p' = 1/3$ and $\delta q'/\delta p' = 1/2$ are shown in Figure 12.

Contraction and dilation can be caused by application of shear stresses as well as by changes in the mean normal stress. In the constant $p'$-test the increment $\delta p'$ is zero and the elastic volumetric strain increment is therefore also zero. In this test the volumetric strains are caused entirely by shear stresses. The test shows shear-induced contraction in the beginning, and it is possible to define a characteristic state, as shown in Figure 11. As expected, the contraction becomes more pronounced as the stress ratio $\delta q'/\delta p'$ increases, and there are distinct differences between the characteristic states obtained from different stress paths, as shown in Figure 11.

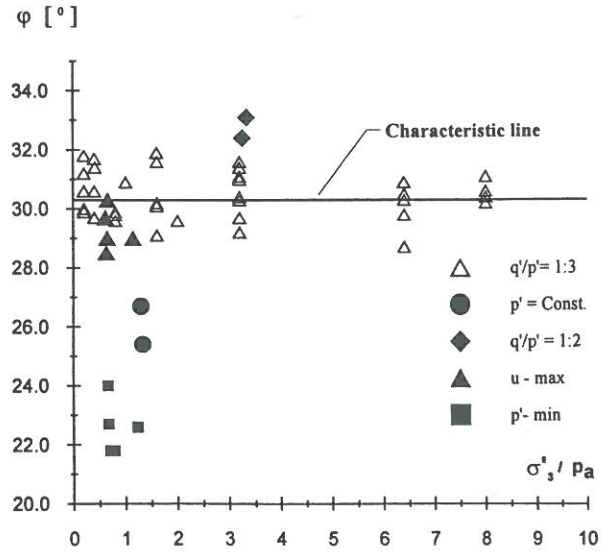


Figure 13. Angles of the characteristic, phase transformation and $u_{max}$ stress states evaluated from drained and undrained triaxial tests on Aalborg University sand No. 1.

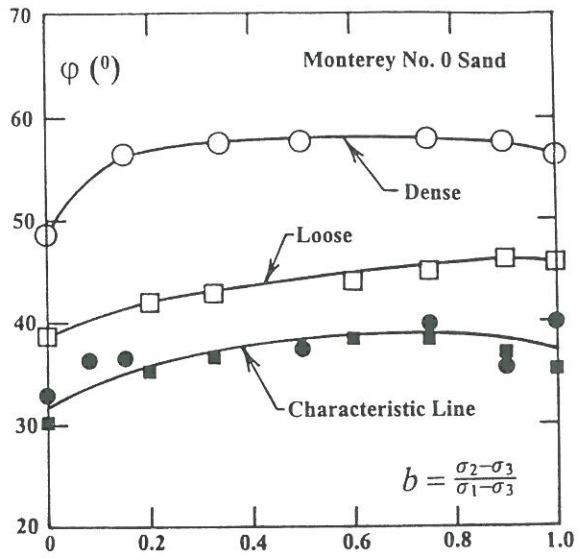


Figure 14. Characteristic angles obtained from cubical triaxial tests on Monterey No. 0 sand.

The characteristic stress states from the three volumetric strain curves are plotted in Figure 12. The characteristic line determined from the results in Figure 7 and two experiments for each of the conditions, $p' = const$ and $\delta q'/\delta p' = 1/2$, are also plotted in this diagram. The characteristic stress states from the $p' = const$ tests are located below and the stress states form the $\delta q'/\delta p' = 1/2$ are located above the characteristic line. The characteristic angle $\varphi_{cl}$ from these four tests are also plotted in Figure 13. It is seen that $\varphi_{cl}$ from the $p' = const$ tests is 26°, and it is 33° in the tests with the stress path $\delta q'/\delta p' = 1/2$. The characteristic angles are outside the general scatter of the $\delta q'/\delta p' = 1/3$ tests, and it appears from these experiments that the characteristic stress state and therefore the characteristic angle is a function of the stress path.

### *4.4 Effects of intermediate principal stress*

The characteristic angles have also been obtained from drained cubical triaxial compression tests on dense and loose Monterey No.0 sand (Lade and Duncan 1973) and shown in Figure 14. The characteristic angles are affected by the intermediate principal stress in a similar fashion as the measured friction angles. Each b-value represents a different stress path in the stress space, and there does not seem to be any pronounced effect of relative density on the characteristic angles. It is observed that for a given stress path, the characteristic stress states are independent of relative density.

## *5 COMPARISON OF PHASE TRANSFORMATION AND CHARACTERISTIC STRESS STATES*

The phase transformation stress state plays a similar role for undrained tests as the characteristic stress state plays for drained tests. Figure 15 shows a schematic illustration of the stress state at which phase transformation occurs along an effective stress path from an undrained test. It is the point at which "the stress path turns its direction in p'- q' space" (Ishihara et al. 1975), i.e. the point where the effective stress path has a "knee" and the effective mean normal stress reaches a minimum value $p'_{min}$. Ishihara et al. (1975) observed that for cyclic undrained triaxial tests "it is necessary for a sample to go at least once through this critical value in order to be taken to a completely liquefied state." In this sense, "the critical stress ratio may be considered as a threshold at which the behavior of sand as a solid is lost and transformed into that of a liquefied state."

Whereas the "knee" described above does not clearly define the location of the phase transformation point, the most consistent definition is one that is independent of the stress path. The phase transformation state is therefore best defined as the point at which the effective stress path has a vertical tangent. This also corresponds to the transition from compressive to dilative behavior. At this point of the undrained test, the increment $\delta p'$ becomes zero, and the elastic volumetric strain increment, $\delta\varepsilon_v^e$, is therefore also zero. Consequently, the plastic volumetric strain increment, $\delta\varepsilon_v^p$, is also zero. This definition theoretically makes the characteristic and phase transformation states identical.

Inspection of the data in Figure 13 shows that the characteristic angles obtained from $p' = const$ tests are slightly higher than the angles defining the phase transformation states. It was expected that the characteristic angle from $p' = const$ tests and the

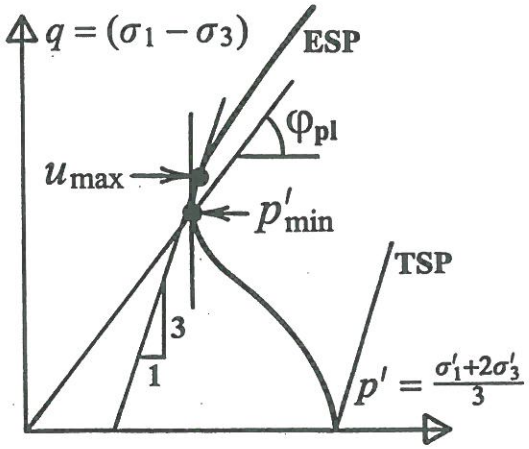


**Figure 15 Schematic diagram of phase transformation state in undrained triaxial compression test on sand.**

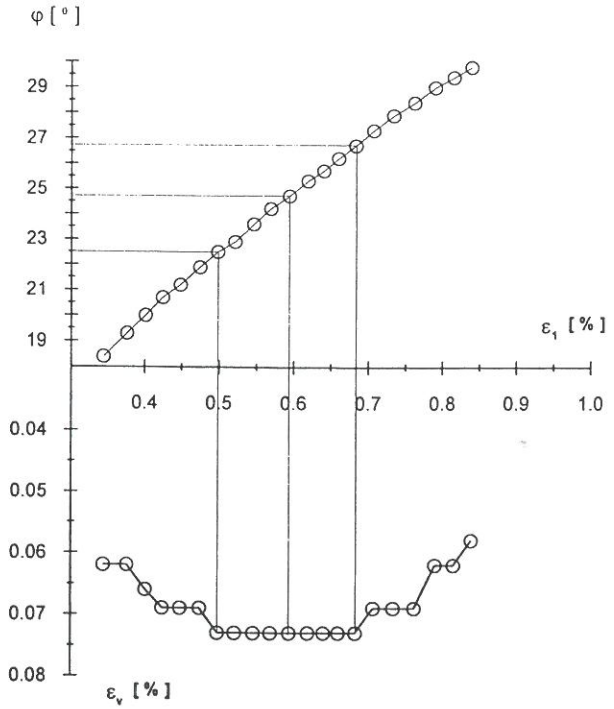


Figure 16. The measured points used to define the characteristic stress state in a p' = constant triaxial test run on Aalborg University sand No. 1 with $I_D = 1.00$.

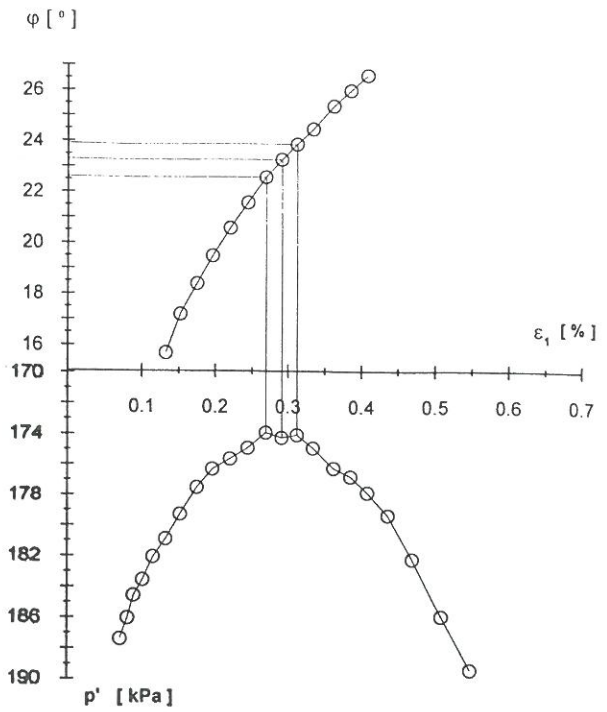


Figure 17. The measured points used to define the phase transformation stress state in a CU triaxial test performed on Aalborg University sand No. 1 with $I_D = 1.00$.

angle of the phase transformation states would be the same, because both stress states are characterized by having $\delta\varepsilon_v^e = 0$. However, the conditions defining the two stress states are not exactly identical. In the undrained test, the total volumetric strain is zero and the elastic and plastic volumetric strains therefore have to compensate for each other, i.e. $\varepsilon_v^e = -\varepsilon_v^p$, while $\varepsilon_v^e = 0$ and $\varepsilon_v^p \neq 0$ in the drained test.

In Figures 16 and 17 the points used to define the characteristic and phase transformation stress states are shown for tests performed on Aalborg University sand No. 1 with $I_D = 1.00$. Figure 16 shows that the transition zone in which $\delta\varepsilon_v = 0$ starts at $\varphi = 22.5°$ and ends at $\varphi = 26.7°$. Previously, and according to Luong (1982), the characteristic stress state has been defined as the mean value in this transition zone producing $\varphi_{cl} = 24.6°$. In comparison, the transition zone for the phase transformation state in the corresponding undrained test is much narrower.

Redefining the characteristic and phase transformation states as the states where $\delta\varepsilon_v$ and $\delta p'$ becomes zero for the first time, produces identical states, if simultaneously, the characteristic state is obtained from a $p' = const$ test, as shown in Figures 16 and 17.

This new definition is used in evaluating the angles shown in Figure 18. The test data are identical with those shown in Figures 7 and 13 for $I_D$ = 1.00. It is seen that the by using this definition, all the characteristic angles, evaluated from CD-tests performed with $p' = const$, become identical with the angles of the phase transformation states. The characteristic angle still shows the same stress path dependency as before, while that evaluated from

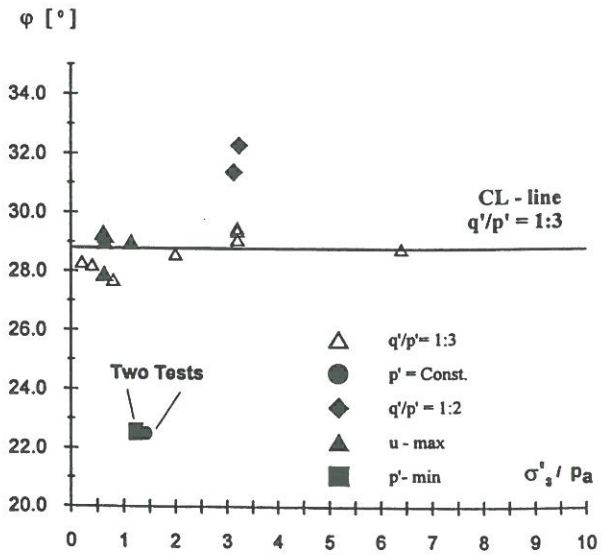


Figure 18. Angles of characteristic and phase transformation states defined as the stress state where $\delta\varepsilon_v$ respectively $\delta p'$ becomes zero. The tests are run on Aalborg University Sand No 1.

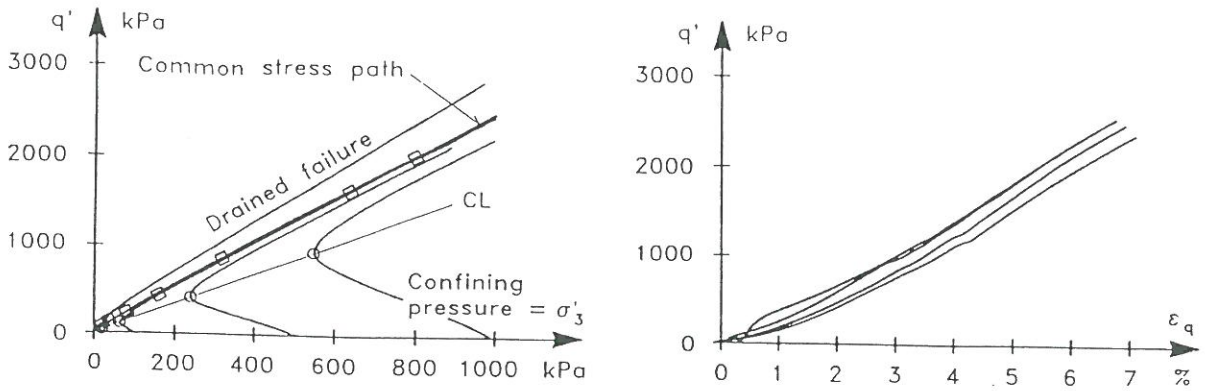


Figure 19. Results of four $CU_{u=0}$ - tests performed on Lund sand No. 0 with $I_D = 0.78$. The tests were performed on specimens with equal height and diameter.

conventional triaxial tests is reduced from $\varphi_{cl} = 30.3°$ to $\varphi_{cl} = 28.8°$.

## 6 *THE CHARACTERISTIC STATE FOR UNDRAINED CONDITIONS*

Along the effective stress path in a undrained test the elastic and plastic volumetric strains have to compensate for each other, i.e. $\varepsilon_v^e = -\varepsilon_v^p$. It has been shown that changes in the effective mean normal stress $p'$ affects both the elastic volumetric strain and the stress state where the soil goes from compression to dilation. In a conventional undrained triaxial compression test, in which the total stress path corresponds to $\delta q'/\delta p' = 1/3$, the phase transformation state does not correspond to the transition from contractive to dilative behavior, i.e. the point where the maximum pore water pressure $u_{max}$ occurs.

The characteristic stress state, as defined by Luong (1982), together with the total stress path, controls the point where the maximum pore water pressure $u_{max}$ occurs in an undrained test. During undrained shear, the pore pressure increases at first in order to prevent the sand from contraction, i.e. $\delta u > 0$. When the deviator stress approaches the characteristic state $\delta u \to 0$. The results of four undrained triaxial tests, shown in Figure 19, indicate that the stress states where $\delta u = 0$ are located on the characteristic line. If $q$ increases further, the effective stress path is located in the subspace which is characterized by dilation. In order to prevent dilation, the pore pressure generation becomes negative, i.e. $\delta u < 0$, as shown in Figure 19a. If the effective stress path in Figure 19a is plotted in a $p' - q$ diagram, the stress state corresponding to maximum pore water pressure $u_{max}$ will occur slightly later than the phase transformation stress state, as indicated in Figure 15.

Stress states corresponding to $u_{max}$ from five undrained tests performed on Aalborg University sand No. 1 with $I_D$ = 1.00, 0.80 and 0.51 are shown in Figure 18. It is seen that $u_{max}$ corresponds to the characteristic stress states for the tests conducted with the stress ratio $\delta q'/\delta p' = 1/3$. It is also recognized that the stress state where $u_{max}$ occurs is quite different from the phase transformation stress state corresponding to $p'_{min}$.

## 7 UNDRAINED SHEAR STRENGTH OF SAND

Figure 19a shows that the effective stress path approaches a common stress path asymptotically, defined by the stress state marked with open squares. This common stress path is identical with the stress path defined by the stress states where the total volumetric strain $\Sigma\delta\varepsilon_v = 0$, marked by open squares in Figure 5.

This common stress path is normally considered to be the undrained failure envelope. In Figure 19b it is shown that the common stress path does not represent any failure state in the sand, and tests covering a $\sigma'_3$ interval from 5 kPa to 2000 kPa do not reveal any maximum on the stress-strain curves. This conclusion is not in agreement with the state of the art. The state of the art is build on undrained tests performed on specimens with double height and it therefore reflects the test errors and not the real properties of the soil, as explained above and also by Ibsen (1994).

### *7.1 Failure restricted by undrained conditions*

Failure under undrained conditions develops when the pore water fails to prevent dilation. From this state $\delta\varepsilon_v$ is no longer equal to zero and the soil starts to dilate. In this way the failure is controlled by the same mechanism as failure under drained conditions. The stress path followed can be explained in view of the relative locations of the characteristic stress state and the drained failure surface.

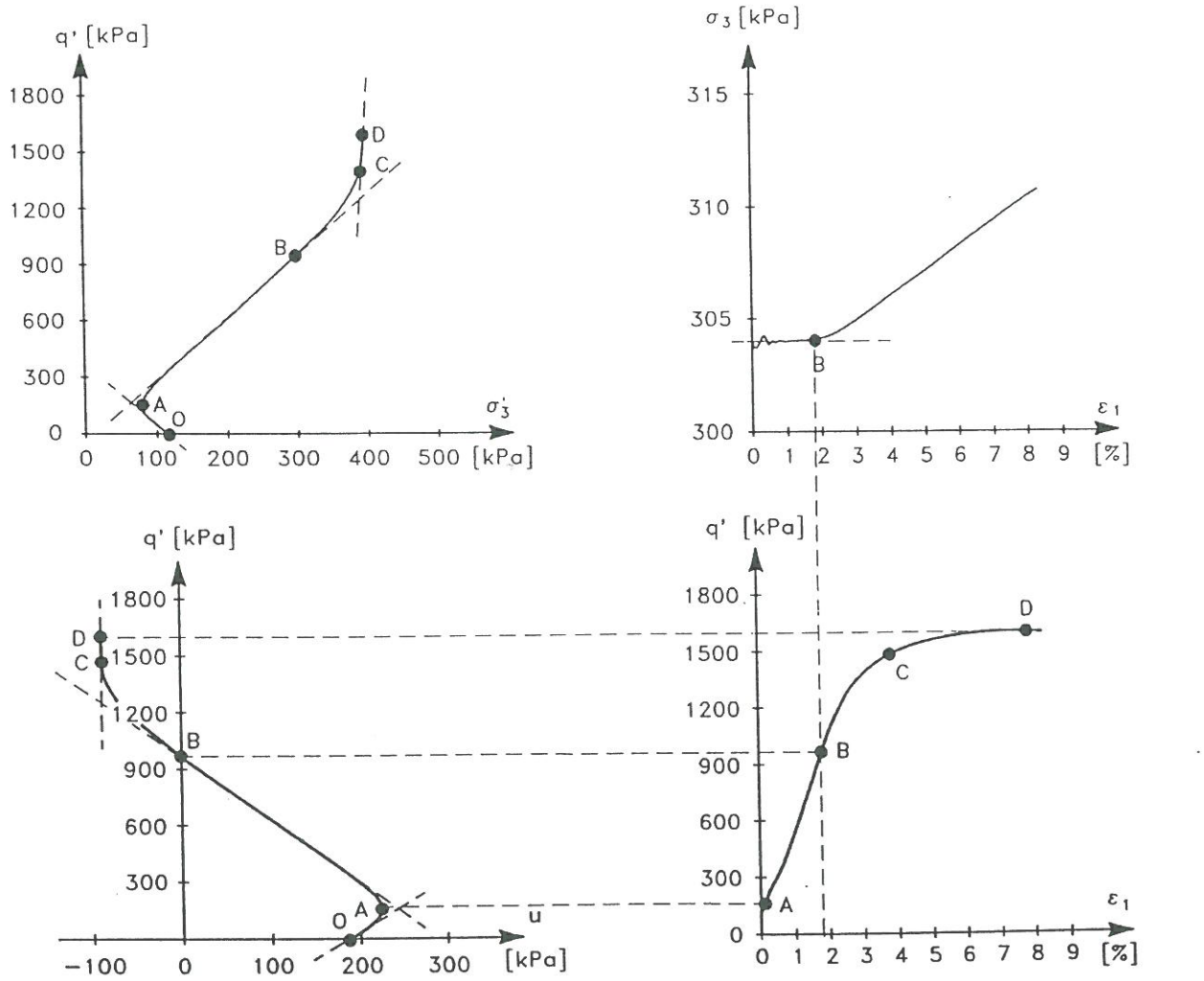


Figure 20. Results of a high deformation rate CU-triaxial test performed on Aalborg University sand No 1. The tests was performed with a constant deformation rate of 1000 % per hour. The specimen was prepared with $I_D = 0.80$.

The variation of the pore pressure during a high deformation rate CU-test is outlined in Figure 20. The figure shows that the pore pressure initially increases to prevent the sand from contraction and $\delta u > 0$. When the deviator stress approaches the characteristic stress state, point A, $\delta u \to 0$. Between point A and B the pore water manages to prevent the sand from dilating and the pore pressure generation is negative, $\delta u < 0$. Up to point B the stress-strain curve, Figure 20d, shows the same strain hardening response as outlined in Fig. 19b, and the stress path follows the common stress path defined by the drained stress states where $\Sigma \delta \varepsilon_v = 0$. When the pore pressure becomes negative the response changes character. The pore water can no longer prevent interlocking disrupture and the material starts to dilate slightly. The dilation causes a strengthening of the material and the response starts to deviate from the common stress path. At point C the pore water provides the maximum resistance and cavitation occurs at approximately -90 kPa. From this state the effective confining pressure remains constant, and further strengthening of the material depends entirely on the dilation. At point D failure occurs, while the negative pore pressure remains constant and does not vanish between C and D, as shown in Figure 20.

A static test is shown in Figure 21. At first, the test is performed as a constant volume test, $CU_{u=0}$ test. After the stress path has followed the common stress path for a while, the undrained restriction is changed to a drained conditions. It is seen that the shift from undrained to drained conditions results in dilation and the observed response is identical to that outlined in Figure 20. It is clearly shown, that the stress path during the drained part of the test in Figure 21 is identical with stress path C - D in Figure 20. It clear that drained failure conditions control failure in both tests, even though the overall conditions are undrained in the CU-test in Figure 20.

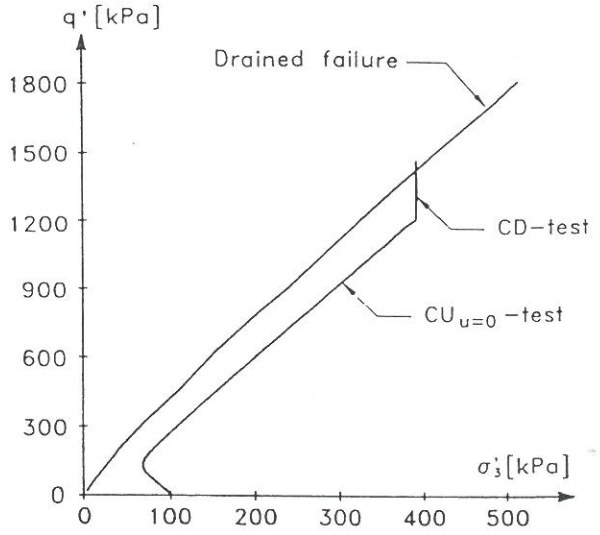


Figure 21. Static $CU_{u=0}$/CD triaxial compression test on Aalborg University sand No. 1. The test was performed with constant deformation rate of 4 % per hour and $I_D$ = 0.80.

If the soil element is located at a water depth where the hydrostatic pressure is high enough to prevent dilation, failure occurs at the intersection point between the characteristic line and the drained failure surface, as shown in Figure 3 and 4. Thus again, the drained failure surface is seen to control failure even though the overall conditions are undrained.

*7.2 Deformation rate effects*

The effect of deformation rate on the sand behavior has been studied by performing triaxial tests with constant deformation rates varying from 40 to 100,000 % per hour. The result of this study is outlined in Figures 22 and 23. The ratio between the dynamic and the static strengths is 1.1 for the tests shown in Figure 22. It has been speculated before (Nash and Dixon 1961, Yamamuro and Lade 1993) that the lower undrained strengths observed in the static tests are caused by higher pore pressures generated at low strain rates where more time is available for particle crushing and rearranging. This would result in more volumetric compression, but since the tests were undrained, higher pore pressures were induced. At higher strain rates, less time was allowed for particle crushing and rearranging to occur, and this caused the specimen to be less compressive. Consequently, lower pore pressures were produced and higher deviator stresses were obtained.

The stress-strain curves shown in Figure 23 indicate considerable rate effects. These effects are important in analyzing the interaction between the

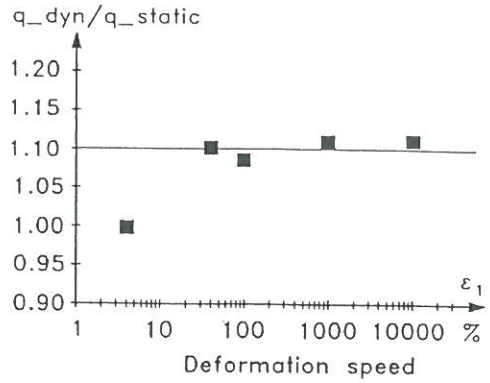


Figure 22. Relative strengths of CU triaxial tests on Aalborg University sand No. 1, $I_D$ = 0.80. The tests were performed with constant deformation rates varying from 40 to 100,000 % per hour.

structure and the soil when calculating the dynamic amplification factors.

*7.3 Effects of height-to-diameter ratio*

As discussed above, a tall specimen may not be capable of producing uniform deformation conditions throughout a triaxial test. This has considerable influence on the results of undrained tests. Test results of drained and undrained triaxial tests performed on specimens with homogeneous stress and strain distributions are shown in Figure 24a. The same sand was also tested in an undrained triaxial test with the height of the specimen equal to twice the diameter, as shown in Figure 24b. Initially the

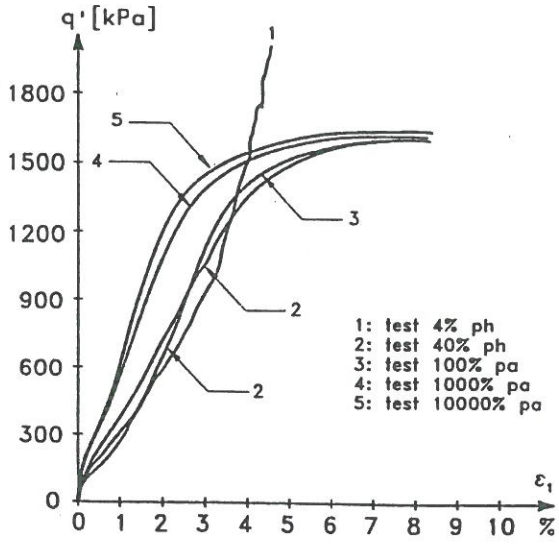


Figure 23. Stress-strain curves from triaxial tests on Aalborg University sand No. 1 performed with different deformation rates. Strength comparisons shown in Figure 22.

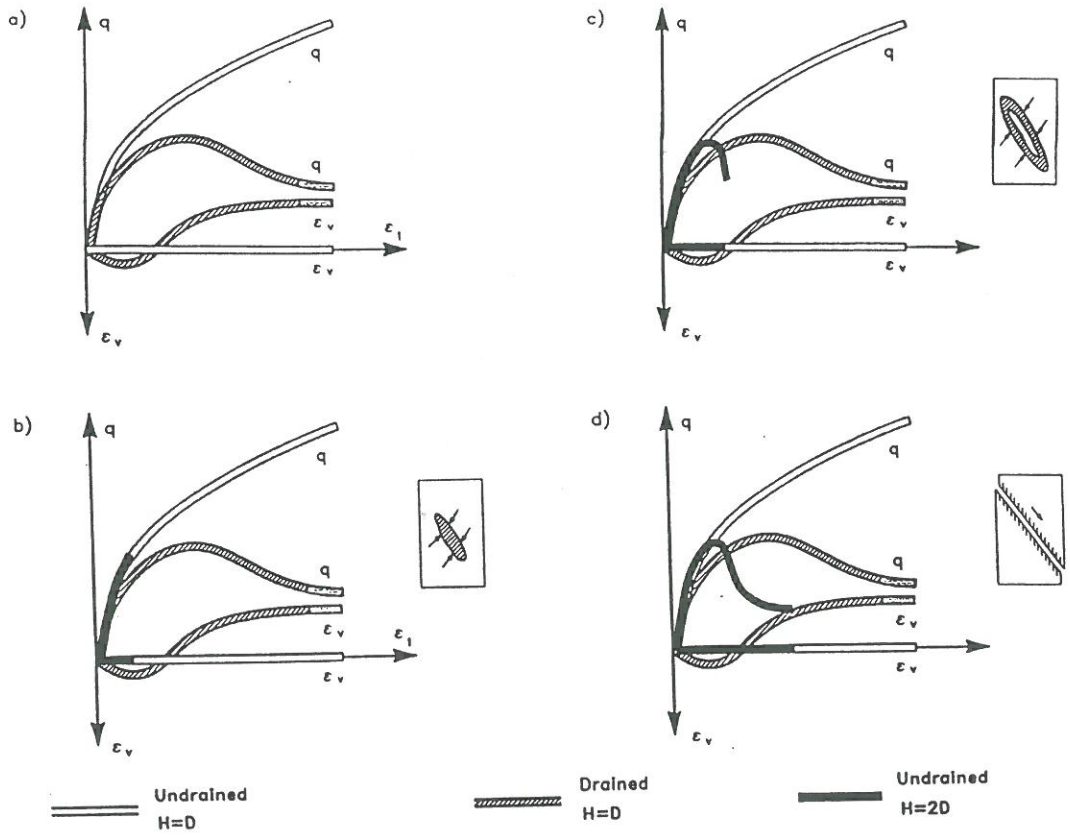


Figure 24. The consequence of an undrained test performed on a specimen with double height. (a) Drained and undrained test with homogeneous strain conditions. (b) Development of the locally weakened zone in which the shear plane subsequently is formed. (c) The drained zone dominates the stress-strain curve. (d) Two practically solid bodies sliding past each other ($H$ = height and $D$ = diameter of the specimen).

two stress-strain curves from the undrained tests coincide. As the deviator stress $q$ increases, the sand will try to expand. Under homogeneous conditions this expansion is impossible since the drains are closed. The resulting pore water suction will increase and hold the grain structure together. But in the tall specimen the deformation is not homogeneous, and some local zones will dilate and others will contract, resulting in zero overall volumetric strain. Inside the specimens water will flow from the zones that contract to the zones that dilate, as shown on the insert in Figure 24b. As a consequence, the test is not truly undrained, even though the overall volume of the whole specimen is kept constant. The stress-strain curve corresponding to these opposing volume change tendencies begin to deviate from the curve obtained from the uniform strain test as the zones with nonuniform strains develop into more distinct

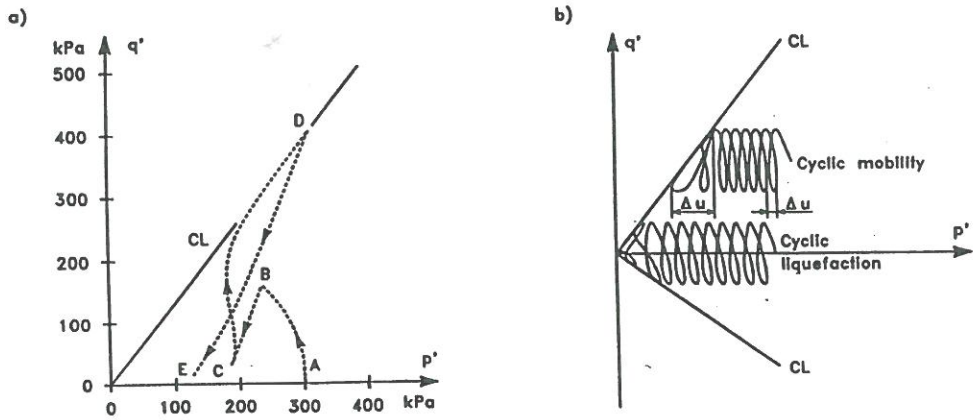


Figure 25. Results of CU-tests performed on specimen with double height submitted to a) static loading, b) cyclic loading. (Ibsen 1995).

localized zones, as illustrated on the insert in Figure 24c. Consequently, the inner drainage of some portions of the tall specimen causes the externally measured stress-strain curve to resemble the curves from the fully drained tests shown in Figure 5b. Critical state conditions develop inside the localized shear zone as the test continues. A shear band develops, and two practically solid bodies slide past each other, as indicated on the insert in Figure 24d. This limits the full development of negative pore pressure, and the shear strengths from such tests are consequently too low.

Figure 25 shows the results of CU-tests conducted on specimens with double height submitted to a) static loading and b) cyclic loading. Similar to the results in Figure 19a, the pore pressure in Figure 25a increases in the beginning, but as soon as the deviator stress approaches the characteristic line cl, the localized zone starts to develop. The inner drainage in the nonhomogeneous specimen causes reduced suction. As a consequence the effective stress path cannot be located correctly in the dilation subspace. In Figure 25a the test results show that the effective stress path therefore follows the characteristic line cl when the characteristic threshold is reached. This has led to the opinion that the undrained failure envelope describes a straight line through the stress origin.

In the case of undrained cyclic loading the stress variation can only be located in the subspace which is characterized by contraction and the stress variation will therefore always lead to pore pressure buildup. If the cyclic loading involves negative deviator stresses and the number of cycles is large enough, the effective stress variation will approach the characteristic line cl. Similar to static loading, the localization zone starts to develop and the stress variation is seen in Figure 25b to follow the characteristic line in both compression and extension. This phenomenon is described by many authors and called *Cyclic Liquefaction* (initiated by Seed and Lee 1966). If the cyclic loading involves negative deviator stresses, *Cyclic Mobility* can occur as described by Casagrande (1971). In both phenomena the shear plane is developed progressively as the cyclic stress variation continues to follow the characteristic line in each cycle. Large residual deformations are observed and the phenomenon is normally considered an expression of failure due to cyclic loading. As the effective stress variation follows the same effective stress path, both under cyclic and static loading, the "Undrained failure envelope" - which is seen to be identical to the characteristic line - is widely accepted to control the development of failure due to cyclic loading, see for instance Guzmann et al. (1988).

## *8 CONCLUSIONS*

By studying the basic sand behavior in triaxial tests under uniform conditions, identical responses of the sand due to static and dynamic loading have been discovered. The static and dynamic responses of sand can be explained with help of the characteristic state, and the strength of sand under undrained conditions is found to be controlled by the drained failure condition for both static and dynamic loading.

The negative pore pressure remains during failure Thus, the negative pore pressure can be counted on as a reliable stabilizing factor in calculations for design of foundations subjected to variable or dynamic loads.

The ratio between the dynamic and static strengths is approximately 1.1 in the interval from 40 to 100,000 % per hour. The tests also showed that the stress-strain curves indicated great rate effects. These effects are important in analyzing the interaction between the structure and the soil when calculating the dynamic amplification factors.

In this paper, the characteristic state is redefined as the stress state where $\delta\varepsilon_v$ becomes zero for the first time in a test with $p' = const.$ Further, the phase transformation state is defined as the state where $\delta p'$ becomes zero for the first time. As a consequence, the characteristic and phase transformation lines become identical. These definitions are mutually consistent, and they may therefore be useful in controlling the plastic potential function for description of plastic volume changes of soils.

In comparison, the characteristic angle defined by Luong (1982) is not an intrinsic parameter, independent of stress path, and it not useful for development of elasto-plasticity models.

The characteristic line has been studied in view of experimental results from drained and undrained triaxial compression tests and cubical triaxial tests on different sands. Experiments have shown, that the relative density and the minor principal stress do not influence the location of the redefined characteristic line and the characteristic angle is therefore unique for a given sand.

It is also shown that nonuniform deformations, which develop at very small strains in tall specimens, may influence the measured characteristic angles and the conclusions regarding the effect of the minor principal stress. It is therefore recommended to determine the characteristic and the phase transformation states from experiments with uniform stress and strain states. These are best produced in tests on specimens with height equal to diameter and lubricated ends.

REFERENCES


Bishop, A.W. and Green, G.E. 1965. The influence of end restraint on the compression strength of a cohesionless soil. Geotechnique, 15(3), 243-266.

Casagrande, A. 1971. On Liquefaction phenomena. *Geotechnique,* September, 1971 XXI(3), 197-202.

De Groot, M.B, Andersen K.H, Burcharth H.F, Ibsen. L.B, Kortenhaus. A, Lundgren H, Magda W, Oumeraci H, Richwien W. Foundation Design of Caisson Breakwaters. *Norwegian Geotechnical Institute. Publicatio No 198. Volume 1.*

Guzmann, A. A. et al. 1988. Undrained monotonic and cyclic strength of sand. *Jurnal of the Geotechnical Engineering Division ASCE*, 114(10), 1089-1118.

Ibsen, L.B. 1994. The stable state in cyclic triaxial testing on sand. *Soil Dynamics and Earthquake Engineering 13,* 63- 72.

Ibsen, L.B 1995. Static and dynamic strength of sand. *Eleventh European Conference on Soil Mechanics and Foundation Engineering*, Copenhagen, Denmark, 29 May - 1 June.

Ibsen, L.B. and Bødker, L. 1994. Baskarp Sand No. 15. *Data Report 9301*, Soil Mechanics Laboratory, Aalborg University, Denmark.

Ibsen, L.B and Lade P.V. 1998. The Role of the Characteristic Line in Static Soil Behavior. 4th Workshop on Localisation and Bifurcaton Theory for Soils and Rocks, A. A Balkema.

Ibsen, L.B. and Jakobsen, F.R. 1996. Lund Sand No. 0, *Data Report 8401, 8402, 8801 & 8901,* Soil Mechanics Laboratory, Aalborg University, Denmark.

Ishihara, K., Tatsuoka, F. and Yasuda, S. 1975. Undrained deformation and liquefaction of sand under cyclic stresses. *Soils and Foundations,* 15(1), 29-44.

Jacobsen, M. 1967. The undrained shear strength of preconmsolidated boulder clay. *Proc. Geot. Conf.*, Oslo, I, 119-122.

Jacobsen, M. 1970. New Oedometer and Triaxial Apparatus for Firm Soil. *DGI Bulletin No. 27*, 7-20.

Jacobsen, M. 1981 Two Comments on Laboratory Tests. Proc. 10th Int. Conf. Soil Mech. Found. Engr., Stockholm, Sweden.

Jakobsen, F.R. and Simonsen, J. 1994 Horizontal resistance of dynamically loaded piles. (in Danish). *M.Sc. Thesis.* Aalborg University.

Lade, P. V. 1982. Localization effects in triaxial test on sand. *IUTAM Conference on Deformation and Failure of Granular Materials*. A.A. Balkema, Rotterdam, 461-471.

Lade, P.V. 1994. Instability and Liquefaction of granular materials. Computers and Geotechnics, 16, 123-151.

Lade, P.V. and Duncan, J.M. 1973. Cubical triaxial tests on cohesionless soil. *Journal of the Soil Mechanics and Foundations Division,* ASCE, 99(10), 793-812.

Lade P.V and Ibsen 1997. A Study of the Phase Transformation and the Characteristic Lines of Sand Behavior. *Deformation and Progressive failure in Geomechanics. IS-NAGOYA '97.* Pergamon Press, 353-358.

Lade, P.V. and Prabucki, M.-J. 1995. Softening and preshearing effects in sand. *Soils and Foundations,* 35(4), 93-104.

Lee, K.L. 1965. Triaxial compressive strength of saturated sand under seismic loading conditions, PhD thesis, University of California, Berkeley.

Lee, K.L. and Seed, H.B. 1967. Drained strength characteristics of sands. *Journal of the Soil Mechanics and Foundations Division,* ASCE, 93(6), 117-141.

Luong, M.P. 1982. Stress-strain aspects of cohesionless soils under cyclic and transient loading. *International Symposium on Soil under Cyclic and transient Loading,* A. A Balkema, Rotterdam, 315-324.

Nash, K.L. and Dixon, R.K. 1961. The measurement of pore pressure in sand under rapid triaxial tests, *Proc. Conf. on the pore pressure and suction in soils*, Butterworths, London, 21-25.

Rowe, P.W. and Barden, L. (1964). Importance of free ends in triaxial testing. *Journal of the Soil Mechanic and Foundation Division, ASCE,* 90(SM1), 1-27.

Yamamuro, J.A. and Lade, P.V. 1993. Effects of strain rate on instability of granular soils, *Geot. Testing J.,* 16(3), 304-313.

# C.2 Hydraulic Response of Caisson Breakwaters in Multidirectional Breaking and Non-breaking Waves

GRØNBECH J., KOFOED J. P., HALD T.,
FRIGAARD P. and BURCHARTH H. F.
Hydraulics and Coastal Engineering Laboratory
Dept. of Civil Engineering, Aalborg University, Denmark

## ABSTRACT

The present paper concerns the results and findings of a physical study on wave impacts on vertical caisson breakwaters situated in irregular, multidirectional breaking seas. The study has taken place as part of the framework programme "Dynamics of Structures" financially supported by the Danish Technical Research Council, during the period of January 97 to December 97. The tests were carried out in the 3D wave basin at the Hydraulics and Coastal Engineering Laboratory, Aalborg University. The objective of the study was to asses the effects of wave obliquity and multidirectionality on the wave induced loading and overtopping on cassion breakwaters situated in breaking seas. Regarding the wave forces only minor differences between breaking and non breaking waves in deep water were observed, and it was found that the prediction formula of Goda also seems to apply well for multidirectionally breaking waves at deep water. The study on wave overtopping showed that the 3D wave overtopping formula suggested by Franco et al., 1995b, predicts the wave overtopping reasonable well for both non breaking and breaking waves at deep water.

## 1. INTRODUCTION

Attention has been addressed to the effects of wave obliquity and multidirectionality on wave loads and wave overtopping on vertical caisson breakwaters situated in non-breaking seas. Within the joint European (MAST-LIP-TAW) research project, a 3D model investigation was carried out at Delft Hydraulics to asses these effects. The results have been published by several researchers, among them Franco et al., 1995a and Franco et al., 1995b. Several researchers have investigated the effects of wave breaking and impact forces on vertical structures in the past, and it is still generally acknowledged that the impact loading of vertical structures is the main damage source, see Oumeraci et al., 1995. The research work on impact forces has mainly been based on 2D breaking waves. So far, no attention has been paid to the effects of wave obliquity and mulitidirectionality on the wave loads and wave overtopping on caisson breakwaters placed in deep water breaking seas. The effects

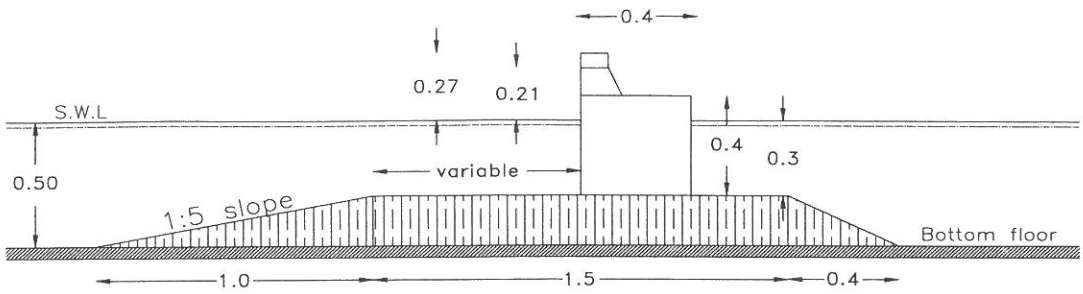


Figure 1 - Cross section of caisson model(s).

of wave obliquity and multidirectionality on the wave loads were investigated by measuring the wave induced pressure at 50 locations on a 6.0 meter wide caisson breakwater model, enabling determination of the horizontal force in one section as well as the lateral distribution of the horizontal force. The results and findings on the effects on the lateral distribution of the horizontal force are not included in this paper, but is published in the test report Results of Caisson Breakwater Tests in Multidirectional Breaking Seas. The present paper intends to stress the effects of wave obliquity and multidirectionality on the horizontal force in one vertical section.

The wave overtopping was measured on a 1.0 meter wide section of the caisson breakwater model, and the findings regarding the effects of wave obliquity and multidirectionality of the waves are presented in terms of the mean average overtopping discharge.

## 2. EXPERIMENTAL SETUP

The cassion breakwater model was constructed in plywood and placed on a smooth one layer foundation berm. Since the wave induced uplift pressures at the caisson bottom was not considered in the study, the foundation berm was constructed in concrete. The cross section of the model is seen in Figure 1, and as it appears a crest element is placed on the top of the model in order to vary the crest height. The size of the model does not refer to any particular prototype structure, however, a Froude scaling of 1:20 - 1:25 seems appropriate for this type of structures. In order to generate a sea state representing breaking waves in deep water in front of the caisson model, a relatively short 1:5 slope was constructed and placed as seen in Figure 1.

For harbor type structures situated at deep water, the percentage of breaking waves in a storm event depends on the structure location and at the wave climate at this location, however, for this study it is decided to keep the number of breaking waves at about 5 to10 per cent of the total number of waves. Using the numerical wave transformation model "MildSim", developed at the Hydraulics Laboratory at Aalborg University, tests with 2D irregular waves with a significant wave height of 0.18 m and a peak period at 1.2 s showed that about 6 to 7 per cent of the waves are breaking.

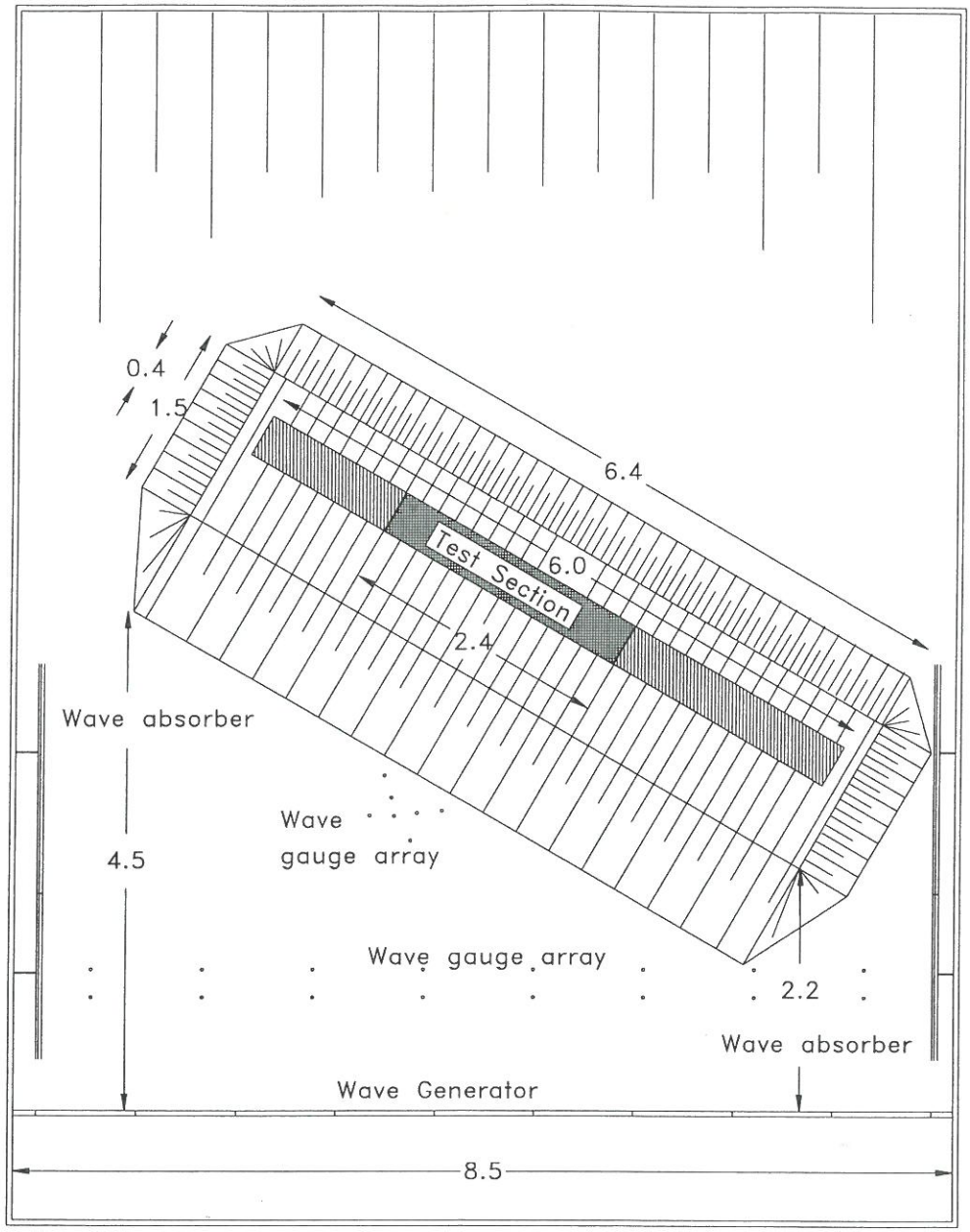


Figure 2 - Plan view of the 3D wave basin layout. Measures in meters.

Due to the wave diffraction processes around the two ends of the breakwater, the sea states in the vicinity of the ends would be disturbed during the tests. Therefore, since the lateral distribution of the horizontal force was to be considered in this study, it was important that the sea state in front of the test section not was influenced by the diffraction at the two ends. The numerical wave transformation tests showed, depending on the wave obliquity, that the sea state at the two ends was disturbed at a distance corresponding to approximately 1-1.5 times the wavelength. Therefore, to take into account the disturbance from the diffraction

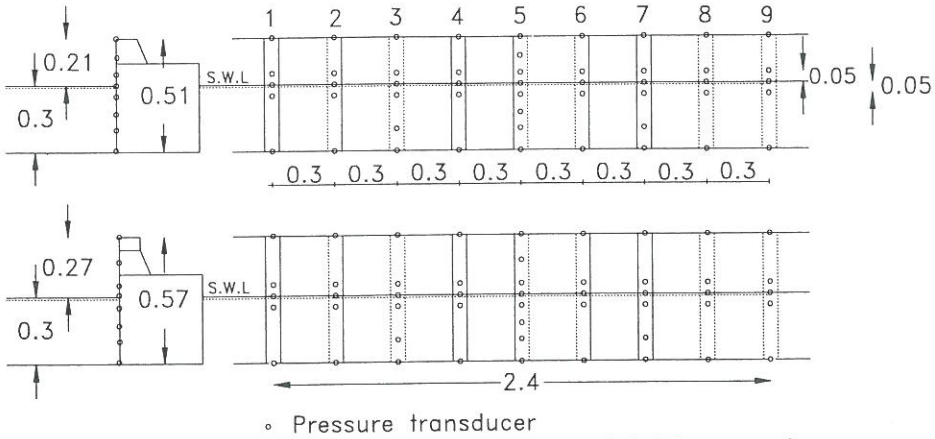


Figure 3 - Instrumentation of the caisson model. Measures in meters.

processes, and to obtain a width of the test section corresponding to one wavelength, the total width of the model should be about 6 meter.

The experiments were carried out in the 3D deep water wave basin at Aalborg University. The wave basin is capable of generating irregular multidirectional waves. A plan view of the wave basin and the caisson model is seen in Figure 2. Although the amount of wave energy passing through the gabs between the caissons and the side walls of the basin is small compared with the reflected wave energy, the rear end of the basin is equipped with a spending beach constructed of gravel material. Along the side walls of the basin, vertical steel absorbers are placed to damp any cross modal activity occurring during the tests. Due to limitations in the wave generation, the obliquity of the generated waves should be kept less than 30°, and therefore the model was placed under 60° with the wave paddles of the wave generator, as seen in Figure 2. Due to the high reflection from the caissons, a three dimensional active wave absorption system is applied to avoid too much re-reflected wave energy in front of the caissons. The active absorption system operates on-line by digital filtering of surface elevations measured in 16 individual positions in the wave field in front of the wave paddles, as seen in Figure 2. The wave absorption system is in its complete form outlined in Hald and Frigaard, 1997. In front of the model the wave field is measured by an array of 7 wave gauges, see Figure 2. The wave gauges are placed at deep water, i.e. in front of the 1:5 slope, which is about 1.5 meter, seaward the model. The incident wave field was estimated based on the Bayesian Directional spectrum estimation Method (BDM). Furthermore, the caisson has been instrumented with two wave gauges on the front. Thus, by assuming full reflection and therefore neglecting that some water is overtopping the water height can also be estimated at the structure.

The wave pressures were measured by a set of 50 pressure transducers placed as shown in Figure 3. The position of the pressure transducers enables the study of the vertical distribution of the

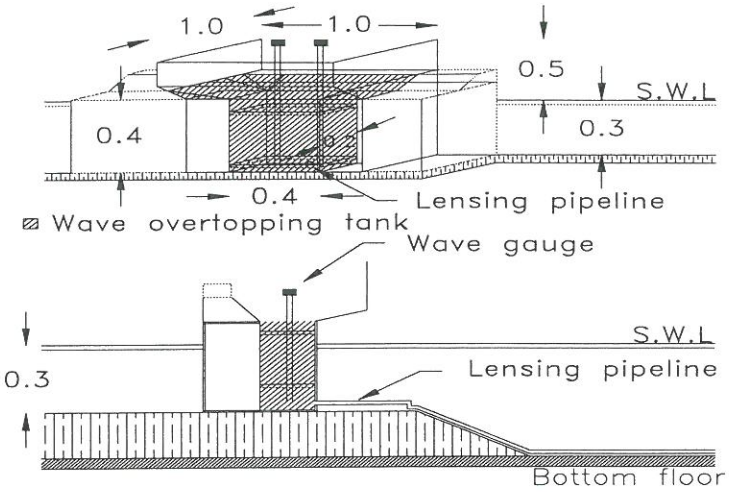


Figure 4 - Wave overtopping measuring device. Measures in meters.

horizontal pressure in different sections along the caisson model. By means of these vertical distributions of the horizontal pressures, the lateral distribution of the horizontal forces can be studied, and not only the lateral distribution of the horizontal pressures. This is important due to the unknown correlation between the lateral distribution of the horizontal pressure and the lateral distribution of the horizontal force.

Sideways, the pressure transducers are placed within a distance of 0.3 m enabling the study of the vertical distribution of the horizontal pressure in 9 sections along the 2.4 meter wide test section. A row of pressure transducers is placed at still water level. Furthermore, a row of transducers is placed 5 cm above and 5 cm below the still water level.

The wave overtopping measurements concern the determination of the mean discharge of a test sequence, the number of wave overtopping events and finally the determination of the water volume in each of the individual overtopping events. In this study, the wave overtopping is determined by recording the water level in a water tank, in which all the overtopping water is collected. The collected overtopping water corresponds to a width of 1.0 m of the test section. The amount of water collected in the tank is determined by recording the water level in the tank during the tests. The water level is measured by a set of two wave gauges placed in the water tank. Due to the irregularity of the waves, the amount of overtopping water varies from wave to wave, and in order to obtain reasonable increments of the water level in the tank even for the smallest wave overtopping events, the cross section area of the tank must be kept relatively small.

## 3. TEST CONDITIONS

As the main objective of the study was to assess the effect of wave obliquity and multidirectionality the changes on test conditions were mainly the incident mean direction of the waves and the directional spreading of the waves, i.e. the energy distribution around the mean direction of the waves. The

| | |
|---|---|
| Wave spectrum | JONSWAP, $\gamma = 3.3$ |
| Peak period, $T_p$ | 1.2 sec |
| Significant wave height | 0.16 m to 0.18 m |
| Crest freeboard, $R_c$ | 0.21 and 0.27 |
| Water depth, $h_d$ | 0.3 m |
| Angle of wave attack , $\theta$ | 0°, 15°, 30°, 45°, ( 60° ) |
| Type of spreading | Cosine squared, with s=10 and s=29 |

Table 1 - Wave parameters.

mean direction or the incident angle of wave attack was varied from 0° (head on waves) to 50° for some of the tests. A cosine squared ($\cos^{2s}(\theta/2)$) spreading function with fixed s-values of 10 and 29 was used in the tests, which corresponds to standard deviations of 25° and 15°, respectively. See Frigaard et al., 1997. The incident target significant wave height was fixed at 0.16 m for the non breaking waves and 0.18 m for the breaking waves. A JONSWAP wave spectrum with a peak enhancement factor of 3.3 and a peak period of 1.2 sec was applied in all the tests, giving a steepness at 0.07 for non breaking waves and 0.08 for breaking waves. To obtain an adequately statistically validity of the test results, rather long test series were performed with no test series having less than 1800 waves. In table 1, the various target parameters of the test series are shown.

Regarding this paper, the results are all based on the test cases listed below and with a crest freeboard of 0.27.

- 3D non breaking waves, $H_s = 0.16$ m, $\sigma = 15°$, $\theta = 0°$ to 40°
- 3D non breaking waves, $H_s = 0.18$ m, $\sigma = 25°$, $\theta = 0°$ to 40°
- 3D breaking waves, $H_s = 0.16$ m, $\sigma = 15°$, $\theta = 0°$ to 48°
- 3D breaking waves, $H_s = 0.18$ m, $\sigma = 25°$, $\theta = 0°$ to 40°

## 4. WAVE FORCE ANALYSIS

The horizontal wave forces are determined by a linear integration of the measured pressure time series. The horizontal forces presented below are all based on the pressure measurements of section 5, see Figure 3, where 8 pressure measurement positions are used representation of the vertical distribution of the horizontal pressure. In Figure 5, a plot of the measured horizontal pressures are shown along with the calculated force time series. The plot shows 10 sec of the test series with head on breaking waves and a spreading corresponding to $\sigma = 25°$.

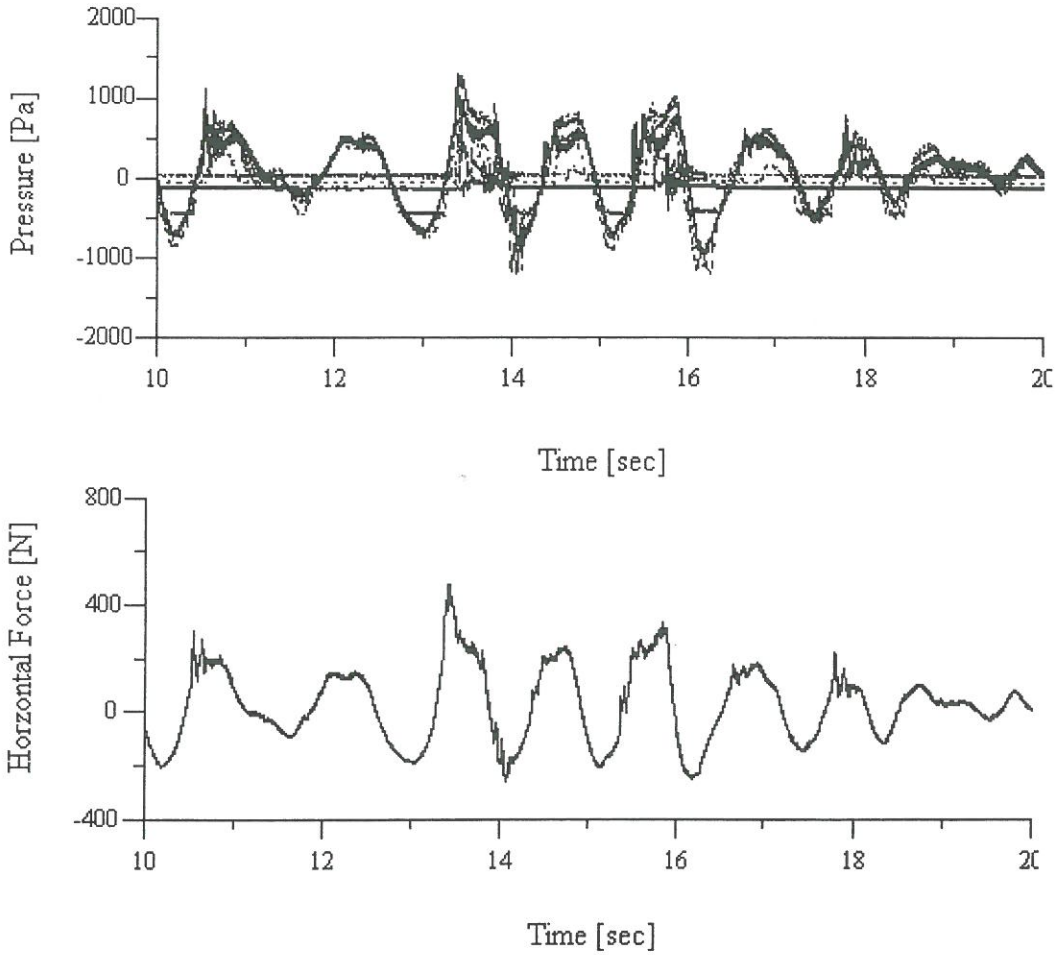


Figure 5 - Pressure record with corresponding force time series.

The pressure time series are sampled at 800 Hz, and only the maximum peaks within one wave period are used for the determination of the probability distribution of the horizontal forces.

In order to compare the results with the prediction formula of Goda, the statistical force parameter $F_{1/250}$ are calculated from the force time series. Due to the applied number of waves this force is calculated as an average value of the 7 largest forces found by the analysis of the force time series. In order to compare the results of the tests with non breaking waves with the tests with breaking waves, the calculated $F_{1/250}$ forces are normalized by the predicted Goda force corresponding to the actual wave obliquity and wave height measured by the wave gauges placed at deep water. Such normalization is however not unambiguous because due to shoaling the waves at the model structure are quite different from the recorded waves at deep water, whereas this was not the case in the tests of Goda. For this reason, alternative normalization is presented in Section 6 of this paper.

The results of the normalization based on the recorded non shoaling waves are shown in Figure 6. Deeper interpretation of the results should not be done because of the normalization as

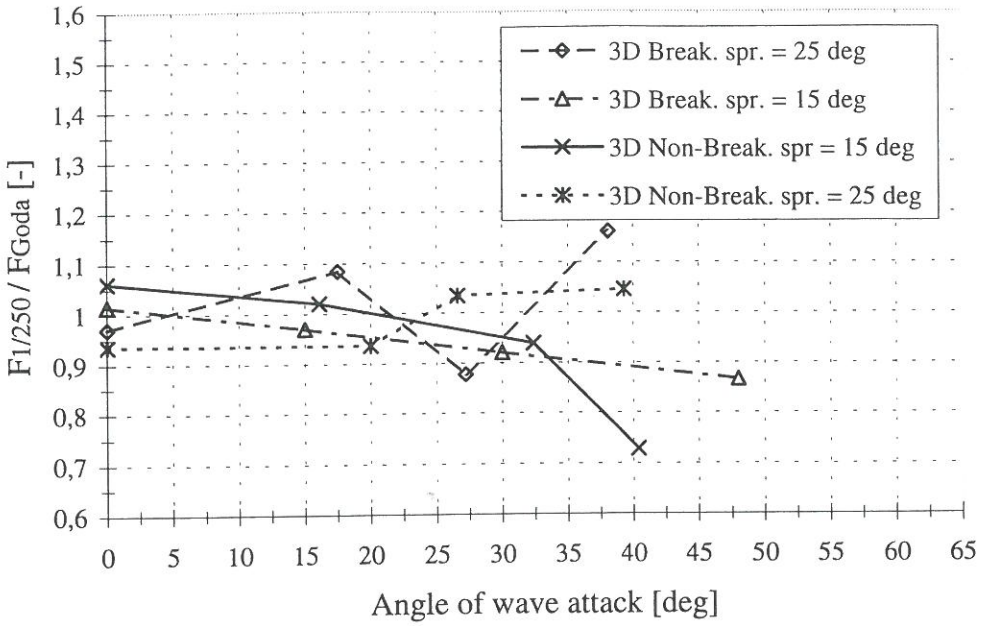


Figure 6 - Comparison with Goda predicted forces based on recorded non shoaling waves at a distance from the structure.

discussed above. However, if this is disregarded it can be seen that the formula of Goda seems to apply well for both the non breaking as well as the breaking waves. Most of the calculated forces are seen to deviate less than 10% from the Goda predicted forces. Apparently, the Goda formula applies best in case of waves within the range of 0 to 35 degrees. However, the pronounced scatter for waves with larger obliquity than 35 degrees could also be due to the relative error of these forces.

Franco et al. 1995a found for non breaking waves that the forces predicted by the formula of Goda, which does not take into account the multidirectionality of the waves, should be reduced with about 10%. This trend is, however, not seen in the results of this study.

One would expect the breaking waves to produce higher forces than the non breaking waves due to the impact forces. This is also seen if the shoaling waves at the structure are used as reference waves instead of the non shoaling waves, cf. Section 6.

## 5. WAVE OVERTOPPING ANALYSIS

For each test series, the wave overtopping was determined by recording the water level in the overtopping tank. The water levels were measured by a set of two wave gauges during the tests, and each of the overtopping events were recorded as a small (or large) increase in water level. In Figure 7 the measured overtopping rate is shown for the test with head on non breaking waves, and a spreading corresponding to $\sigma = 25°$. The total amount of water collected in the water tank during a complete time series is determined by calculating the water

volume of each of the individual overtopping events.
The non dimensional mean overtopping discharge is defined as:

$$Q=\frac{q}{\sqrt{gH_s^3}}$$

where q is the average wave overtopping discharge per meter structure length, $H_s$ is the significant wave height and g is the gravity acceleration.

The basic assumption, confirmed by many researchers, is that the main parameters influencing the wave overtopping performance, i.e. the significant wave height, the crest height and the average wave overtopping discharge are related through a exponential function as:

$$Q=ae^{\left(-b\frac{R_c}{H_s}\right)}$$

Based on more than 80 hydraulic model tests performed in the directional wave basin at Delft Hydraulics,

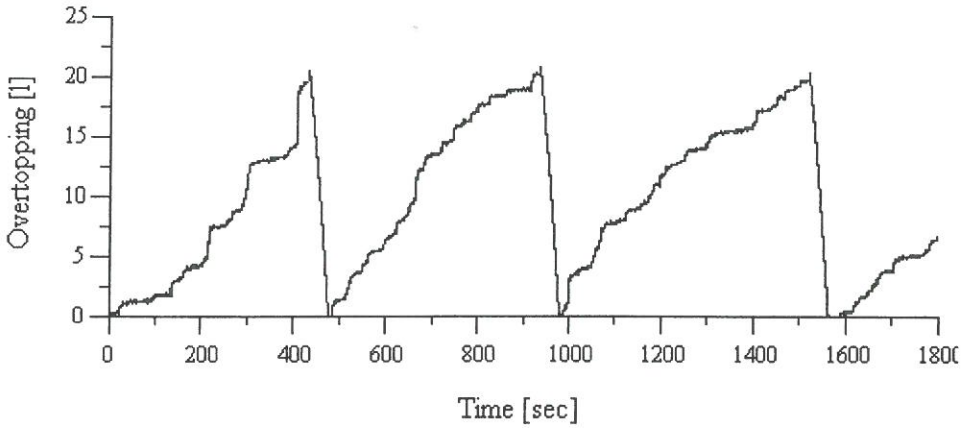


Figure 7 - Recorded wave overtopping time series.

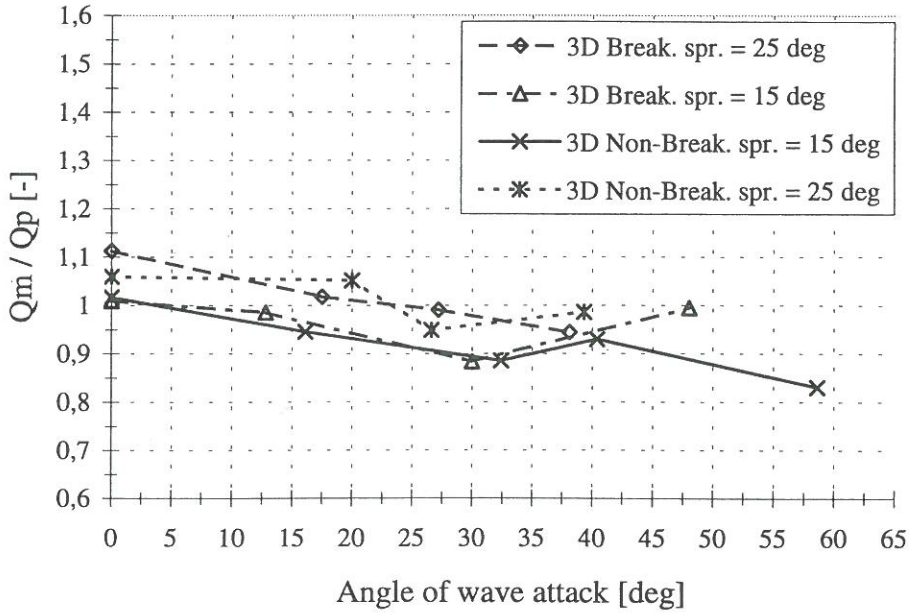


Figure 8 - Comparison of measured and predicted wave overtopping based on non shoaling waves at a distance from the structure.

Franco et al., 1995b, suggested the use of a = 0.082 and b = 3.0 for plain vertical structures exposed to head on waves. To take into account the effects of wave obliquity and multidirectionality a reduction factor was introduced to the non dimensional expression.

$$Q_p = ae^{\left(-\frac{b\ R_c}{\gamma\ H_s}\right)}$$

Through best fit regression analysis Franco et al., 1995b suggested the following relation between $\gamma$ and the wave obliquity for multidirectional waves.

$\gamma = 0.83$ for $0° \leq \theta \leq 20°$
$\gamma = 0.83 \cos(20° - \theta)$ for $\theta \geq 20°$

In Figure 8 the results of the 4 test cases are shown. The wave overtopping is expressed in terms of the measured average overtopping discharge $Q_m$ normalized by the predicted average wave overtopping discharge $Q_p$.

As it appears, the suggested prediction formula of Franco et al., 1995b seems to apply well with most of the compared data deviating less than 10%. It is, however, observed that for angles of wave attack smaller than approximately 20°, the predicted wave overtopping tends to be smaller than the measured wave overtopping, whereas, the wave overtopping seems to be over predicted for angles of wave attack larger than approximately 20°.

Comparing the results of non breaking waves to the results of breaking waves, it is seen, that no apparent difference exist, indicating that in terms of 3D waves, it is not necessary to distinguish breaking waves from non breaking waves. However, it was visually observed during the tests with breaking waves that the breaking process causes a significant increase in spray, which of course should be considered in the prototype case.

## 6. RESULTS BASED ON WAVE HEIGHTS AT THE STRUCTURE

As described in Section 2 it is the sloping bottom in front of the caisson that introduces the wave breaking in the breaking waves test series. This means that the wave height in these tests varies as the waves approaches the caisson. Thus, the wave heights determined by the BDM analysis of the waves measured at the deep water is not the wave heights of the breaking waves as they reach the cassion. This wave height at the structure is very difficult to estimate, due to the high amount of reflection. But by using the wave gauges placed on the front of the caisson, the wave height at the structure has been estimated. Using these wave heights Figures 6 and 8 will change into the plots shown in Figure 9 and Figure 10.

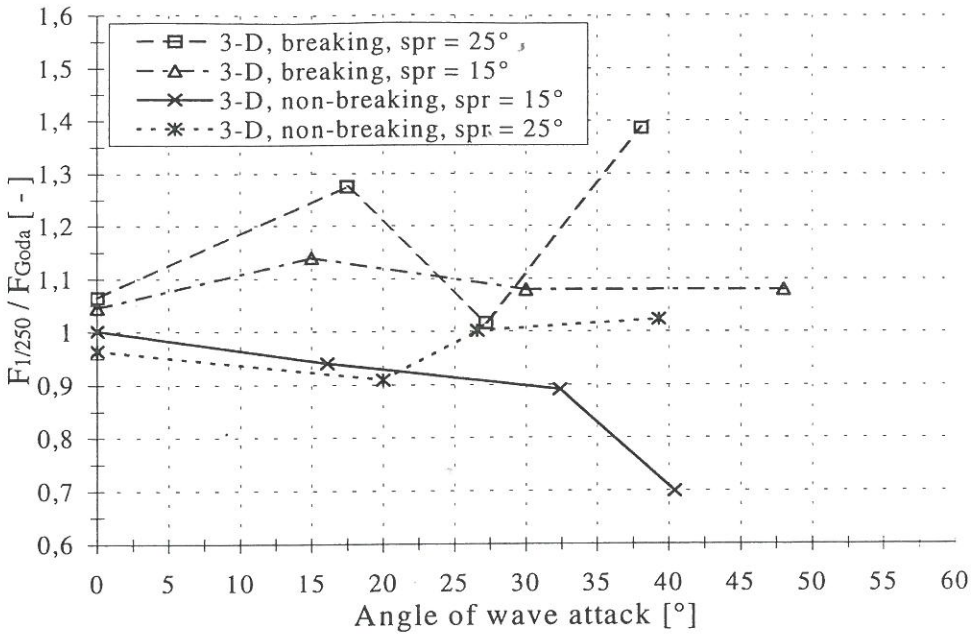


Figure 9 – Comparison with Goda predicted forces (wave heights at the structure).

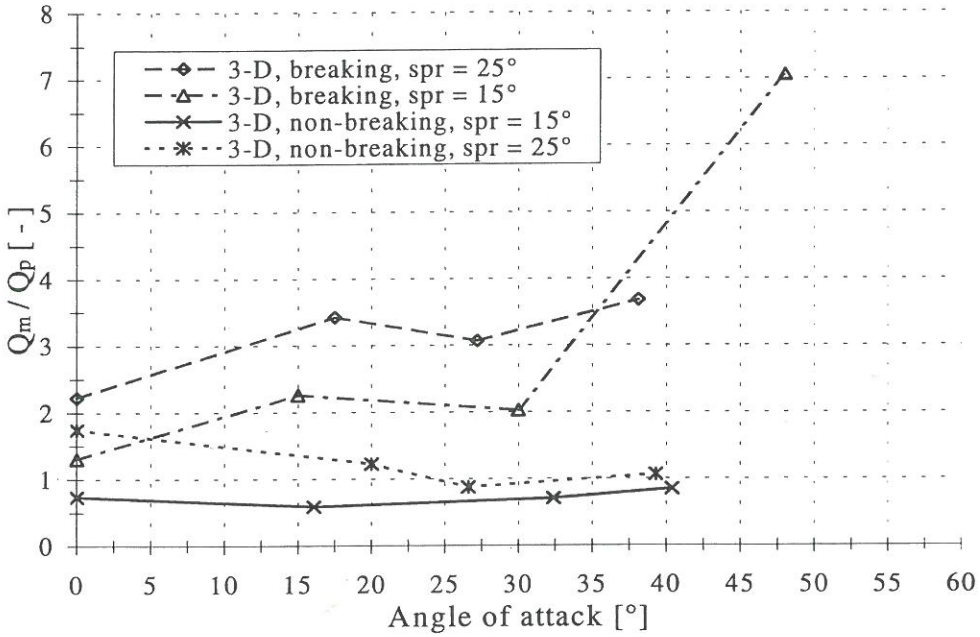


Figure 10 – Comparison of measured and predicted wave overtopping (wave heights at the structure).

The new plots show more scatter than the previous plots due to the poorer estimation of wave heights. As expected the breaking waves loose more energy on the slope than the non breaking waves, and the normalized forces and overtopping rates are therefore increased for the breaking waves compared to the previous plots, while the rates for the non breaking waves are relatively unaltered. Thses results seems more logic than those presented in Figure 6.

## 7. CONCLUSION

Regarding the effects of wave obliquity and multidirectionality on wave loading and wave overtopping on caisson breakwaters only minor differences were observed between breaking and non breaking waves when the results were normalized with deep water wave heights. In the case where the forces were normalized with wave heights at the structure larger wave force rates where observed for the breaking waves.

Despite the observed amount of spray during the tests, the measured overtopping rates for breaking waves seem to agree well with the prediction formula for 3D non breaking waves given by Franco et al., 1995b as long as the deep water wave heights where used. Using the wave heights at the structure results in significantly larger overtopping rates for the breaking waves, than predicted by the overtopping formula by Franco for non breaking waves. The rates for the non breaking waves were better predicted by the Franco formula.

## 8. ACKNOWLEDGEMENTS

This work has been carried out with support from the frame work programme *Dynamics of Structures* of the *Danish Technical Research Council.*

## 8. REFERENCES

Battjes, J. A. and Jansen, J. P. F. M. (1978). *Energy loss and set-up due to breaking of random waves*, Proceedings of the 16th International Conference on Coastal Engineering, Hamburg.

Hald, T. and Frigaard, P. (1997). *Alternative Method for Active Absorption in Multidirectional Waves*. IAHR seminar on Multidirectional Waves and their Interaction with Structures, 27th IAHR Congress, San Francisco, 10-15 August 1997.

Franco, C., Franco, L., Passoni, G., Restano, C., van der Meer, J.W. (1995a). *The effect of wave obliquity and short-crestedness on the horizontal and uplift forces on caisson breakwaters.* Final proceedings, MAST II, (MAS2-CT92-0047), MCS-Project: Monolithic (Vertical) Coastal Structures, Paper 4.8, 22 pp.

Franco, C., Franco, L., Restano, C., van der Meer, J.W. (1995b). *The effect of wave obliquity and short-crestedness on the overtopping rate and volume distribution on caisson breakwaters.* Final proceedings, MAST II, (MAS2-CT92-0047), MCS-Project: Monolithic (Vertical) Coastal Structures, Paper 4.9, 37 pp.

Frigaard, P., Helm-Petersen, J., Klopman, G., Stansberg, C. T., Benoit, M., Briggs M. J., Miles, M., Santas, J., Schäffer, H.A., Hawkes, P.J. (1997). Grønbech J., Hald, T. and Frigaard, P., Burcharth H. F. (1997). *Wave Loading and Overtopping on Caisson Breakwaters in Multidirectional Breaking Seas.* IAHR seminar on Multidirectional Waves and their Interaction with Structures, 27th IAHR Congress, San Francisco, 10-15 August 1997.

*IAHR List of Sea State Parameters.* IAHR seminar on Multidirectional Waves and their Interaction with Structures, 27th IAHR Congress, San Francisco, 10-15 August 1997.

Oumeraci, H., Hewson, P., Juhl, J. and van der Meer, J.W. (1995). MCS-Project: *Multi-Disciplinary Research on Monolithic Coastal Structures*, Final proceedings, MAST II, (MAS2-CT92-0047), MCS-project: Monolithic (Vertical) Coastal Structures. Papers Task 1-2.

*Results of Caisson Breakwater Tests in Multidirectional Breaking Seas (Internal Laboratory Test Report).* Hydraulics and Coastal Engineering Laboratory, Dept. of Civil Engineering, Aalborg University, Denmark, December 1997.

Project C3: Dynamics of Sports Stadiums

# Development of models for determination of the dynamic load from spectator movement

Jeppe Jönsson
*ES-Consult, Staktoften 20, 2950 Denmark*

Lars Pilegaard Hansen
*Aalborg University, 9000 Aalborg, Denmark*

*In the design of sports stadiums the dynamic effects from spectator movement constitutes an important part. In the present project the main focus has been on the development of spectator load models that give a realistic representation of the vertical force exerted by the individual spectator on the structure, when performing repetitive motion. Analytical expressions of force amplitude spectra for both deterministic and stochastic pulse trains have been found for a variety of different impulse shapes. Experimental investigations have been performed for vertical motions at different motion frequencies in order to determine the relevant motion parameters, the experimental load spectra, the influence of the structural eigenfrequency and the structural stiffness. A theoretical, a computational and two experimental investigations have been performed. These investigations show that it is possible to use impulse based models for assessment of the vertical force exerted by repetitive vertical human motion.*

## Development of analytical load models

The theoretical research reported in [1] concerns the investigation of the mechanics of repetitive human motion and involves an analysis of the influence of different impulse shapes, i.e. different force-time functions. The Fourier transforms of pulse trains of the impulse functions are used to find deterministic and stochastic force amplitude spectra. In the theoretical work it has been assumed that the structure is infinitely stiff. The validity of this assumption is sought in the second experimental investigation, [2]. The first experimental investigation, [3], concerns the determination of the main parameters needed to describe the loads for motion on a very stiff structure.

Introducing the impulse starting time within each mean period or the period between impulses as a stochastic variable it has been possible to develop analytical load models in the frequency domain, which include the variance of the impulse starting times or the variance of the pulse periods. These models can be expanded to crowd loads using a corresponding crowd variance. (This can be done by summing up multiple impulses within a period).

### Computational investigation of stochastic repetitive load

The analytical models for the spectral distribution of repetitive vertical human loading, mainly jumping, have been validated through the use of simulated discrete time series of the load. The computational investigation is described in [4]. The simulation is performed on the basis of halfsine impulse shapes and experimentally determined mean values and standard deviations of the pulse period, the pulse starting time and the contact durations. The simulations show that the developed analytical expressions for the spectral load distribution are adequate.

### Experimental investigation of repetitive vertical human loading

The first experimental investigations reported in [2] involves **one** person performing repetitive vertical motion on a very stiff square measuring platform 0.80 m x 0.80 m. Time series of the loads on the platform and the motion of the waist are recorded. The experiments are performed at motion frequencies varying from 0.5 Hz to 3.2 Hz using a metronome. Two test series with two different test persons were performed. The motions performed at each frequency include movements, where the amplitude of the vertical motion is as large as possible, for example by repetitive jumping from a position with bent knees. Mechanical and experimental analysis shows that the maximum movement is obtained for low frequencies. At each frequency the person is asked to perform the following motions:

a) high jumping with the largest possible movement (bending of knees)
b) high jumping with the smallest possible contact duration (on toes)
c) jumping with the largest possible contact duration (stamping)
d) normal jumping
e) large amplitude vertical motion with continuous contact (knee bends)

These motion types are believed to be sufficient for the purpose of defining spectral force envelopes to be used in the ultimate state and the serviceability state. The influence of the number of people is not considered in the experimental work, but the mechanical investigations have opened a path for further investigations.

The experimental investigations show that it should be possible to use the developed impulse based load models for repetitive vertical human loading. The experiments have been illustrated by direct plots and force amplitude spectra.

### Experimental investigation of the structural influence

The second experimental investigation reported in [3] was performed in order to investigate the influence of the structural stiffness (the structural displacement amplitude) and eigenfrequency on the repetitive vertical human motion and the related loads exerted by the human being.

The "structure" used in the experimental setup consists of a 1.6 m x 1.6 m square steel frame supported at the corners on flexible springs. By adding mass to the frame and choosing springs of varying stiffness it is possible to emulate structures of different stiffness and eigenfrequency. On top of the steel frame the small square measuring platform is mounted and a test person is asked to jump at given frequencies or to induce resonance by fast knee bends (with continuous contact). Both normalized load amplitude spectra and normalized structural displacement response amplitude spectra have been calculated for all experiments.

Nine different experimental structural setups have been used. The experimental structural setups have eigenfrequencies of about 3 Hz, 4 Hz or 6 Hz. For each eigenfrequency three different stiffnesses have been chosen. Thus enabling the experimental investigation of the influence of the displacement amplitude and the eigenfrequency on the load spectrum and human behavior.

The experimental investigations performed show that the impulse based load models for repetitive vertical human loading developed in [1] can be used and that the influence of the deflection amplitudes and the motion frequency is limited to a small increase in the standard deviations of the main motion parameters as shown in the previous section. However the influence is not systematic and the number of experiments have been limited. By comparing the variation of the motion parameters to the variations found for jumping on a stiff structure it is found that the contact duration ratio has the same variation with frequency and that the standard deviations of the periodic starting times are in the same order of magnitude, but with greater non systematic deviations between the individual experiments.

The experimentally found normalized force amplitude spectra for jumping show that load models based on repetitive impulses give reasonable representations of the load spectra for motions at different frequencies and with different contact duration ratios. The normalized displacement amplitude spectra show that simple dynamic response analysis can be used to find the structural response.

**Main results**

The main results of the project is that analytical expressions for deterministic and stochastic load spectra for repetitive impulses have been developed and that these can be used for prediction of the load spectra for repetitive vertical human motion. A number of important parameters related to the deterministic and stochastic description of repetitive vertical human motion have been determined experimentally. The structural influence on these parameters have also been investigated experimentally. For the development of a more complete load model for spectator movement research into the spatial distribution of loads from many spectators over larger areas and the participation degree will have to be performed. The influence of heel impact on the high frequency domain is needed if the models are to be applied for analysis of the service state. One method has been proposed for the inclusion of heel impact.

## References

[1] J. Jönsson. *Repetitive Vertical Human Loading, Part 1 - Theoretical Investigation.* Dept. of Building Technology and Structural Engineering, R9753, Aalborg University, Denmark, 1997.

[2] J. Jönsson and L. Pilegaard Hansen. *Repetitive Vertical Human Loading, Part 2 - Experimental Investigation.* Dept. of Building Technology and Structural Engineering, R9754, Aalborg University, Denmark, 1997.

[3] J. Jönsson and L. Pilegaard Hansen. *The Structural Influence on Repetitive Vertical Human Loading.* Dept. of Building Technology and Structural Engineering, R9804, Aalborg University, Denmark, 1998.

[4] J. Jönsson. Computational Investigation of Repetitive Vertical Human Loading, in proceedings of the *Ninth nordic seminar on computational mechanics,* Technical University of Denmark, 1996.

# C.4 DYNAMIC MEASUREMENTS ON THE FREJLEV MAST

## Content

The interest in the ability to model the dynamics of cables in civil engineering have had an increasing interest during the last century since cables are very efficient structural members due to their high strength and light weight and their use has therefore been increased significantly in civil engineering structures such as cable-stayed bridges, guy towers, transmission lines and cable-supported roofs. Cables are flexible and their inherent damping extremely small and consequently, vibration with large amplitudes can be easily induced by external disturbances such as wind.

The aim of this project was to make full-scale measurements on the Frejlev-mast which is a 200 meter high guyed steel mast located 10 km. from Aalborg. The goal was to investigate the uncertainties of the estimated cable forces from vibration measurements. The cables of the Frejlev mast were instrumented in order to measure strains in the cables. However, it was found that the strain signals had a too low signal to noise ratio to be used for a further analysis. Since the strain signals could not be used some of the five cables were supplied with accelerometers. Further, accelerometers were installed at the location where the cable is attached to the mast. These measurements were used to investigate the influence of the motion of the cable support on the dynamic response of the cable.

The acceleration of the cable in three directions were measured with three different types of excitation: 1)Wind, 2) free-decays and 3) harmonic excitation by shaking the cables by the hand.

## Results

During the project a literature review of papers dealing with cable dynamics has been prepared, see Kirkegaard et al. [1]. More than 200 papers have been reviewed and divided into the subject groups linear cable behavior and non-linear cable behavior. Further, all papers were organized in a table with respect to cable theory, cable type and different remarks.

The Frejlev mast, the test setup, measurement conditions and the measurements performed on the mast have been described in a report, Kirkegaard et al. [2]. In total 60 measurements were performed with different cables and different types of excitation. The measured time series were analyzed using the ARMA techniques from the B.1. project. It was found that these techniques was a nice tool to separate closely-spaced modes of the cables.

In order to establish the relationship between frequencies and cable forces different models of the dynamic response of a cable have been investigated. Firstly, the cable forces have been estimated by a simple relationship between estimated natural frequencies and the cables forces in a linear cable. Secondly, the cable forces were estimated using a model taking into account the

measured excitation of the support at the location where the cable was attached to the mast. Before these approaches for estimation of the cable forces were used on the measured data from the Frejlev mast, simulation studies were performed. The results obtained from the simulation studies showed, that it was possible to obtain realible estimates for cables forces based on measured natural frequencies. Further, by comparing the estimated cable forces obtained from the measured data with the assumed cables forces in the cables, it was concluded that reliable cables forces can be estimated based on measured natural frequencies. The results of the estimation of the cable forces were presented in the report Kirkegaard et al. [3].

## Publications

[1] Kirkegaard, P.H & Lars Pilegaard Hansen: Cable Dynamics - A Literature Review. Aalborg University, Fracture and Dynamics, Paper No. 104, ISSN 1395 - 7953 R9813

[2] Kirkegaard, P.H & Lars Pilegaard Hansen: Vibration Measurements on the Frejlev Mast. Aalborg University, Fracture and Dynamics, Paper No. 105, ISSN 1395 - 7953 R9814

[3] Kirkegaard, P.H & Lars Pilegaard Hansen: Estimation of Cable Forces of a Guyed Mast from Dynamic Measurements. Aalborg University, Fracture and Dynamics, Paper No. 106, ISSN 1395 - 7953 R9815